CANADIAN THESES

THÈSES CANADIENNES

NOTICE

The quality of this microfiche is heavily dependent upon the quality of the original thesis submitted for microfilming. Every effort has been made to ensure the highest quality of reproduction possible.

If pages are missing, contact the university which granted the degree.

Some pages may have indistinct print especially if the original pages were typed with a poor typewriter ribbon or if the university sent us an inferior photocopy.

Previously copyrighted materials (journal articles, published tests, etc.) are not filmed.

Reproduction in full or in part of this film is governed by the Canadian Copyright Act, R.S.C. 1970, c. C-30. Please read the authorization forms which accompany this thesis.

AVIS

La qualité de cette microfiche dépend grandement de la qualité de la thèse soumise au microfilmage. Nous avons tout fait pour assurer une qualité supérieure de reproduction.

S'il manque des pages, veuillez communiquer avec l'université qui a conféré le grade.

La qualité d'impression de certaines pages peut laisser à désirer, surtout si les pages originales ont été dactylographiées à l'aide d'un ruban usé ou si l'université nous a fait parvenir une photocopie de qualité inférieure.

Les documents qui font déjà l'objet d'un droit d'auteur (articles de revue, examens publiés, etc.) ne sont pas microfilmés.

La reproduction, même partielle, de ce microfilm est soumise à la Loi canadienne sur le droit d'auteur, SRC 1970, c. C-30. Veuillez prendre connaissance des formules d'autorisation qui accompagnent cette thèse.

THIS DISSERTATION
HAS BEEN MICROFILMED
EXACTLY AS RECEIVED

LA THÈSE A ÉTÉ
MICROFILMÉE TELLE QUE
NOUS L'AVONS REÇUE

Pullout Capacity of Inclined Strip Anchor Plates in Sand

Adolfo Foriero

A Thesis

in

The Department

of

Civil Engineering

Presented in Partial Fulfillment of the Requirements
for the Degree of Master of Engineering at
Concordia University
Montreal, Quebec, Canada

August 1985

ABSTRACT

Pullout Capacity of Inclined
Strip Anchor Plates in Sand

Adolfo Foriero

The work discussed in this thesis provides a theoretical and experimental study of the behavior of a shallow, inclined strip anchor plate subjected to an axial tensile load in sand. The pullout capacity of the anchor is studied in relation to its axial inclination.

Two analytical procedures used to estimate the pullout capacity in terms of anchor geometry, inclination, depth of embedment and soil properties are presented. The analytical methods presented are checked against laboratory and published data.

Model tests were carried out in the laboratory to determine the effect of inclination on the ultimate uplift capacity of the anchor plate when subjected to inclined uplift forces in dense sand. It was found that the ultimate uplift resistance of the anchor increases as the angle of pull increases from the vertical. At ultimate failure, a soil mass of roughly truncated conical shape is lifted up, the surface of which reaches the ground level.

ACKNOWLEDGEMENT

I take this opportunity to express my sincere appreciation to my thesis Advisors - Dr. A. M. Hanna, Supervisor, Associate Professor in the Department of Civil Engineering, and Dr. A. B. von Keviczky (Co-Advisor for Chapter Number 5), Associate Professor in the Department of Mathematics - for their indispensible, unswerving, helpful guidance which brought about the realization of this thesis.

Further thanks go to Dr. H. Poorooshasb for many useful suggestions, Mr. T. Q. Nguyen for advice on designing the experiments' equipment and Mr. C. Kowalewski for constructing this equipment.

Beyond this, I express my deep indebtedness and admiration to my girlfriend, Teri Corbi, for her patience and stamina while typing this thesis and for her support in its completion.

Without NSERC support, these results would not have been possible. Therefore, I acknowledge the financial support accorded to me by Natural Science and Engineering Research Council of Canada during every stage of preparation of this thesis.

I dedicate this thesis to the memory of my deceased Grandfathers, Adolfo Foriero and Felice Di Salvo, for the loving kindness they gave me....

TABLE OF CONTENTS

Page

NOTATIONS

α'_v	Load Inclination From the Vertical Axis
α_h	Load Inclination From the Horizontal Axis
β	Central Angle of Radial Shear Zone
D_o	Depth of Anchor Plate From Ground Surface to the Bottom of the Plate
D_i	Depth of Anchor Plate From Ground Surface to the Center of the Plate
D	Depth of Anchor Plate From Ground Surface to the Top of the Plate
e_{max}	Maximum Void Ratio
e_{min}	Minimum Void Ratio
e	Void Ratio of Soil Deposit
E_p	Passive Force on Retaining Wall
G	Specific Gravity of Solid Particles
H	Anchor Plate Height
h	Height of Wall
i_u	Inclination Factor

k_b	Uplift Coefficient
k_p	Coefficient of Passive Earth Pressure
$k_{p\gamma}$	Coefficient of Passive Earth Pressure due to Weight Component
k_{pz}	Coefficient of Passive Earth Pressure at depth z
k_s	Coefficient of Punching Shear Resistance
$k_{t\gamma}$	Vertical Coefficient of Passive Earth Pressure due to Weight Component
L_i	Distance From Ground Surface to Plate Edge in the Assumed Failure Plane Direction
P_p	Total Passive Earth Pressure
P_f	Total Frictional Resistance
Q_u	Ultimate Pullout Load
Q_{uo}	Ultimate Pullout Load of Vertical Anchors
R_γ	Reduction Factor due to Weight Component
R.D.	Relative Density
V_i	Velocity Field

W	Width of Anchor Plate
z	Depth of Point Along z-axis
γ	Initial Unit Weight of Sand
γ_w	Unit Weight of Water (γ_w) at 4°C
ξ	Angle Between Anchor Plate and Radial Shear Zone
ϕ	Angle of Shearing Resistance of Soil
λ	Parameter Coefficient
ν	Angle of Dilatancy
δ	Average Mobilized Angle of Shearing Resistance on the Assumed Failure Planes
δ_z	Locally Mobilized Angle of Shearing Resistance on the Assumed Plane
δ_p	Anchor Plate Surface Friction
θ	Central Angle Between Anchor Plate and Slip Line
η	Angle of Slip Line (originating from bottom of plate) with respect to the horizontal axis
Ω	Angle of Slip Line (touching the ground surface) with respect to the horizontal axis

LIST OF FIGURES

LIST OF TABLES

CHAPTER 1

INTRODUCTION

1.1 PREFACE

Soil anchors (both on land and offshore) supporting structures subjected to tensile loading are in increasing demand. On land, anchors are of particular importance in the design of transmission towers as well as radio and television towers. Offshore applications of anchors often appear in the design and construction of deep-sea habitats or in repositioning of deep-sea platforms. In these cases, the requirement for uplift resistance is mainly due to wind and earthquake loading.

1.2 RESEARCH OBJECTIVES

The overall objectives of this study are to investigate the effect of some important variables on anchor pullout capacity. More specifically, the objectives of this research are:

a) to develop a method for estimating the pullout capacity of shallow strip anchor plates subjected to axial tensile loads;

b) corroborate these estimations via comparison with published data as well as laboratory testing of a small scale anchor plate.

The variables considered are the depth of the anchor and its inclination. In this thesis, the upper bound limit theorem and the limit equilibrium concept are employed for the theoretical analyses. The plastic limit theorem shall provide an upper bound of the true collapse load. The limit equilibrium method has some similarities to the upper bound method. Unless it can be demonstrated, however, that the chosen rupture surface possesses a kinematically admissible velocity field, it is not quite certain that the solution is an upper bound.

1.3 LITERATURE REVIEW

1.3.1 LABORATORY STUDIES

Extensive investigations of pullout capacity of anchors in ordinary terrestrial soils exist. Numerous experiments were done on anchors at all depths (16, 34, 35, 36, 47, 50, 51) as well as for shallow anchors (6, 7, 10, 14, 18, 19, 42, 48) and deep anchors only. These tests, however, were primarily performed on anchors subjected to vertical and horizontal pullout forces. Only a limited amount of laboratory experiments involved inclined plates pulled out by centrally-inclined loads in the direction of the plate axis.

Model uplift tests on inclined anchor plates of various shapes were carried out in sand (Bhalla, 1970, and Valliappan, 1970) at the Nova Scotia Technical College. The test results were plotted in polar

diagrams to exhibit the ultimate loads for various inclinations of the anchors (see Figure 1.1). From these results, it can be concluded that the uplift capacity of axially-loaded inclined anchors exceeds that of the horizontal plates.

Meyerhof (1968) extended his theory of vertical uplift to inclined anchors under axial loads. His theory and test results demonstrated that the ultimate load is expressible in terms of uplift coefficients which are functions of the friction angle of the soil and the foundation depth. He observed a roughly truncated pyramidal shape which lifted up when the anchor was loaded to failure (see Figure 1.2). For shallow anchors, the failure surface reached the ground level whereas for greater depths, local shear failure occurred near the anchor. For vertical uplift, he expressed the ultimate load of shallow anchors in sand as

$$Q_u = (\gamma D_o^2 k_b / 2H)\, A + W \cos \alpha_v , \qquad 1.1$$

where:

- A = Area of anchor plate
- H = Height of anchor plate
- D_o = Depth of anchor plate from ground surface to the bottom of the plate
- k_b = Uplift coefficient
- W = Weight of the anchor and soil mass vertically above the anchor plate
- α_v = Load inclination from the vertical axis
- γ = Initial unit weight of the soil

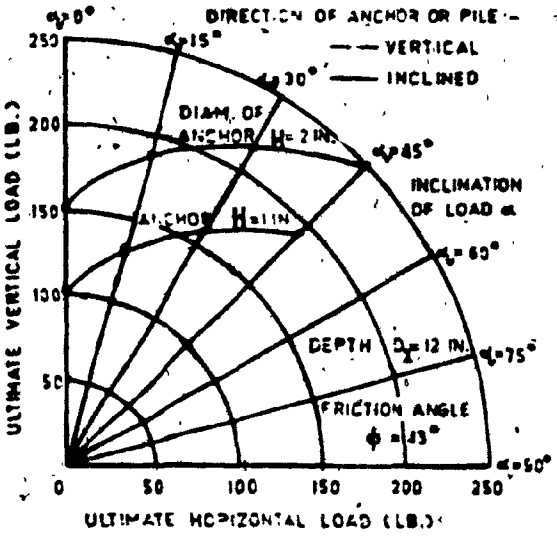

Figure 1.1: Typical Results of Model Tests on Anchors in Sand - Meyerhof (1973)

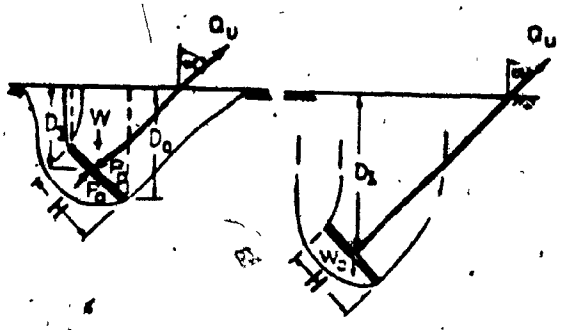

Figure 1.2: Failure of Soil for Shallow Anchor (left) and Deep Anchor (right) - Meyerhof (1973)

The uplift coefficients k_b for shallow strip anchors were determined and graphed (see Figure 1.3). For a given friction angle, the values of k_b decreased with the load inclination from a maximum (for horizontal pull) to a minimum (for a vertical uplift).

Meyerhof (1973) extended his theory further by introducing an inclination factor i_u, which allows the determination of the uplift capacity Q_u of an inclined anchor in terms of the resistance Q_{uo} of an anchor under vertical uplift by means of

$$Q_u = i_u Q_{uo} , \qquad 1.2$$

where: Q_u = Ultimate load of inclined anchor.

i_u = Inclination factor

Q_{uo} = Ultimate load of vertical anchor.

The graph obtained showed the experimental values i_u decreasing with the ratio D/H (see Figure 1.4). For shallow anchors, Meyerhof (1973) developed a theoretical relationship relating the inclination factors to the angle of inclination, which is formulated as follows:

$$i_u = 1 + (\alpha_v/90°)^2, \qquad 1.3$$

where: i_u = Inclination factor

α_v = Inclination of base.

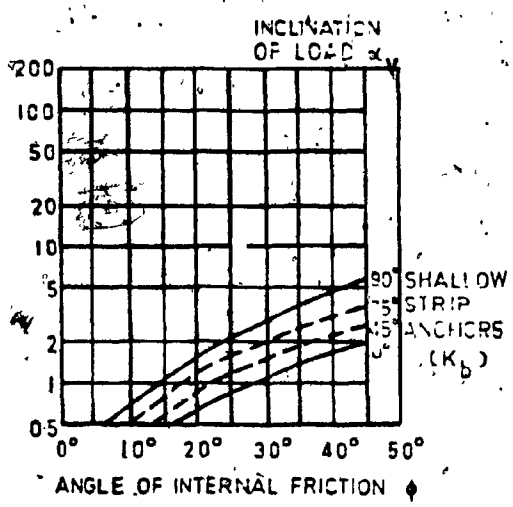

Figure 1.3: Theoretical Uplift Coefficients for Anchors - Meyerhof (1973)

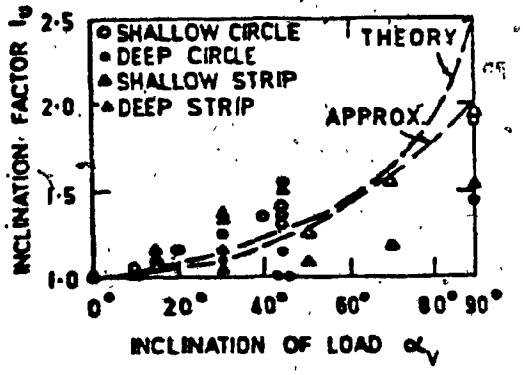

Figure 1.4: Inclination Factors for Anchors in Sand - Meyerhof (1973)

Trân-Vo-Nhiem (1971) used a two-dimensional analog model to study the behavior of a pulverulent soil during the oblique uplift of an anchor plate normal to the tensile load. He observed the uplift of a large zone of soil mass against the upper face. At the same time, there was settlement of the soil towards the lower face of the anchor (see Figure 1.5). These two zones of major deformation spread out when the inclination of the anchor, and hence of the force, increased. On the basis of the preceding observations it was shown that it is possible, assuming perfect plasticity of certain zones of the soil mass, to calculate the limit of resistance to oblique uplift of this type of anchor. Test results are compared with theoretical results for different anchor-soil frictions (see Figure 1.6).

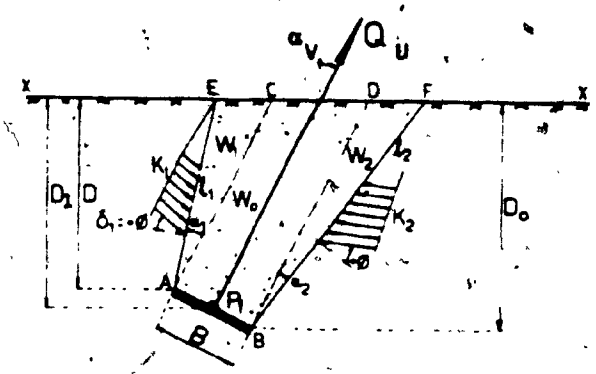

Figure 1.5: Assumed Failure Planes for Inclined Load - Trân-Võ-Nhiem (1971)

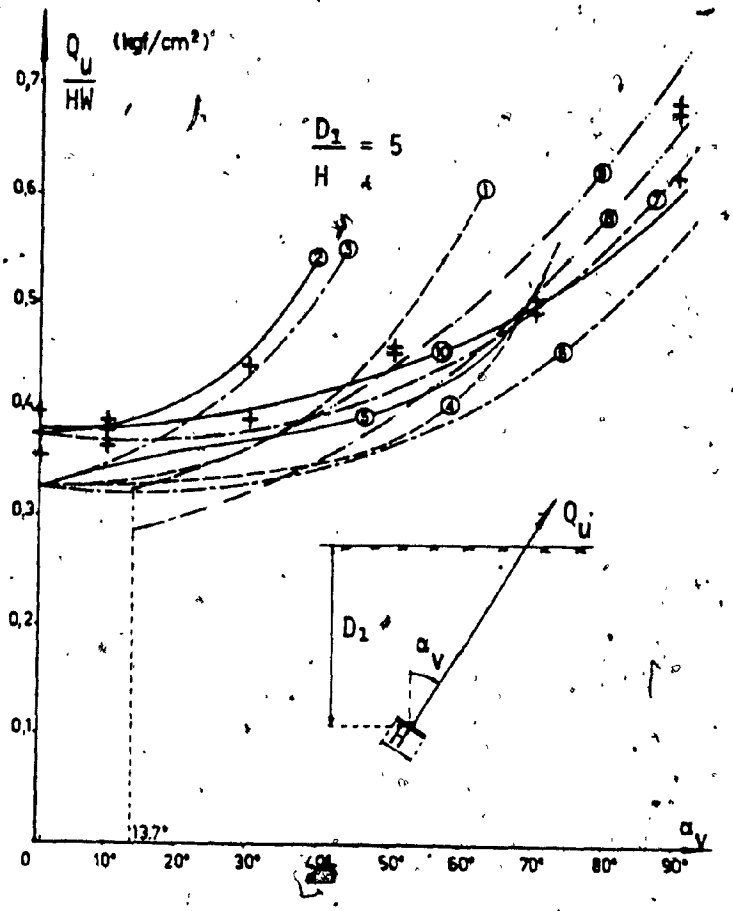

+ Tests on analogous model: $\phi = 26°$, H = 10 cm.

1: wedge angles $\alpha_1 = \alpha_2 = 0$

2: wedge angles $\alpha_1 = \alpha_2 = \phi$

3: wedge angles $\alpha_1 = -\alpha_v$, $\alpha_2 = 0$

4: wedge angles $\alpha_1 = -\alpha_v/2$, $\alpha_2 = 0$

5: wedge angles $\alpha_1 = -\alpha_v$, $\alpha_2 = 0$

6: hypothesis $\delta_b = \delta_p = 0$, $K_{f_1} = P\phi$

7: hypothesis $\delta_b = \delta_p = 0$, $K_{f_1} = P\phi$, $K_{f_2}\upsilon. = b_1\upsilon.$ max.

8 and 9: $\delta_p = \phi$, $K_{f_2} = b_1\phi$, $K_{f_2}\upsilon = b_1\upsilon.$ max

Figure 1.6: Experimental and Theoretical Results for Inclined Anchor - Trần-Vũ-Nhiem (1971)

In a recent study carried out by Wang and Wu (1980), the anchor problem was investigated both analytically and experimentally. The theoretical analyses was conducted using the upper bound limit theorem, which will be used in this thesis. The variables investigated were anchor orientation, embedment depth, internal friction angle of sand and anchor friction. Based on experimental observations, the failure zone was approximated by two straight lines and one segment of logarithmic spiral (see Figure 1.7). Although the experimental results agreed fairly well with the theory, an associative flow rule was assumed. The theory did not take into account the fact that the generated soil particle displacement is different from the stress characteristic pattern on which the stresses have the maximum obliquity of the angle ϕ. In this thesis, this fact has been considered by introducing the angle of dilatancy ν.

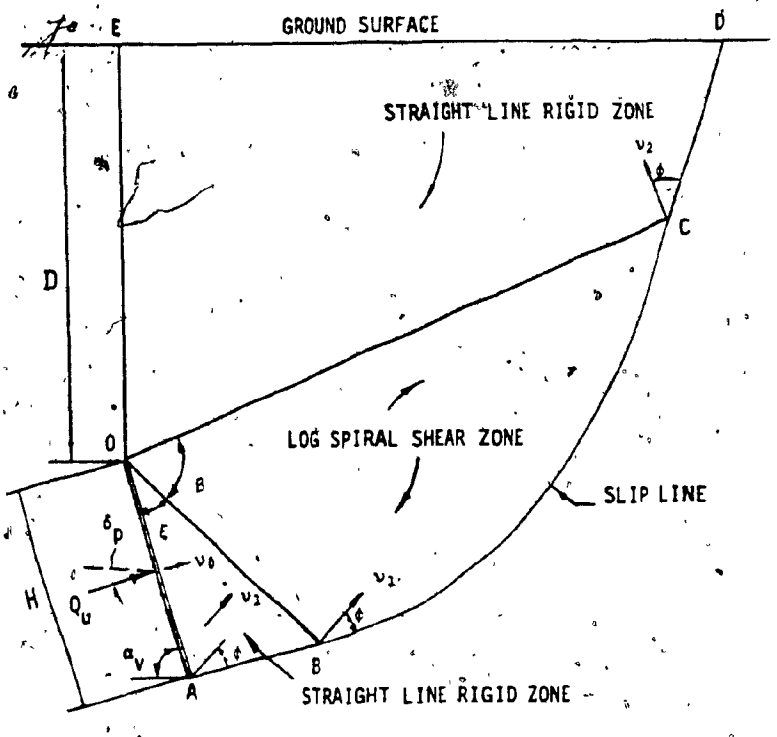

Figure 1.7: General Shear Failure for Shallow Anchors - Wang & Wu (1980)

1.3.2 FULL SCALE FIELD STUDY

Kanayan (1966) performed experiments under field conditions on foundation models with a slab, whose diameter was 1/3 the size of the support foundations of electrical transmission lines. The purpose of his test was to ascertain the pullout capacity under vertically- as well as obliquely-acting forces at constant depth. The size and shape of the zones of propagation were also investigated. Graphs of the pullout inclined force (depending on axial displacement) showed that the inclination of the anchor increases the pullout capacity. This increase is due to an increase of the surfaces of shear and of their change in form (see Figures 1.8 and 1.9). Consequent to the asymmetric character of the conditions of the slab, Kanayan also observed that the displacement of the anchor proceeded with a deflection upward and not in the direction of the acting force.

On the basis of his experimental data, diagrams of surface displacements for different steps of loading were constructed (see Figures 1.10 and 1.11). Vertical displacements reach a maximum in a zone situated above the slab. For inclined anchors, failure with an upward movement of the soil occurs in a zone situated above the slab, just as for the vertical case.

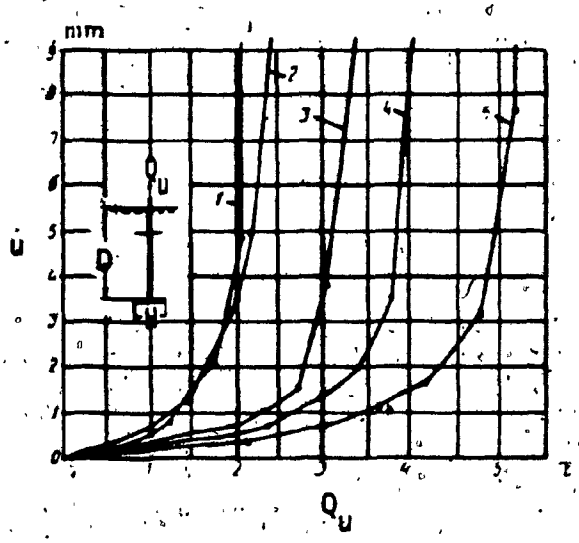

Figure 1.8: Graph of Dependence of Displacement u on Vertical Withdrawing Forces Q_u - Kanayan (1966)

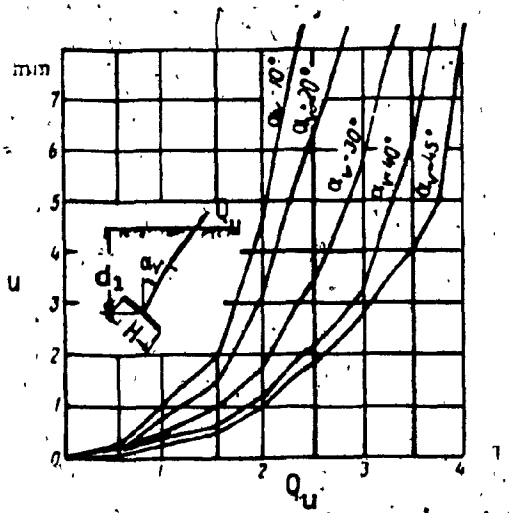

Figure 1.9: Graphs of the Dependence of u on Q_u with an Inclined Position of the Anchor - Kanayan (1966)

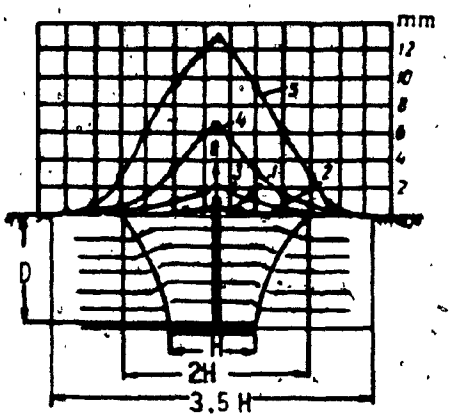

Figure 1.10: Cross Section of Diagram of Deformation of Upward Yielding Zone of Soil and Displacements of the Surface - Kanayan (1966)

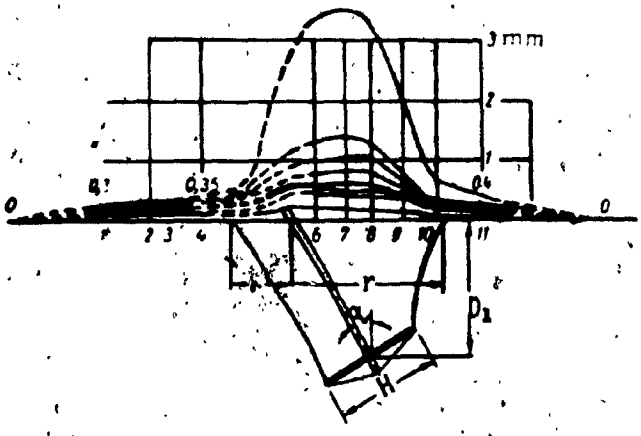

Figure 1.11: Diagram of Displacements of the Earth Surface - Kanayan (1966)

1.3.3 PASSIVE EARTH PRESSURE THEORIES

The classical earth pressure theory was formulated in 1776 by Coulomb. The principle behind his method consists of considering an earth wedge bounded by the surface, the wall and a straight rupture-line through the foot of the wall. By projecting all forces (acting upon this wedge) onto a line making an angle ϕ with the rupture line, he was able to obtain the critical failure plane, which yielded the minimum value of E_p (see Figure 1.12).

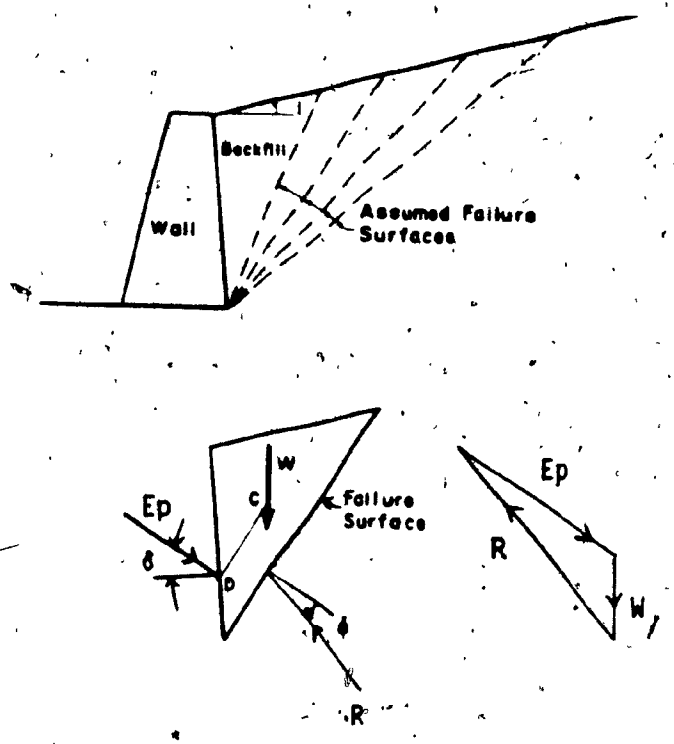

Figure 1.12: Coulomb's Method for a Vertical Wall

In 1857, Rankine approached the earth pressure problem from an entirely different point of view. He considered the case of a semi-infinite cohesionless earth mass with a sloping surface and assumed the whole earth mass to be in a state of failure. Thereupon, he showed that two systems of straight parallel lines, intersecting at angles of $90 \pm \phi$ formed the rupture line (see Figure 1.13). On a smooth retaining wall, Rankine's passive earth pressure is

$$E_p = 1/2\, k_p\, \gamma\, h^2 , \qquad 1.4$$

where: $k_p = \tan^2 (45 + \phi/2)$

γ = Initial unit weight of the soil

h = Height of wall

E_p = Passive force on the retaining wall.

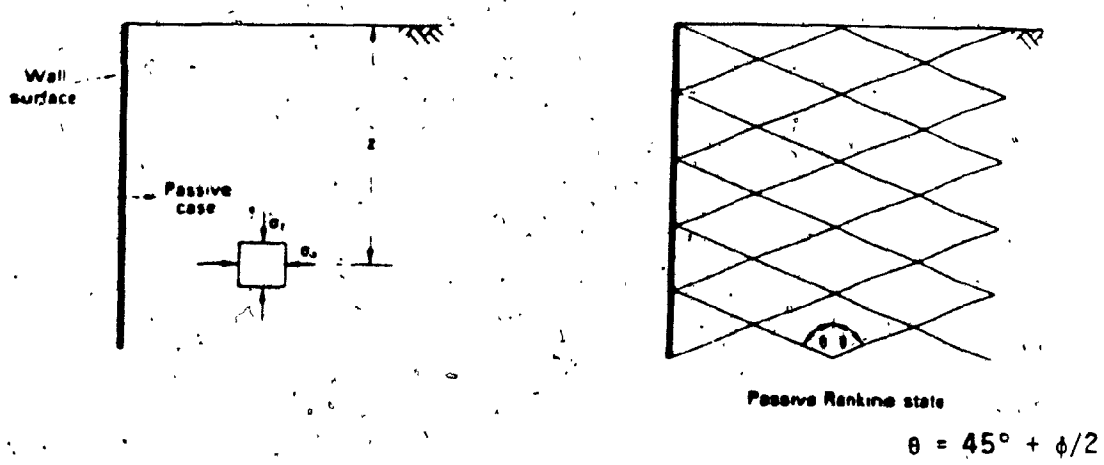

Figure 1.13: Passive Rankine State of Vertical Wall

Terzaghi (1948) adopted an alternate method for predicting the passive earth pressure. A moment equilibrium condition for the soil wedge in front of a slab was studied by taking moments of all forces about the center of the logarithmic spiral. Utilizing a trial and error procedure, the rupture surface giving the minimum passive resistance was obtained (see Figure 1.14).

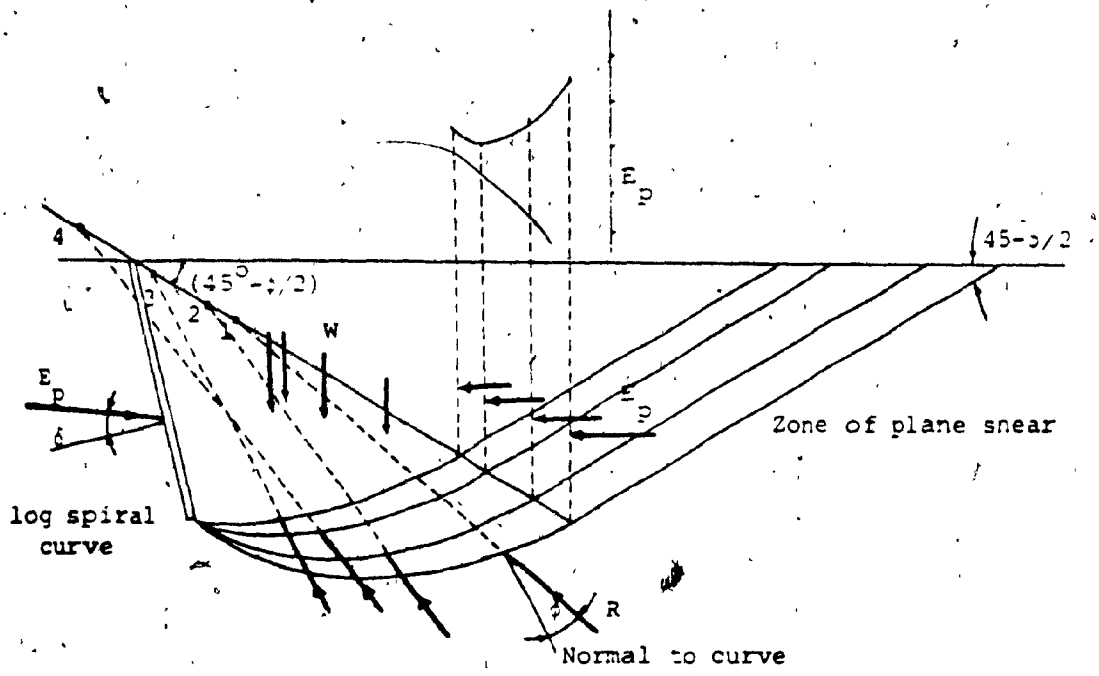

Figure 1.14: Passive Resistance by Logarithmic Spiral (Terzaghi, 1948)

Caquot and Kérizel (1948) derived solutions for the passive pressure acting on the face of a wall. The values were obtained by integrating the differential equations governing the conditions of limiting equilibrium in a soil mass. Such conditions give rise to infinite limiting equilibrium conditions of which only one is valid for a given angle of stress (exerted against the plane). An important aspect of this theory is that the wall friction angle δ depends on the direction of wall movement relative to the soil. In all of the previously-discussed earth pressure theories, the relationship between the direction of wall movement and the change in wall friction angle is rarely discussed.

Via limit analyses, Chen (1975) developed tables for passive pressure results. By using slip line and velocity fields, the coefficients of passive pressure were calculated by equating the rate of work done (by external forces) to the rate of internal energy (dissipated). Assuming that the motion is everywhere continuous on a simply-connected body (in the mathematical sense), the velocity field was defined to be "kinematically admissible". Hence, for kinematically admissible velocity fields, the load computed by equating the dissipated internal energy to the external work done is an upper bound of the true collapse load.

1.4 CRITIQUE

It is interesting to note that in the previously-mentioned passive pressure theories, there is no difference between slip lines and failure planes. If the normality condition is obeyed (the plastic limit theorem holds), then the directions of the stress and velocity characteristics will coincide. Poorooshasb et al (1967) demonstrated that velocity and stress characteristics have, nevertheless, different directions. In spite of this, the plastic limit theorem shall still be utilized for comparative purposes in this thesis. Therefore, the slip lines (observed in the model test) represent a velocity characteristic. The direction of the resultant tractions (along a velocity characteristic) form an angle ϕ with the normal to the velocity characteristic, just as they would along a stress characteristic.

Furthermore, it should be noted that the concept of progressive failure has also been neglected in such theories. Hanna (1978) discussed shear failure in the soil under a footing in terms of progressive rupture at variable stress levels. These results indicated a decrease of the δ values. Consequently, a variation of the locally-mobilized angle of shearing resistance was assumed. This hypothesis was acceptable and represented reality because the proposed parabola was the difference between the assumed and real failure planes, which in turn had a direct effect upon the δ values. This method shall also be used in the limit equilibrium analyses of the problem considered herein.

CHAPTER 2

EXPERIMENTAL INVESTIGATION

INTRODUCTION

Model tests were carried out with a continuous aluminum plate in a homogeneous medium of sand. The purposes of these tests were:

(i) to verify the accuracy of the proposed theory for predicting the holding capacity of inclined anchor plates.

(ii) to gain more knowledge in the characterization of anchor plate behavior.

(iii) to study, experimentally, the pressure distribution developed on the plate surface.

(iv) to study plate movement.

2.1 GENERAL DESCRIPTION

The experimental set-up comprises a Plexiglas test tank. The inside dimensions of the tank are 6 inches wide, 48 inches long and 40 inches high (see Figures 2.1-a to 2.1-d). The rainfall method

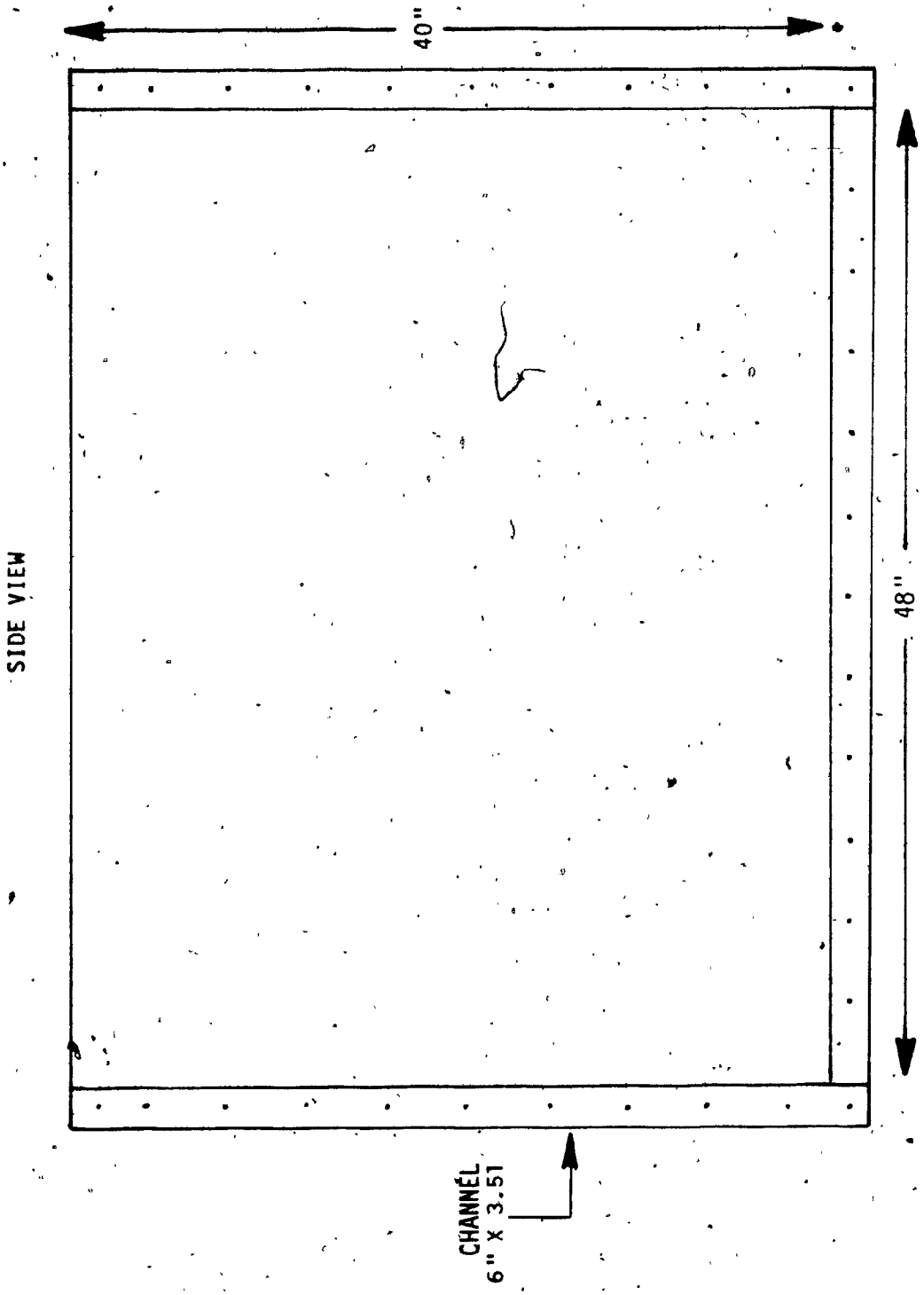

Figure 2.1-a: Plexiglass Tank

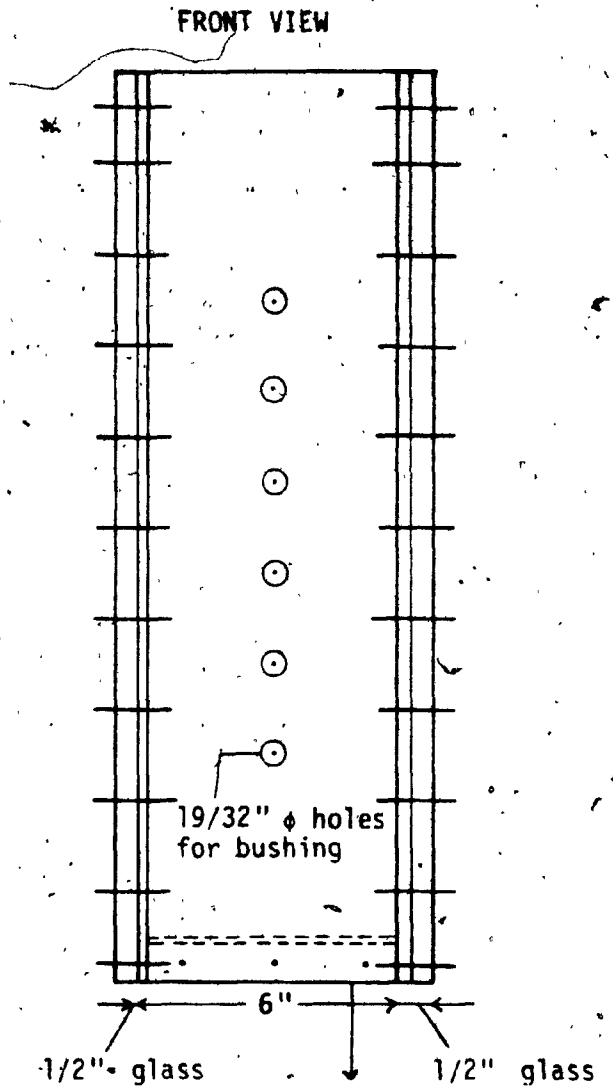

Figure 2.1-b: Plexiglass Tank

DETAIL (A)

FRONT VIEW

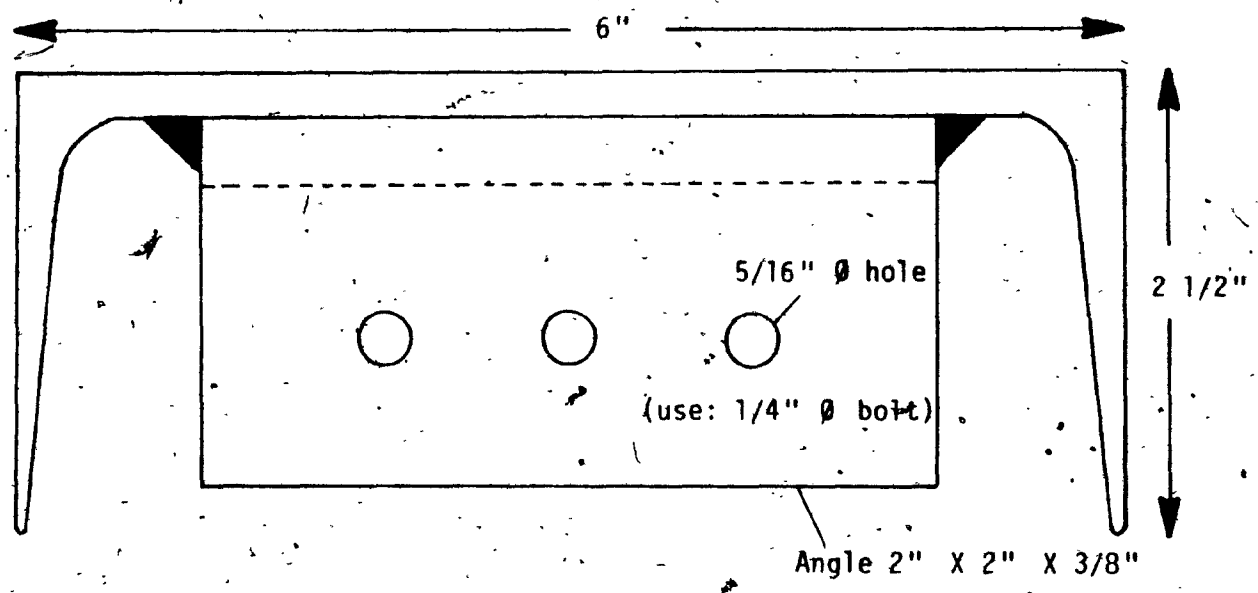

Figure 2.1-c

DETAIL (A)

SIDE VIEW

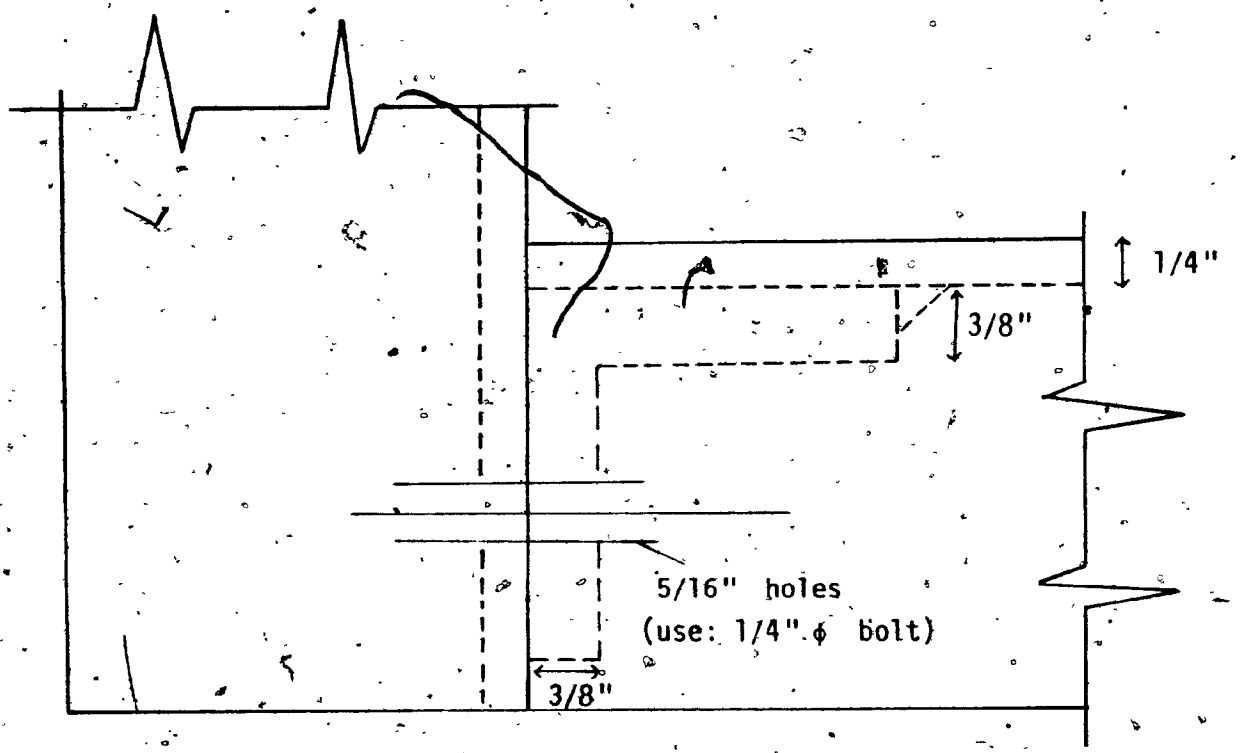

Figure 2.1-d

was used to place sand in the tank. The sand was deposited in a box lying on a frame at a fixed height above the tank. Once an arborite plate was pulled through a slot at one end of the box, the sand filtered through a metallic mesh.

The test anchor was placed at a constant height and at various angles of inclination. It was pulled by a motor at a constant displacement rate. The design allows maximum axial loads of up to 500 pounds. After the completion of one test series, the tank was emptied by a vacuum suction pump.

2.2 TESTING FACILITIES

The loading frame and the loading equipment made up the main facility used in this experimental set-up (see Figure 2.2).

2.2.1 LOADING FRAME

The frame was designed for uplift loads of up to 500 pounds. The major consideration was deflection as it could influence the experimental results. A detailed description of the frame is given in Figures 2.3-a to 2.3-c and in Table 2.1.

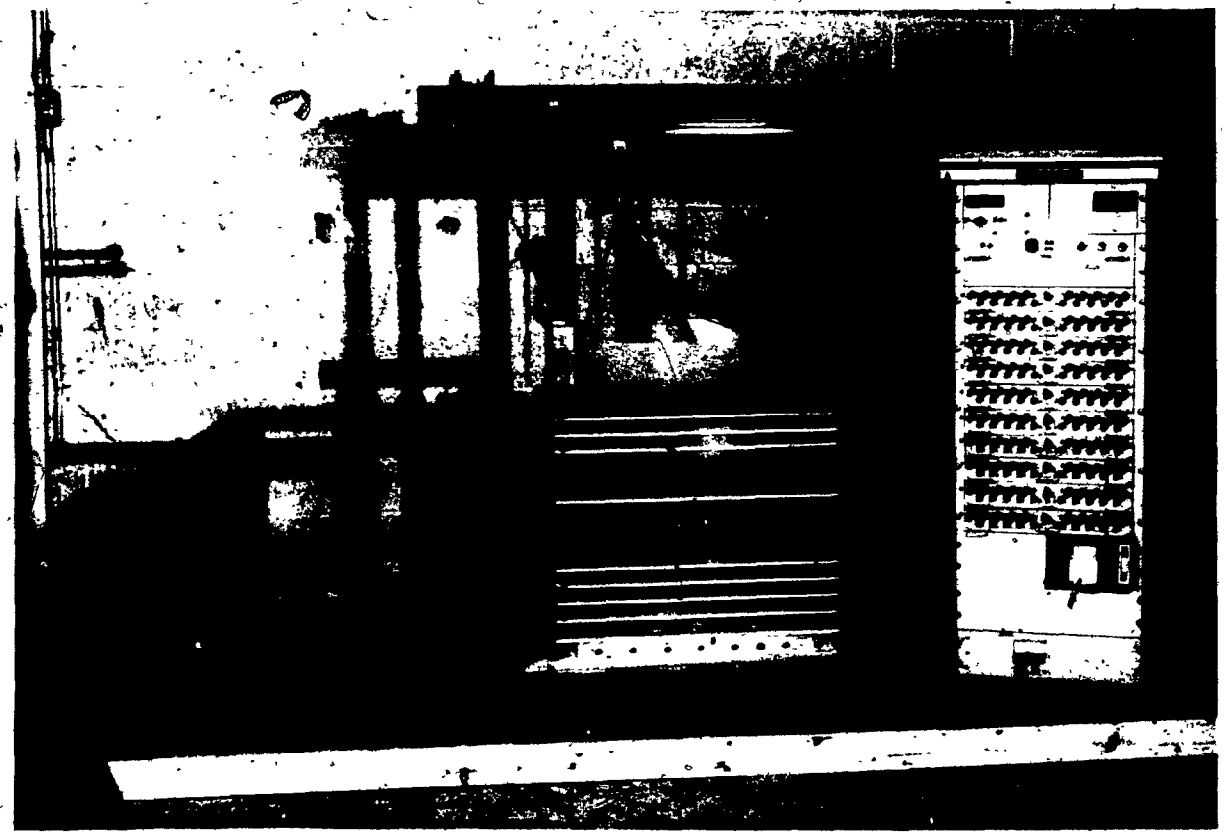

Figure 2.2: Loading Frame and Loading Equipment

STRUCTURAL MEMBER TYPE	MATERIAL	LENGTH	QUANTITY	REFERENCE FOR DETAILS
Steel Channel 4" X 5.40	Mild Steel	68"	2	A
Steel Tubing 2" X 2" X 1/8"	Mild Steel	63"	4	B
Steel Tubing 2" X 2" X 1/8"	Mild Steel	48"	2	C
Steel Tubing 2" X 2" X 1/8"	Mild Steel	104"	2	D
Steel Tubing 2" X 2" X 1/8"	Mild Steel	12"	4	E
Steel Channel 4" X 5.40	Mild Steel	36"	2	F
Steel Angle 2" X 2" x 1/4"	Mild Steel	16"	2	G
Steel Channel 4" X 5.40	Mild Steel	8"	2	H
Steel Channel 3" X 5"	Mild Steel	8"	2	I
Steel Angle 2" X 2" X 1/4"	Mild Steel	13 1/2"	2	J
Steel Plate 20" X 13 1/2" X 1/2"	Mild Steel	13 1/2"	1	K
Steel Plate 11 1/4" X 6" X 1/4"	Mild Steel	11 1/4"	1	L

Table 2.1: Structural Members

SIDE VIEW

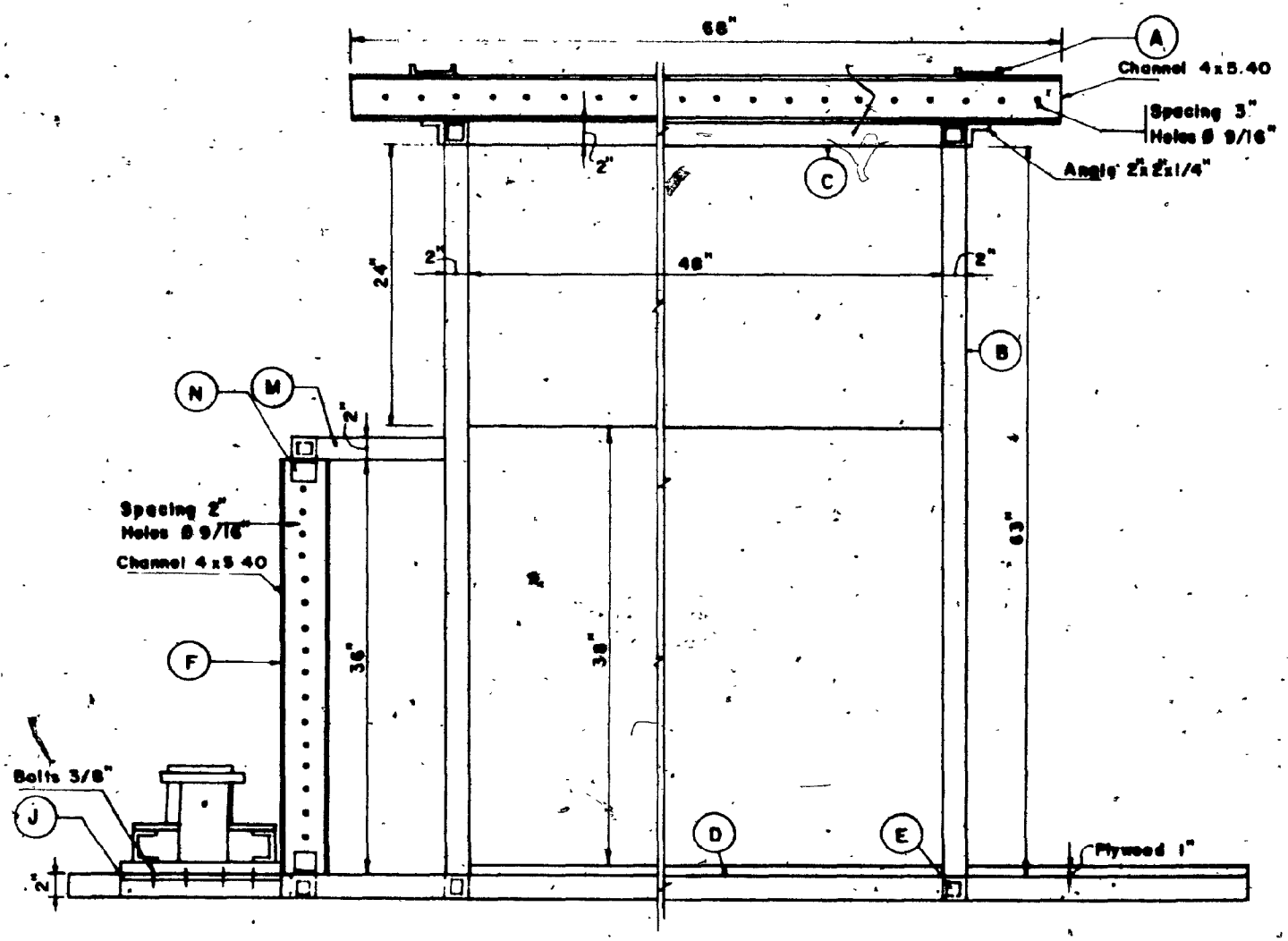

Figure 2.3-a : Experimental Loading Frame

FRONT VIEW

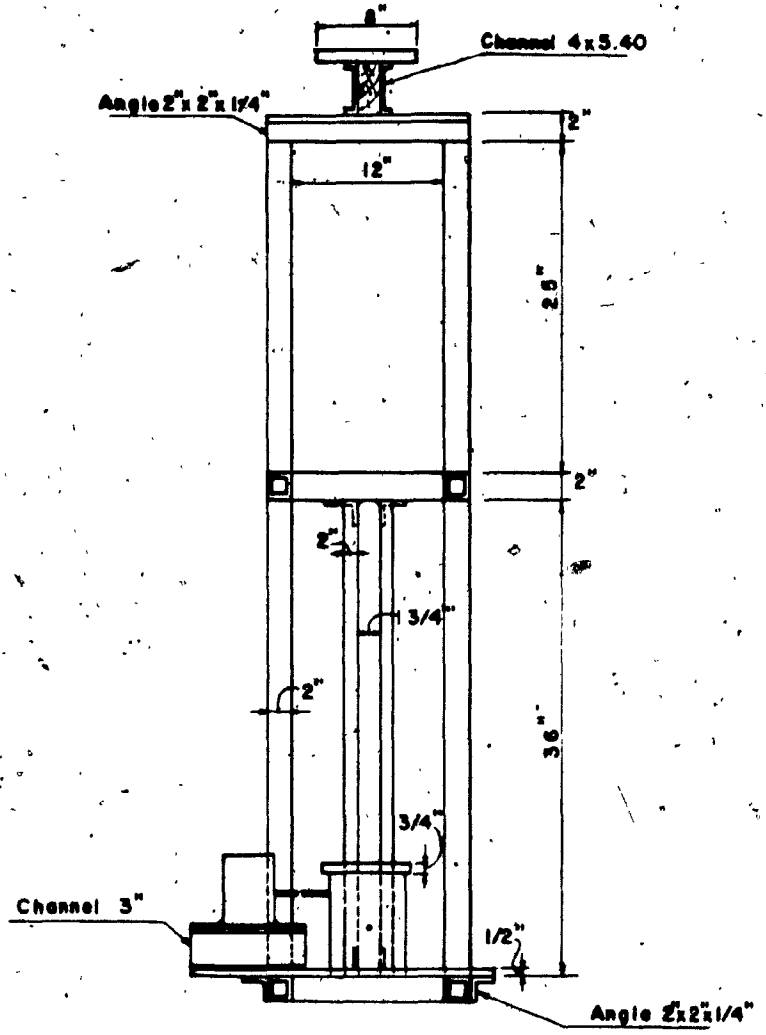

Figure 2.3-b: Experimental Loading Frame.

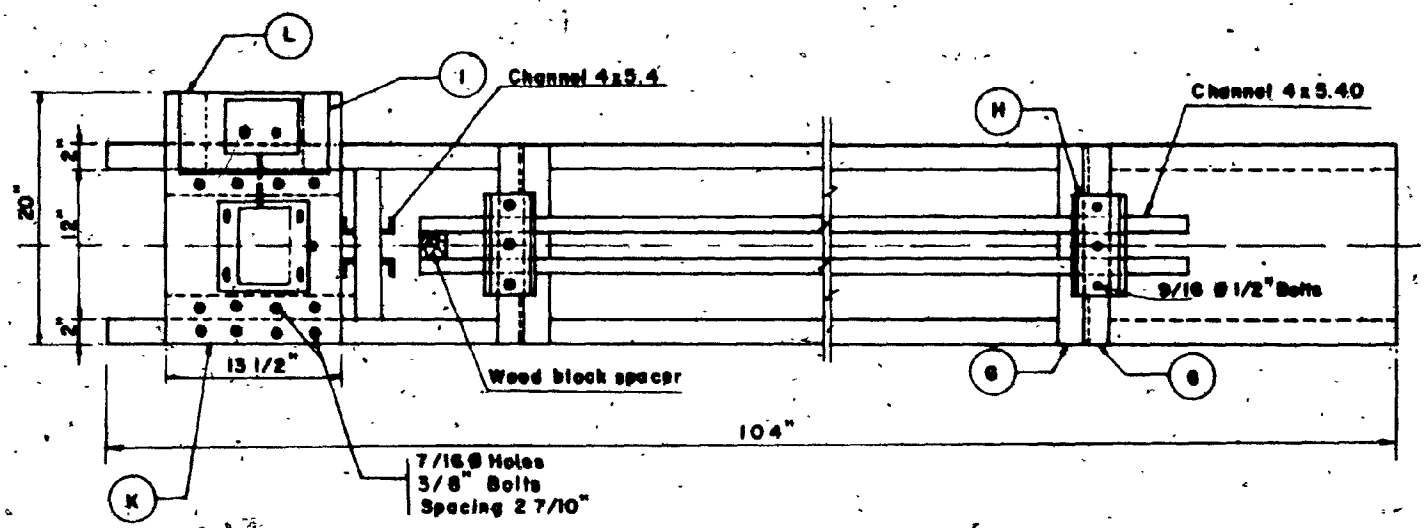

Figure 2.3-c: Experimental Loading Frame

2.2.2 LOADING EQUIPMENT

The loading equipment includes a motorized screw jack with a three-foot maximum travel mounted on a steel plate bolted onto the steel tubing of frame. The combination of a gear shift, a gear reducer and an electronic speed-controlled device provide the screw jack with a loading and unloading speed varying from 0.01" to 1.0" per minute (see Figures 2.3-d, 2.3-e and 2.4-a to 2.4-d).

2.2.3 MODEL ANCHOR

The model anchor used in this investigation is a square aluminum plate 6" X 6" . Pressure transducers were placed in circular openings cut out of the plate. The plate was covered with sand paper to ensure that the surface characteristics of the plate remain consistant during testing. A one-inch outer diameter, steel, hollow rod was rigidly fastened to the center of the plate. The rod served two main functions: (a) pull of the anchor plate and, (b) enclosure of the wiring (see figures 2.5-a to 2.5-l).

2.3 SOIL PROPERTIES

A detailed study of the physical properties of the sand used in all model tests was given by Afram (1984). A brief description of some aspects of these properties will be given here.

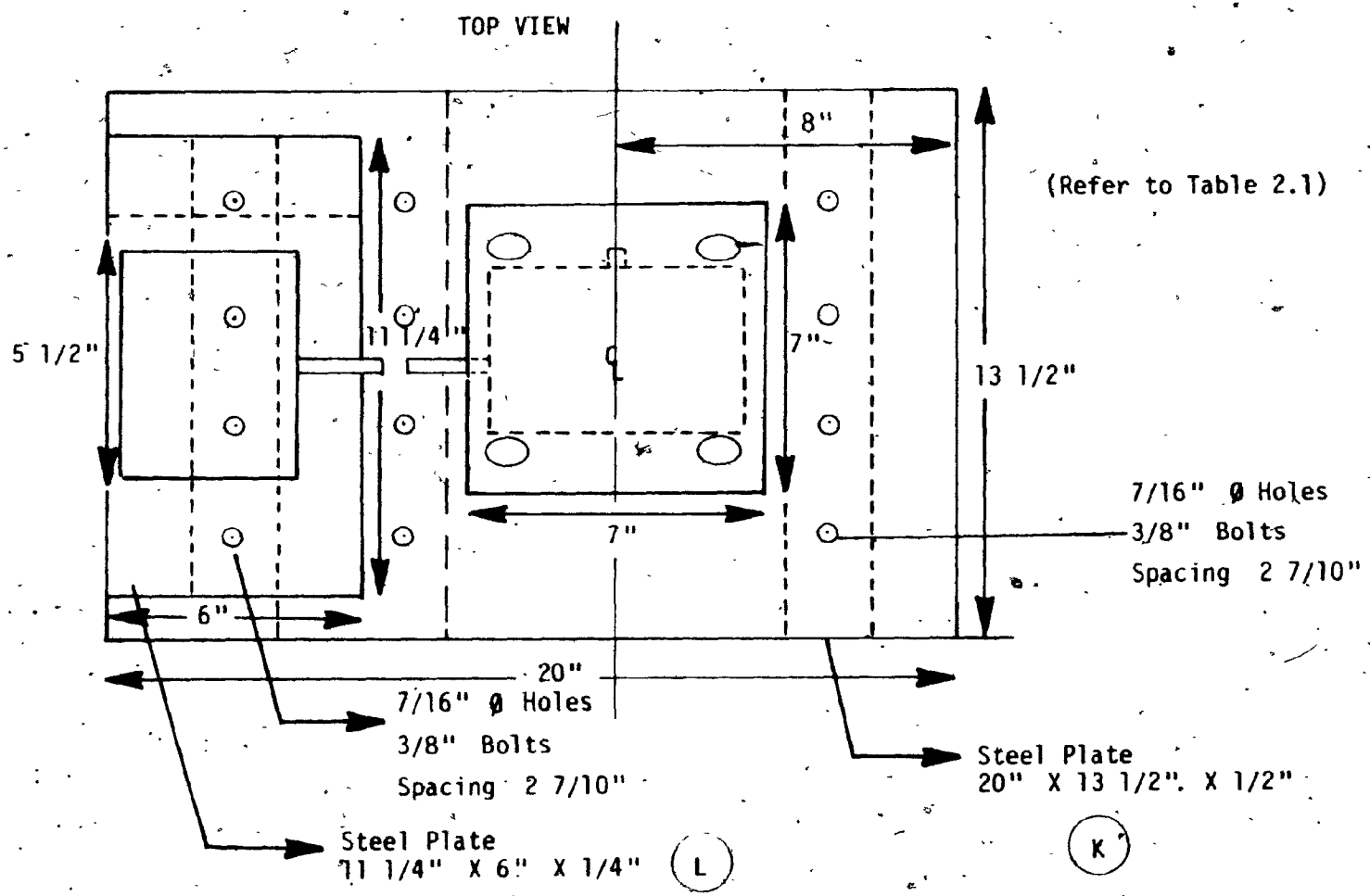

Figure 2.3-d : Loading Equipment

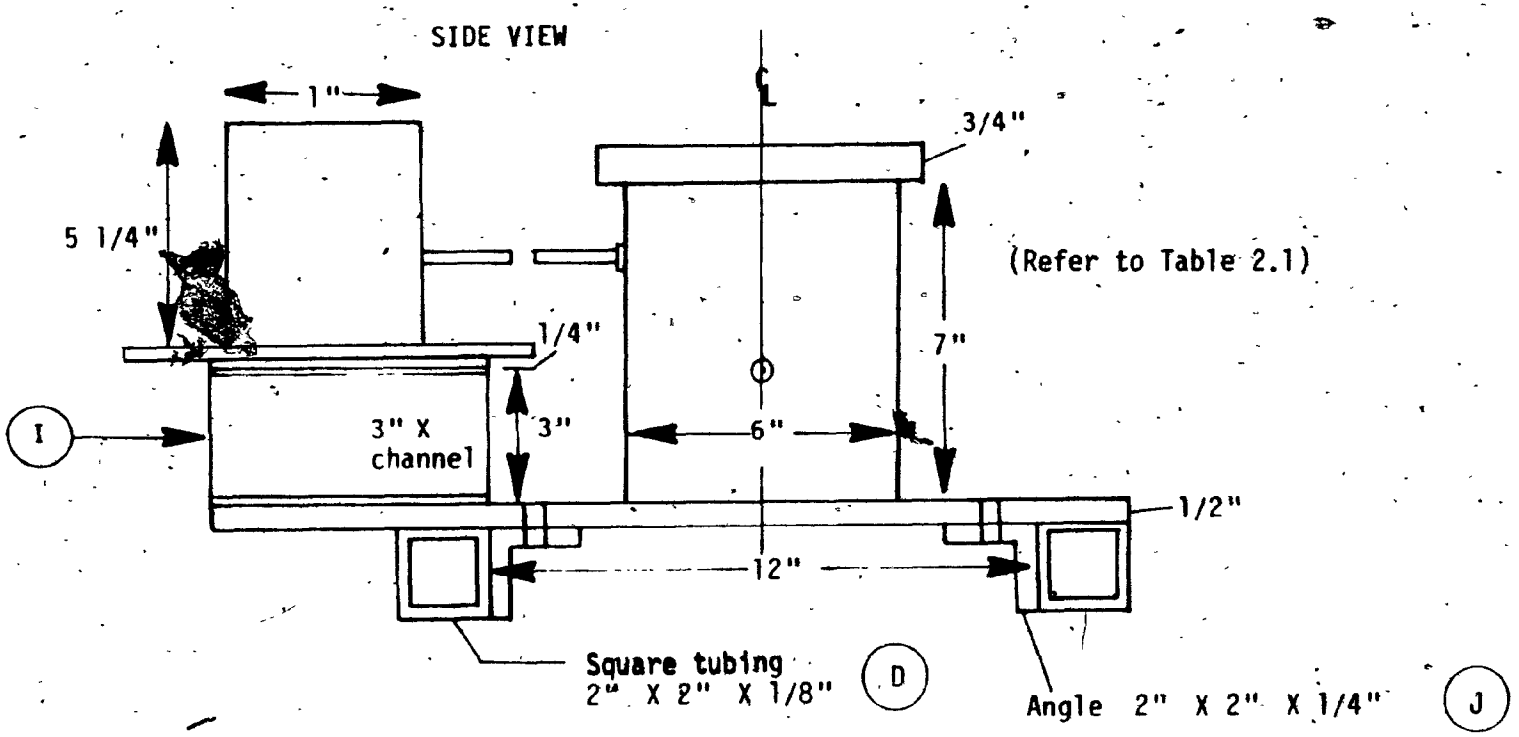

Figure 2.3-e : Loading Equipment

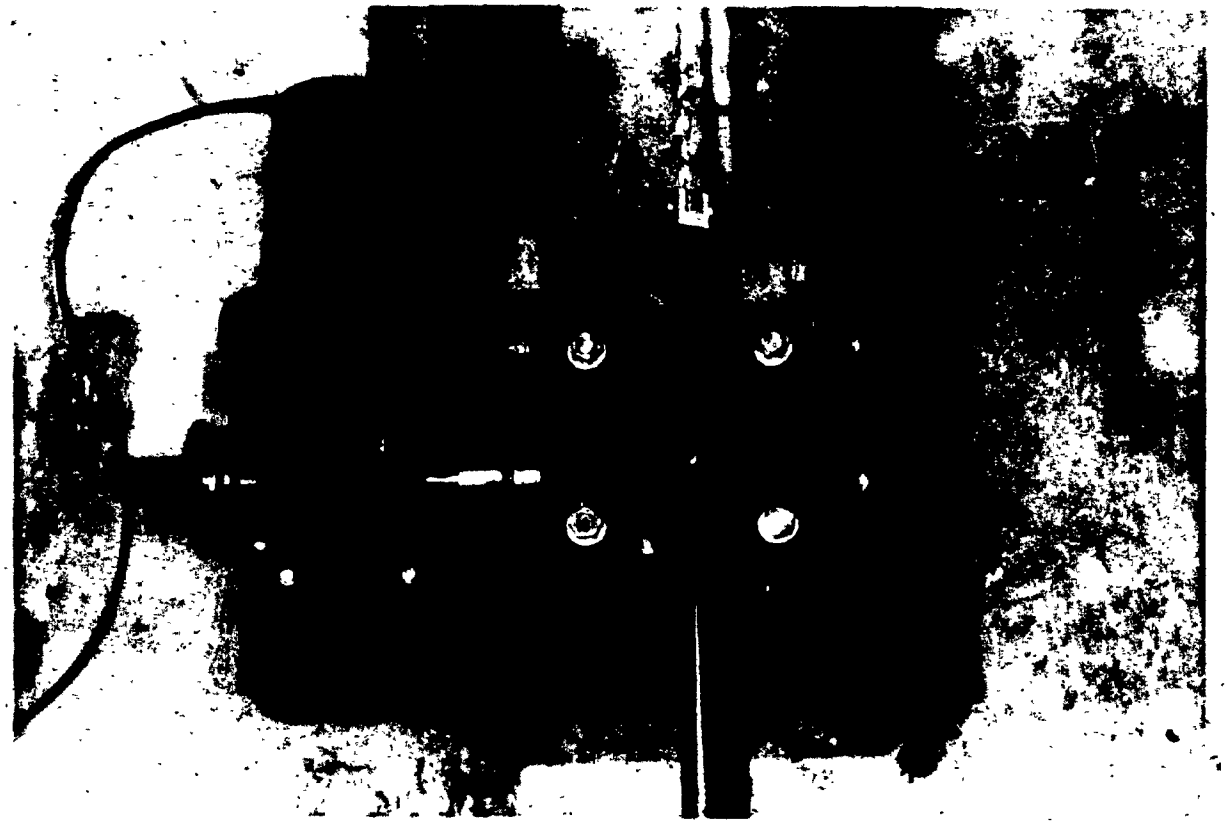

Figure 2.4-a: Loading Equipment

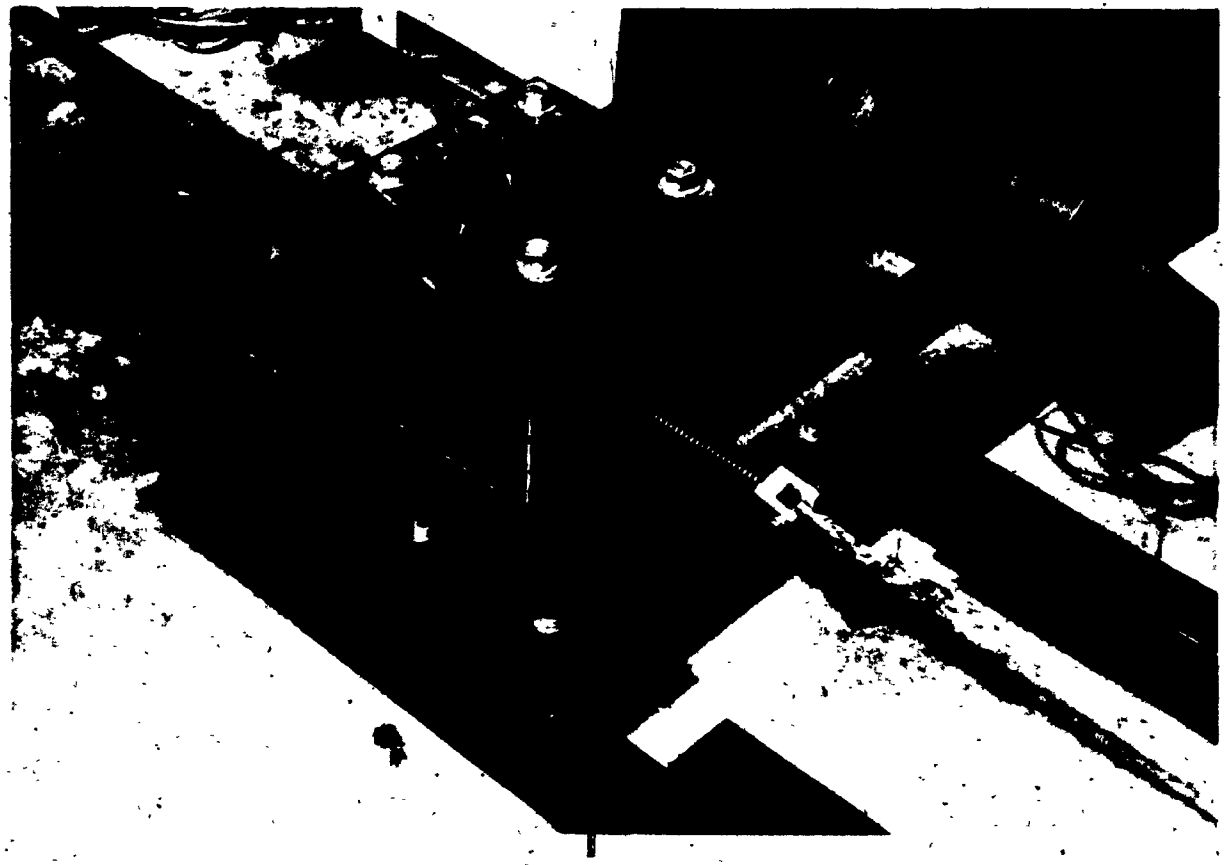

Figure 2.4-b: Loading Equipment

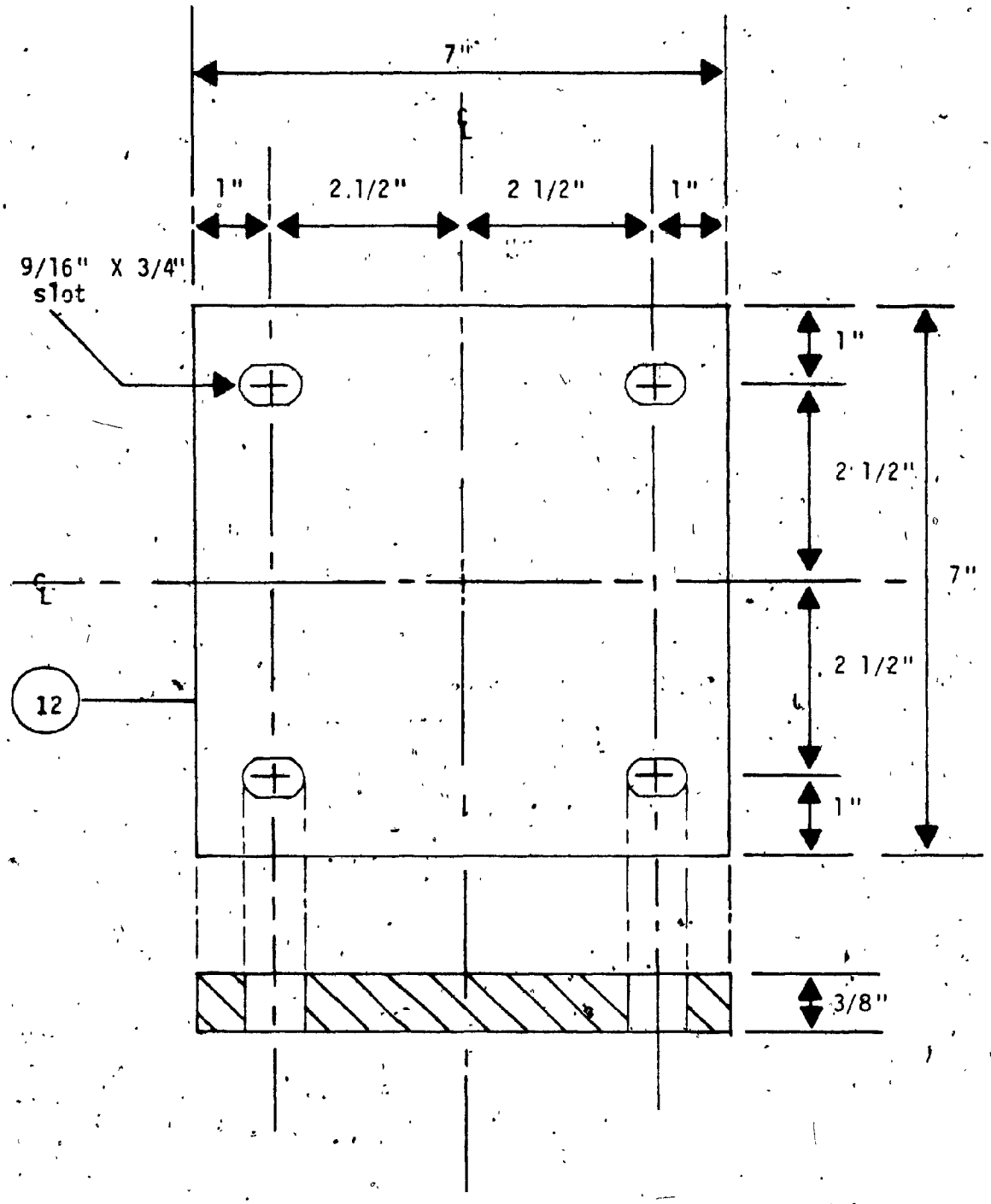

Figure 2.4-c: Top Plate for Screw Jack

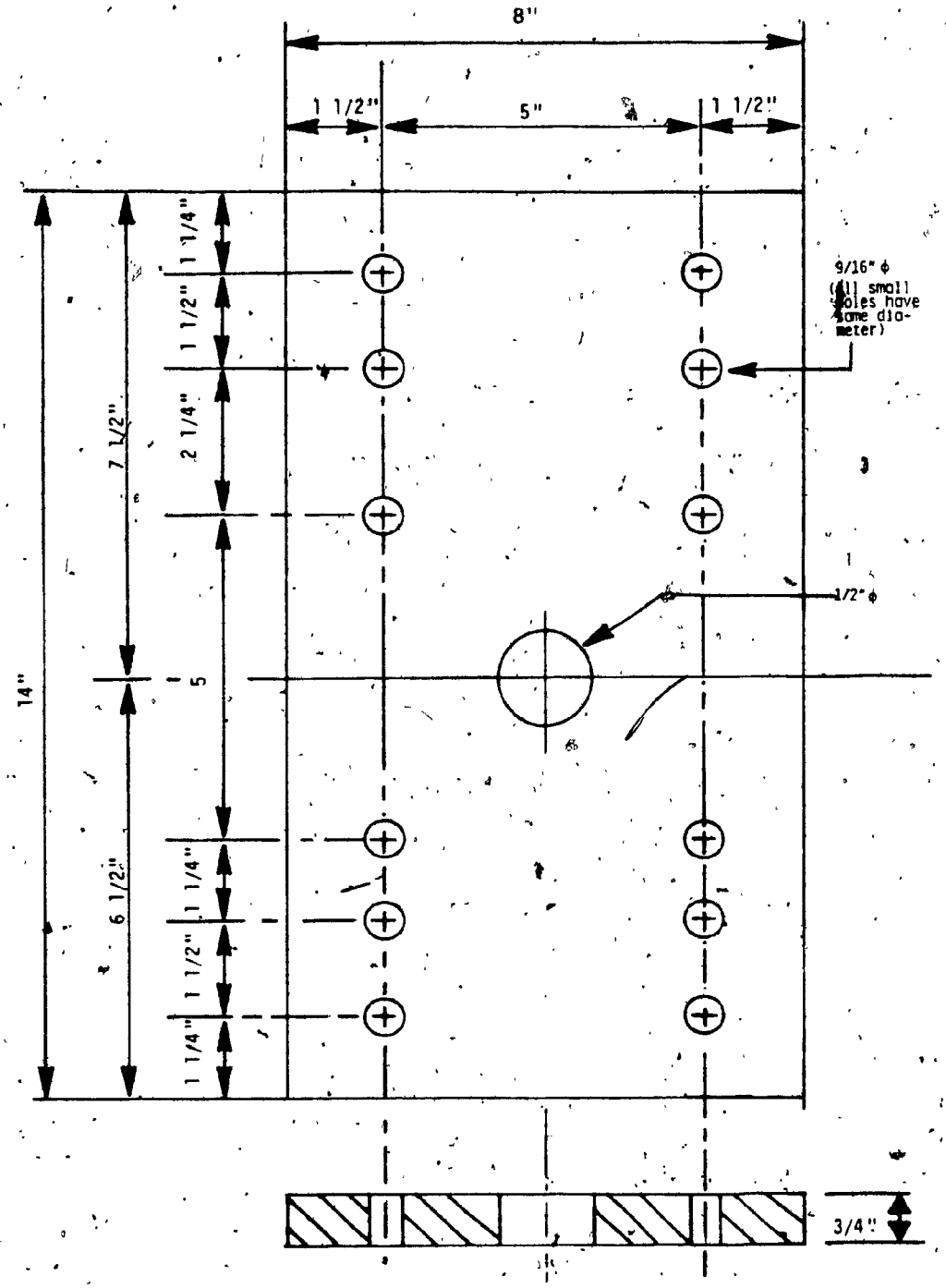

Figure 2.4-d: Base Plate for Screw Jack

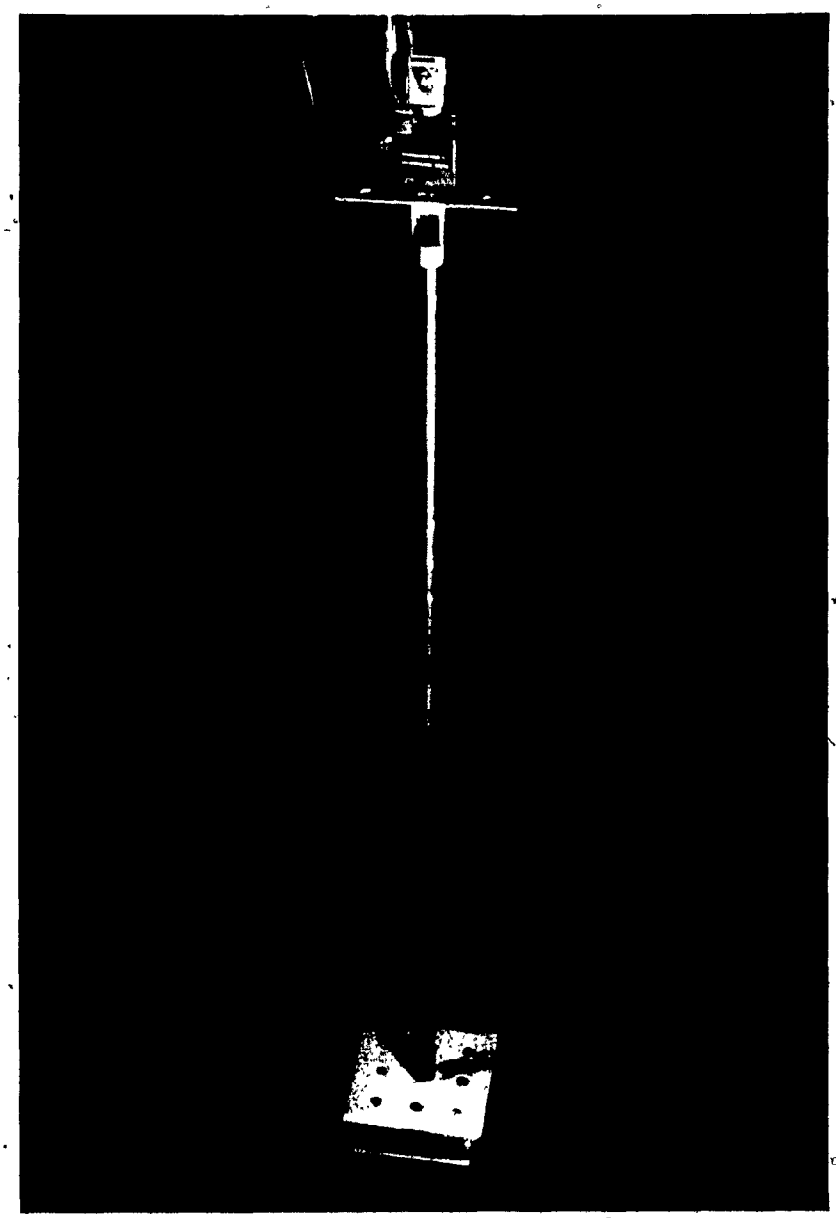

Figure 2.5-a: Model Anchor

INSIDE VIEW

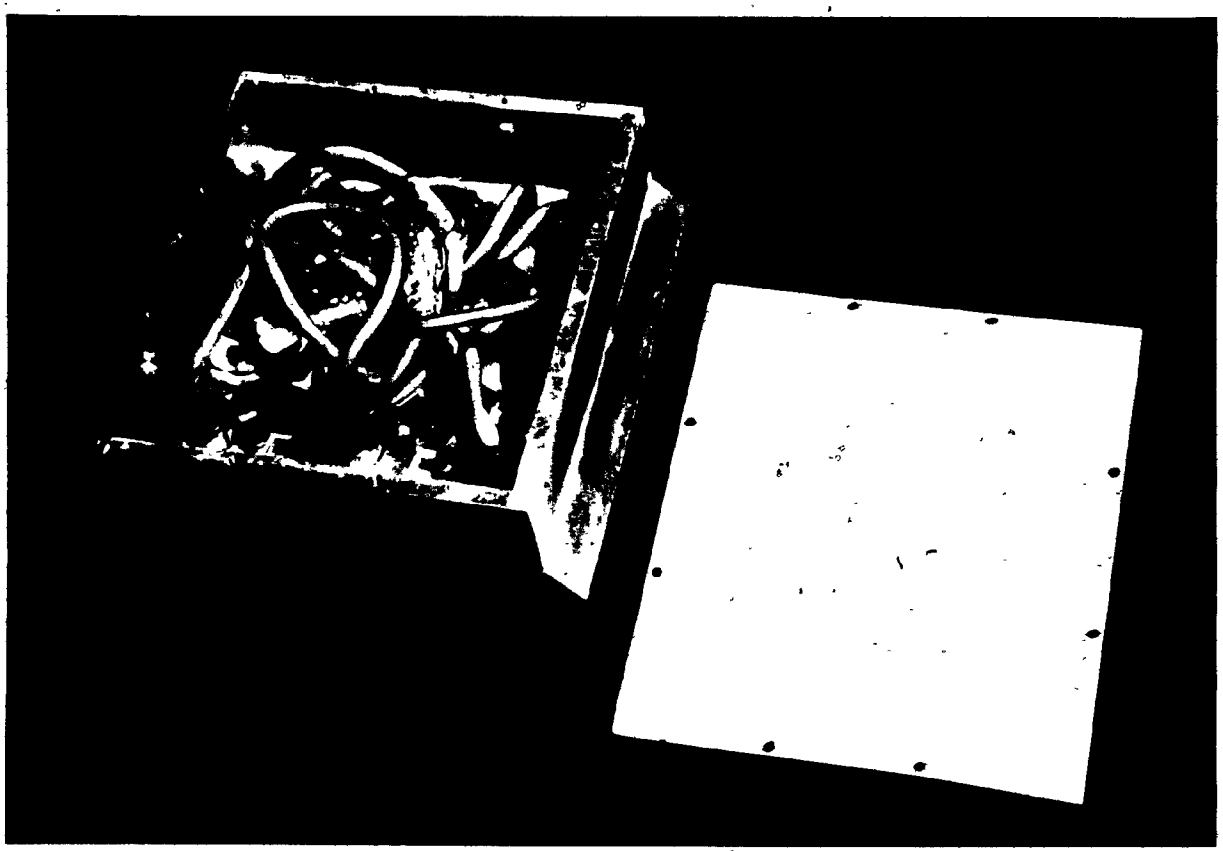

Figure 2.5-b: Model Anchor

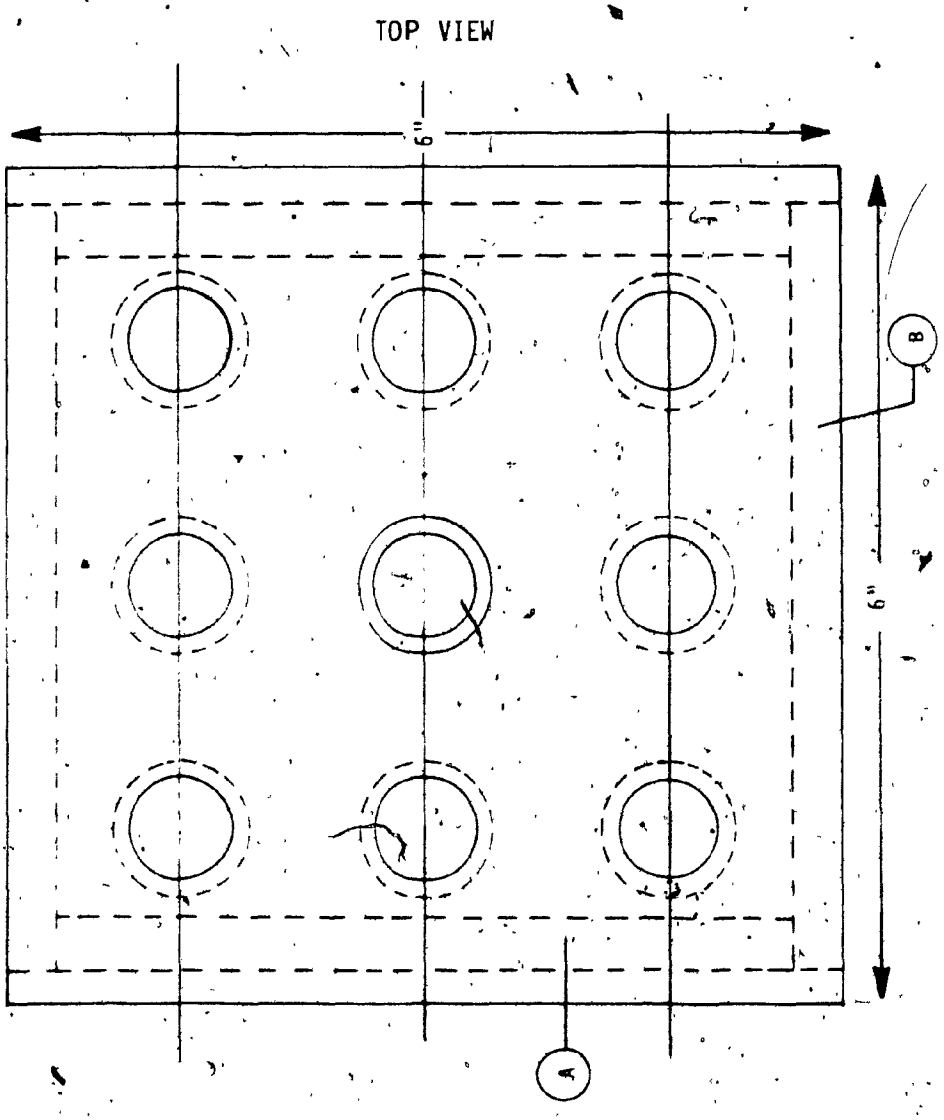

Figure 2.5-c: Model Anchor Plate

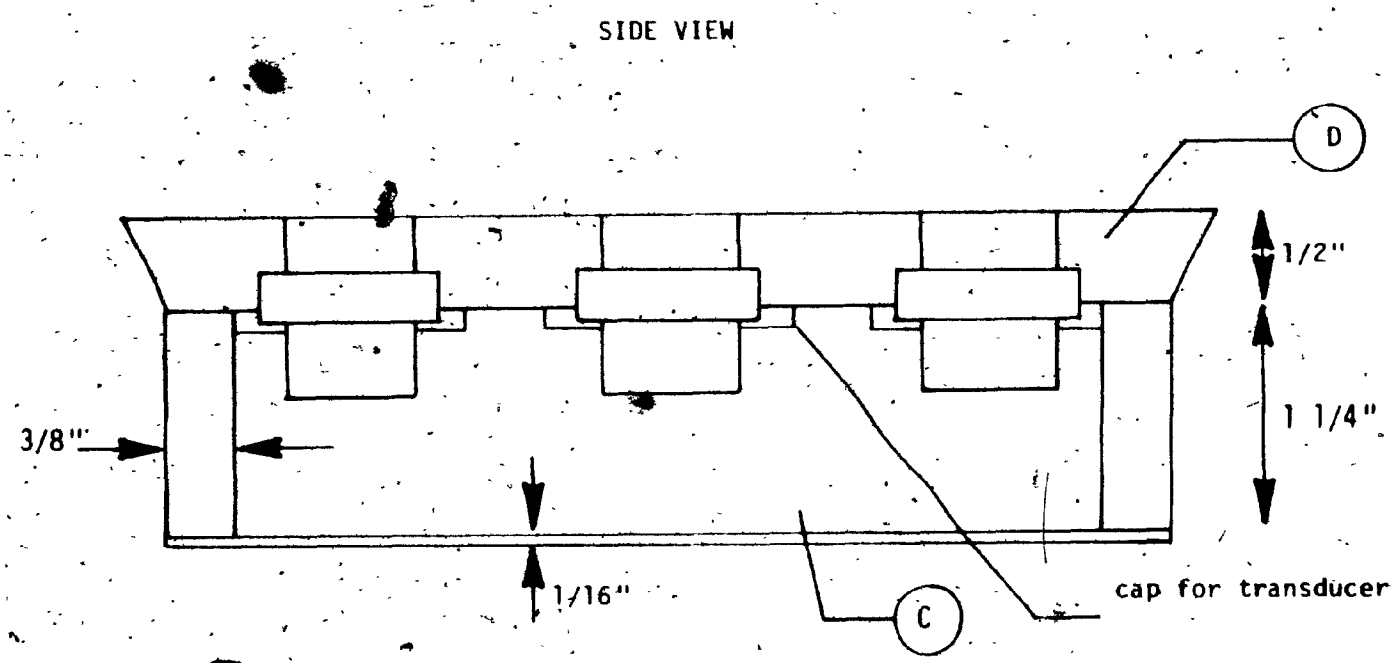

Figure 2.5-d: Model Anchor Plate

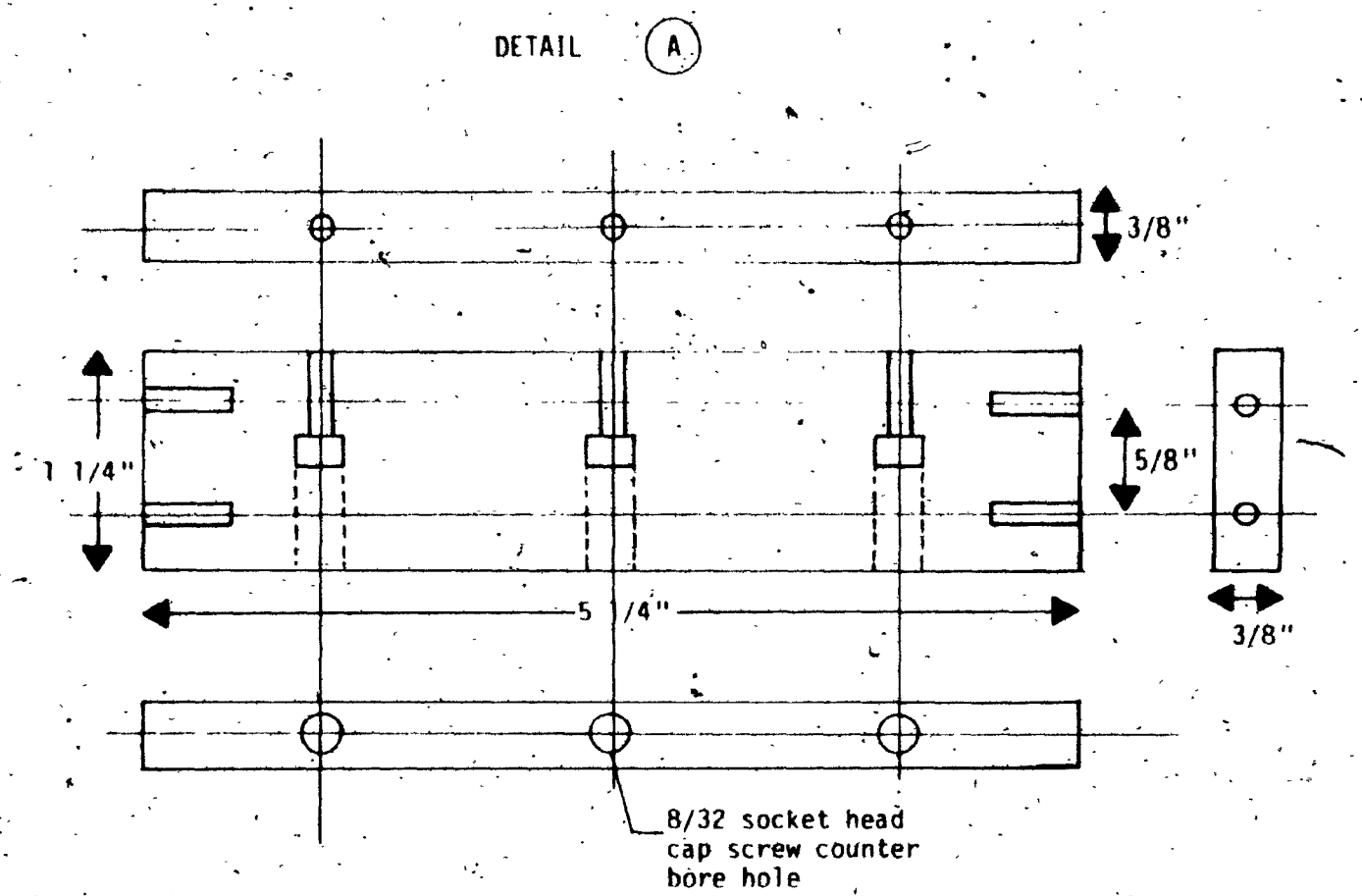

Figure 2.5-e: Edge of Anchor Plate

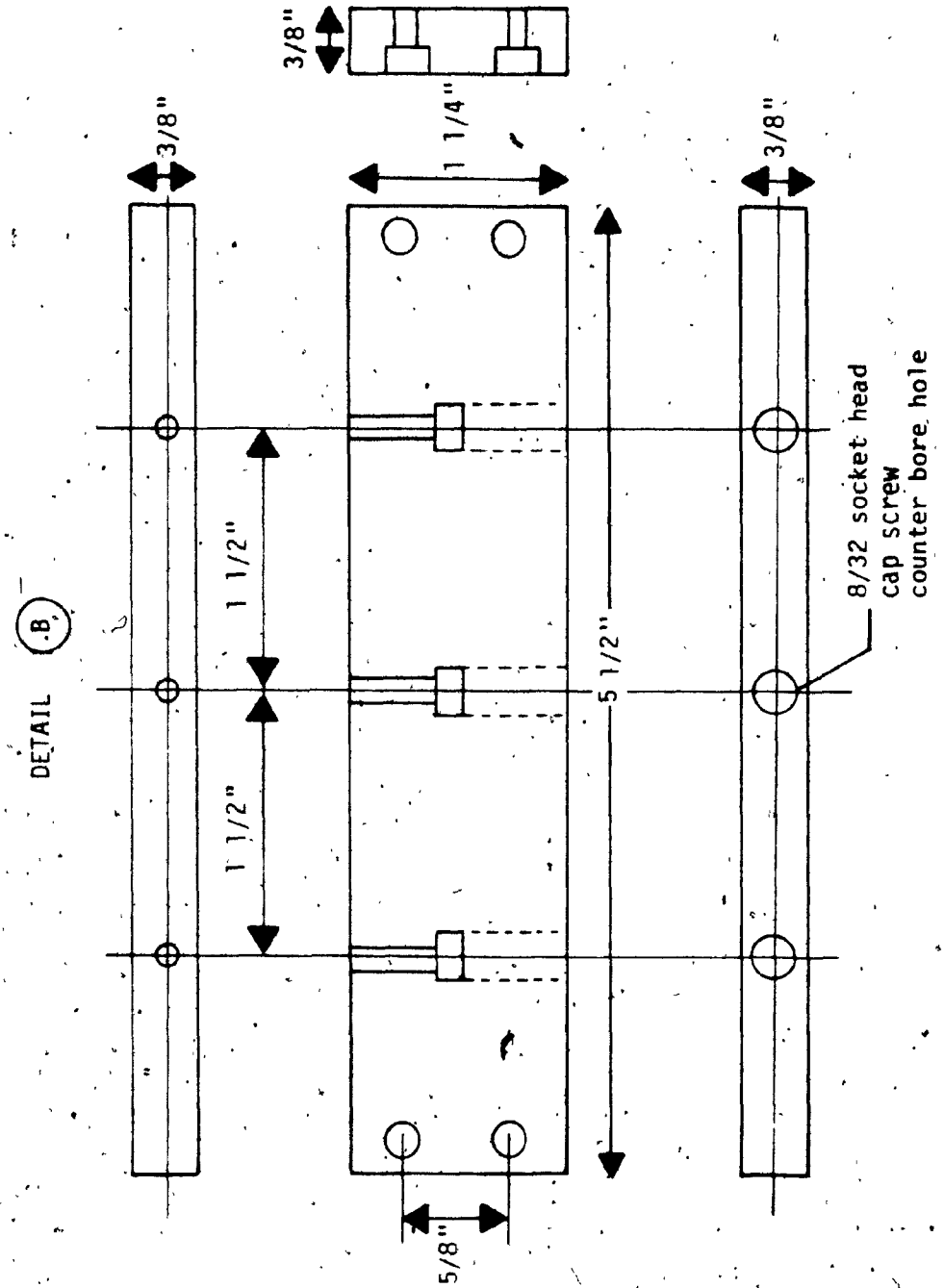

Figure 2.5-f: Edge of Anchor Plate

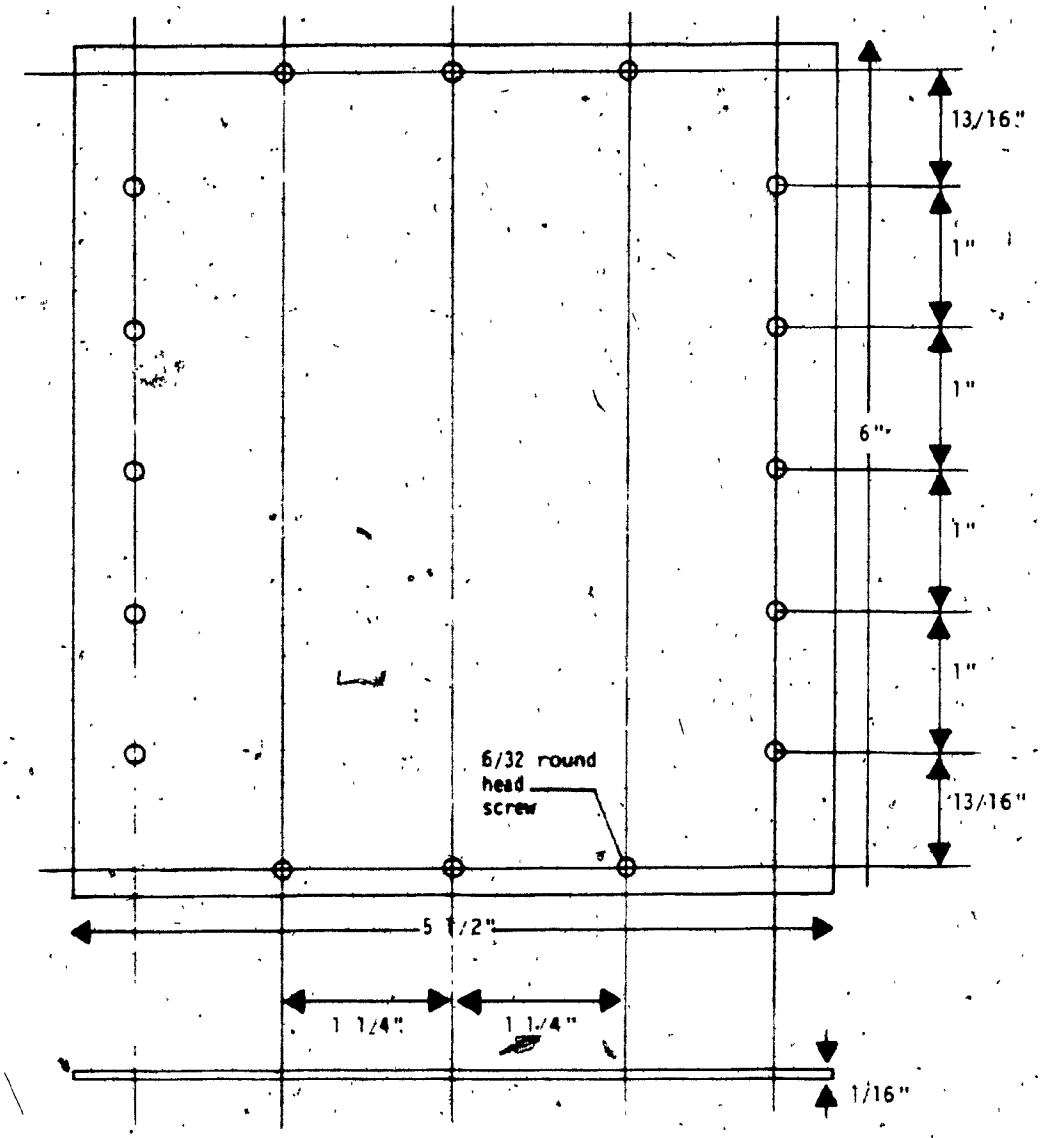

Figure 2.5-g: Back Cover of Plate

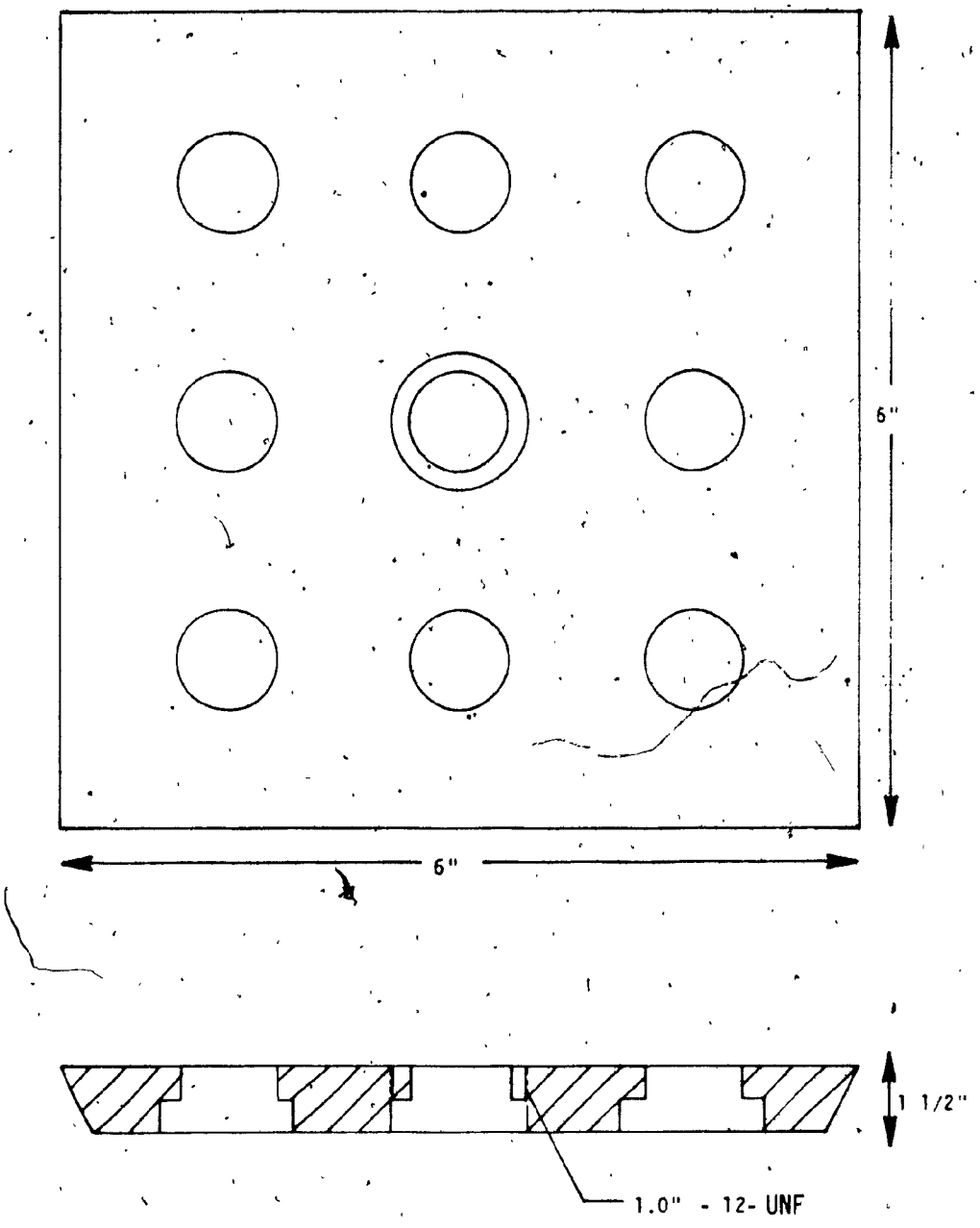

Figure 2.5-h: Plate Frontal Surface

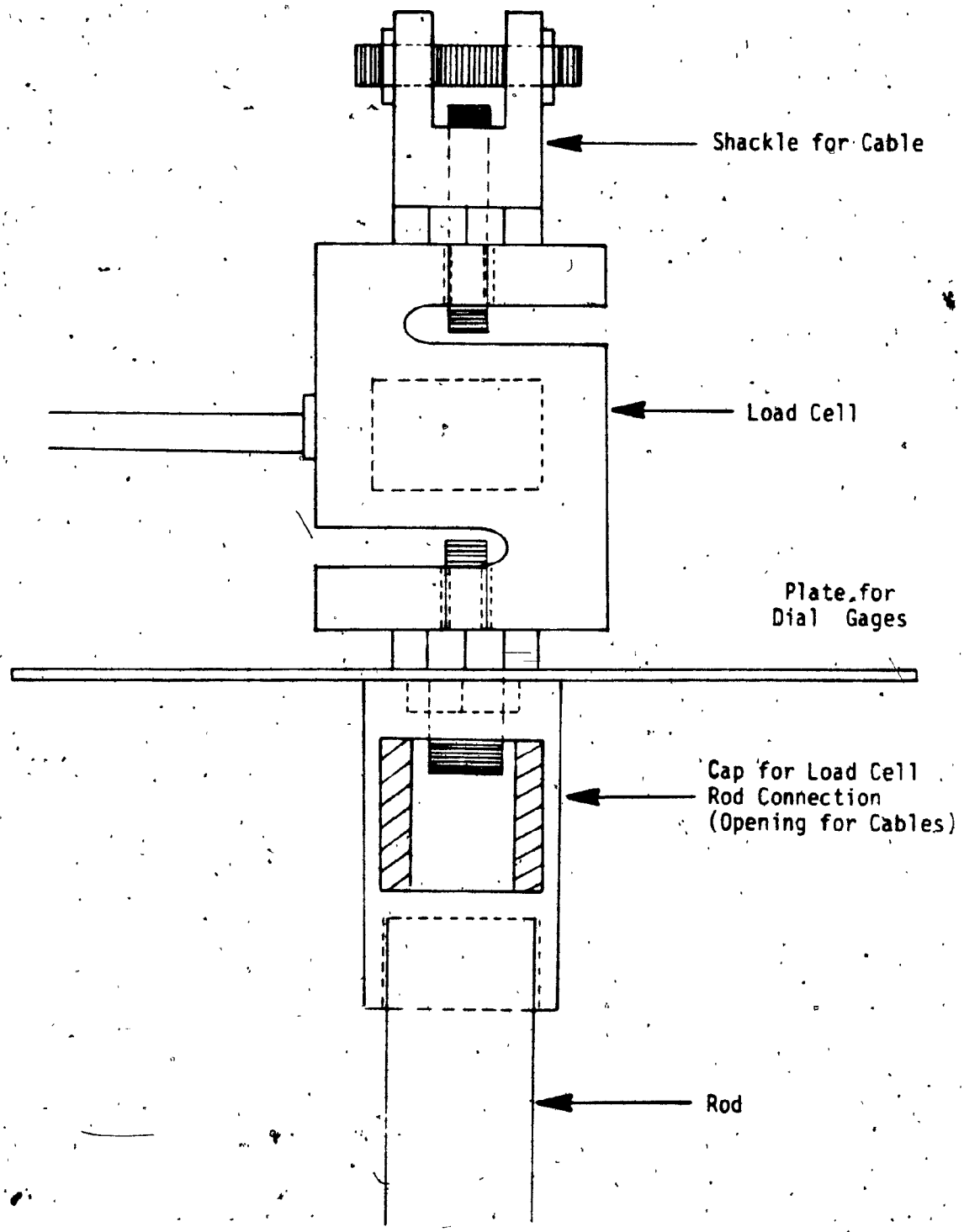

Figure 2.5-i: Cable Load Cell Rod Connection

PKG. SIZE	CAP. LBS. (Kg or TON)	A	B	C	D MAX	E	F TH'D
2	500 (226.8)	2.50 (63.50)	2.00 (50.80)	0.75 (19.05)	1.00 (25.40)	1.25 (31.75)	1/2-20 UNF-2B

MECHANICAL RATINGS		
STD. CAP. LBS. (Kg or TON)	DEFLECTION (In. or MM)	WT. LBS. (kg)
500 (226.8)	.015 (.38)	1 (.5)

Table 2.2: Load Cell Details

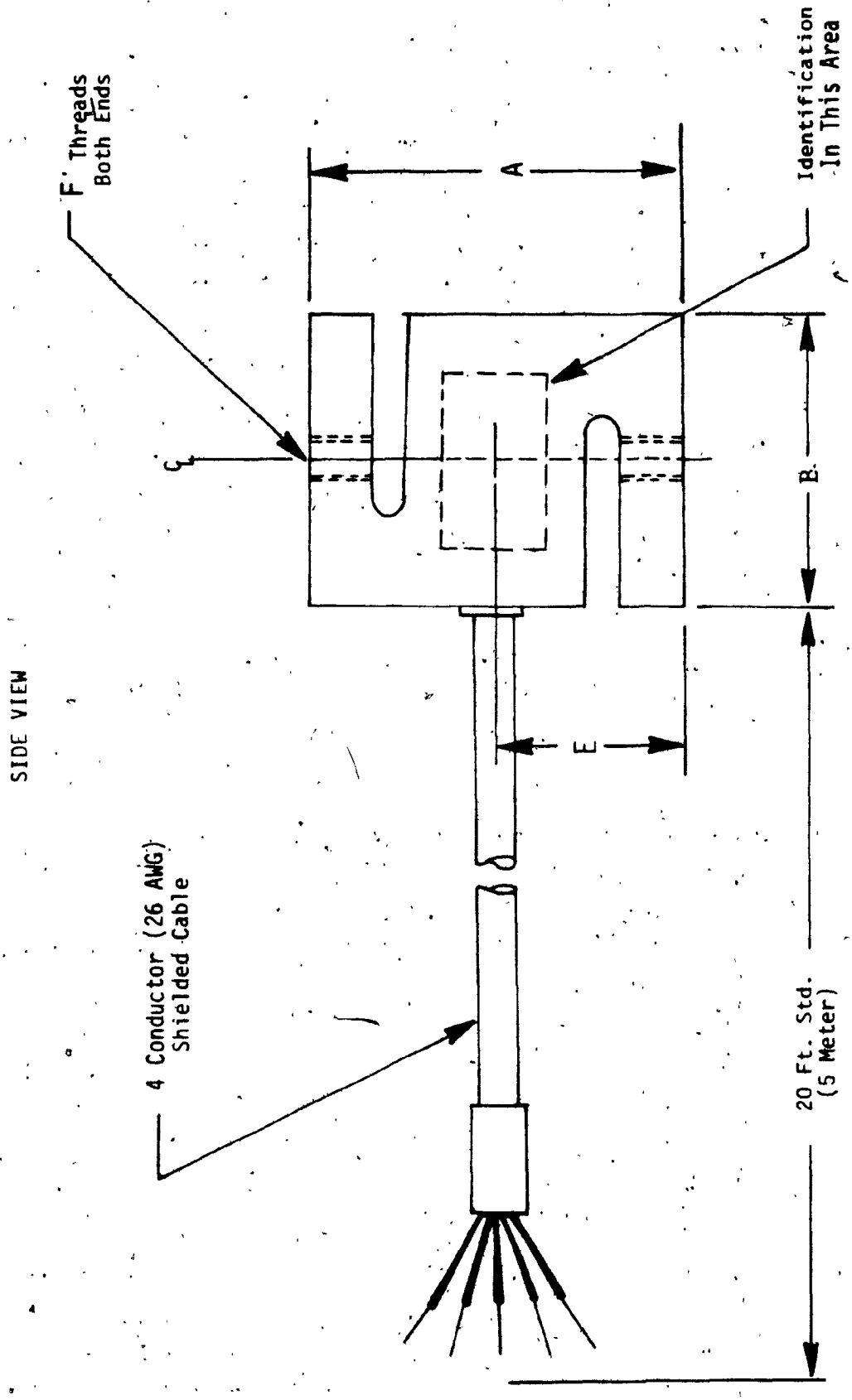

Figure 2.5-j: Load Cell

FRONT VIEW

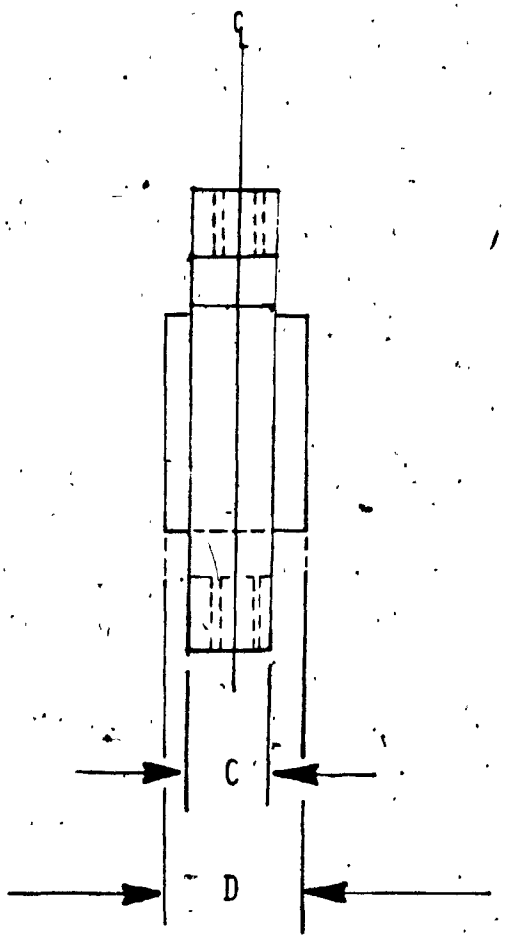

Figure 2.5-k: Load Cell

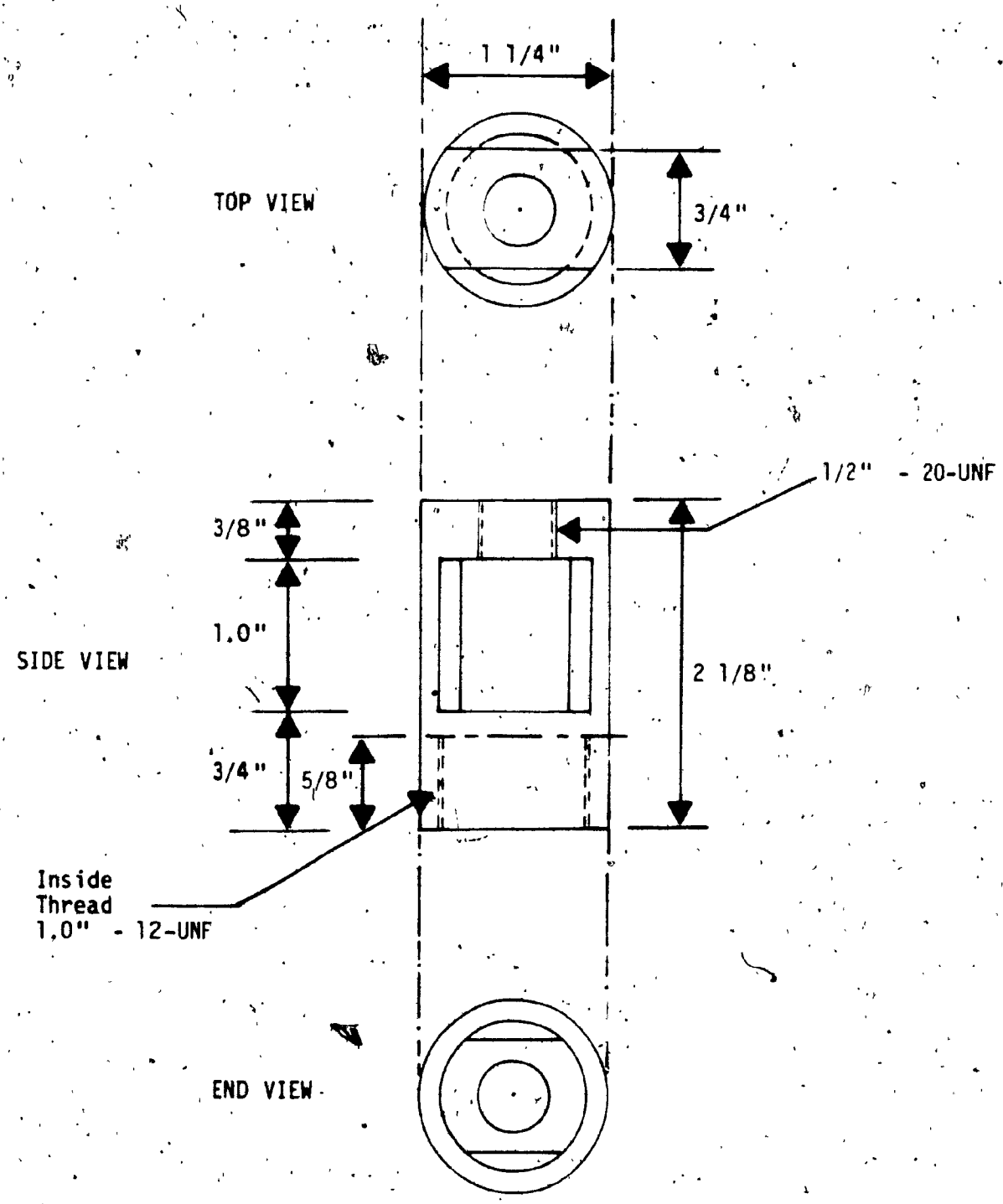

Figure 2.5-1: Rod Load Cell Connection

The sand used in this study is called «morie sand» and is imported from the United States.

An investigation on the grain-size distribution indicated medium sand with a uniformity coefficient of 1.45. The effect of this uniformity is reflected in the measured minimum and maximum densities of 91.5 percent and 104.5 percent respectively.

Test results showing the variation of the angle of friction with relative density is shown in Figure 2.6.

2.4 DETERMINATION OF UNIT WEIGHT

An excellent way of obtaining the density at any location in the test pit is by using density pots (see Figure 2.7). Fifteen pots of known weights and volumes were placed on a levelled surface of sand. After each test, the pots were carefully removed and the excess sand was scraped off. Each pot was then weighed and the density calculated (see Tables 2.3 to 2.5).

2.5 RELATIVE DENSITY CALCULATION

Using the equations:

$$e = \frac{G\gamma_w}{\gamma} - 1 \qquad \text{and} \qquad R.D. = \frac{e_{max} - e}{e_{max} - e_{min}}$$

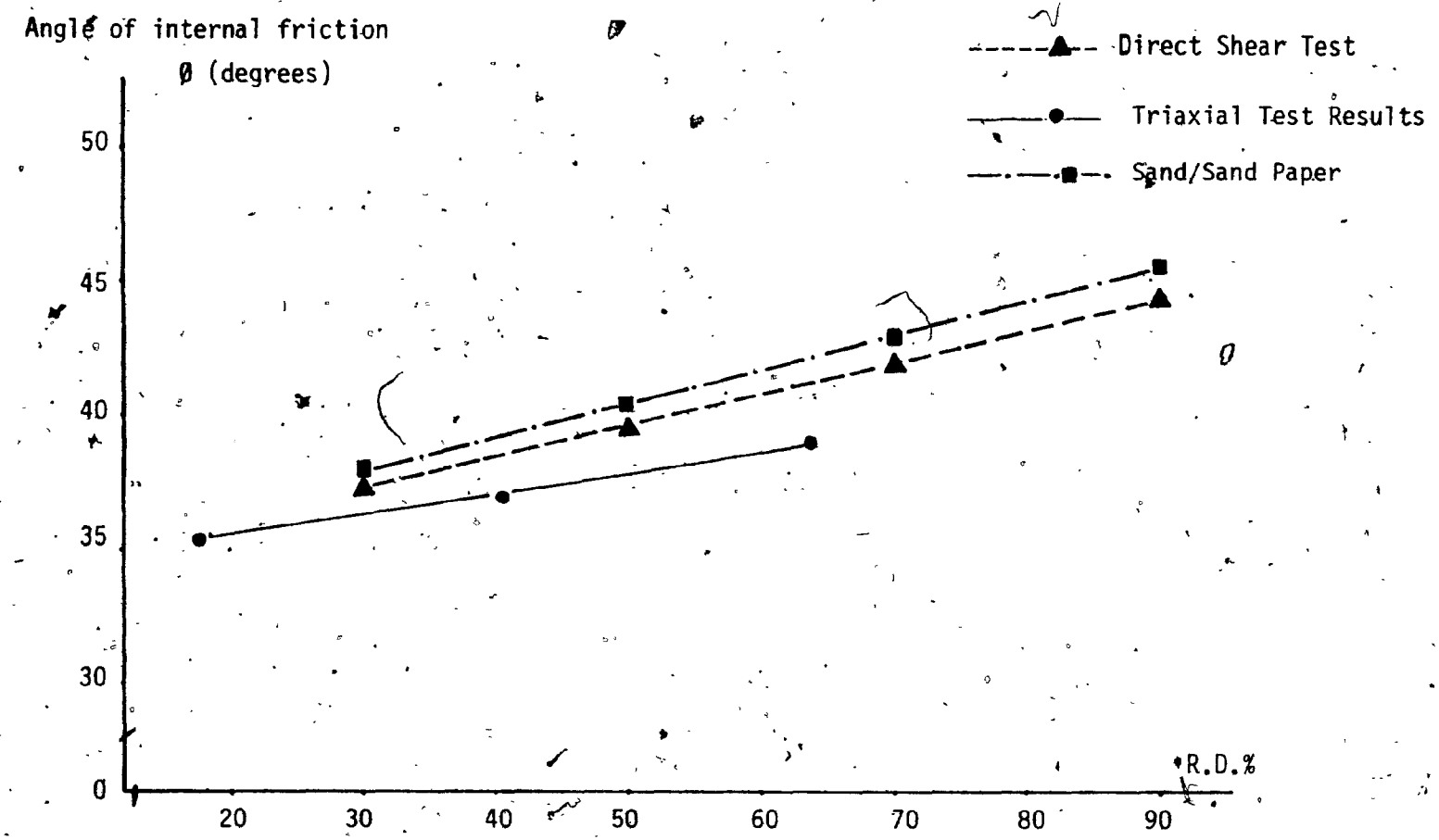

Figure 2.6: Angle of Internal Friction vs R.D. of Sand
(Afram, A. 1984)

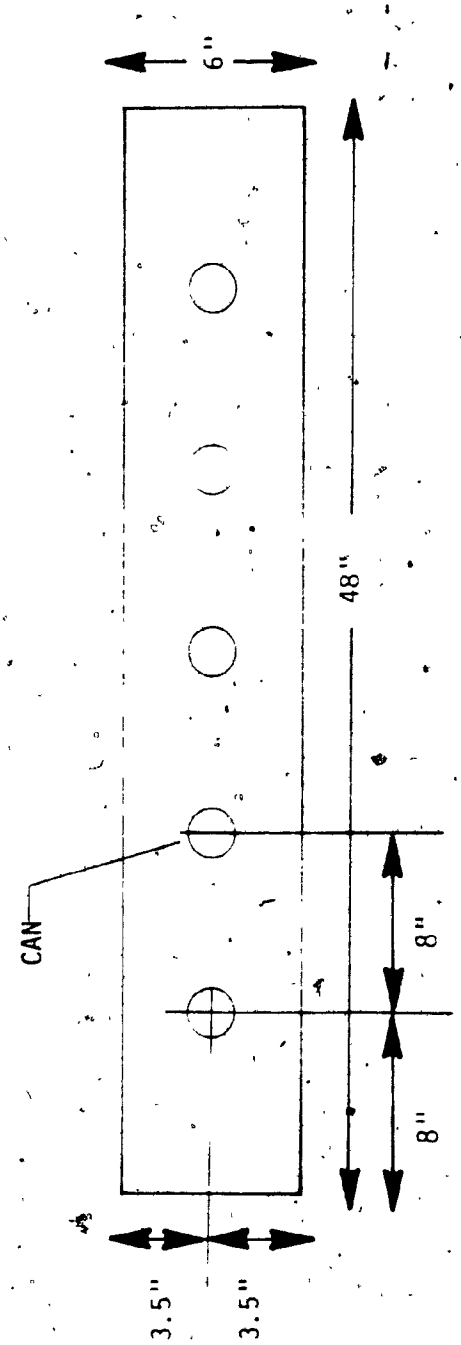

Figure 2.7: Density Pot Placement

TEST 1

CAN NO.	VOLUME OF CAN in^3 (cm^3)	WEIGHT OF CAN Lbs (g)	WEIGHT OF CAN AND SOIL Lbs (g)	NET WEIGHT Lbs (g)	UNIT WEIGHT Lb/ft^3 (KN/m^3)
1	9.02 (147.81	.0698 (32.00	.58 (268.70	.52 (23?.70	99.61 (15.65
2	7.81 (127.99	.0437 (20.00	.49 (266.10	.45 (206.10	99.55 (15.64
3	8.16 (133.65	.0436 (20.00	.50 (232.00	.47 (212.00	99.57 (15.64
4	8.16 (133.65	.0458 (21.00	.52 (236.50	.47 (215.50	99.58 (15.64
5	8.16 (133.65	.0436 (20.00	.51 (233.50	.47 (213.50	99.58 (15.64
6	8.50 (139.32	.0698 (32.00	.56 (255.30	.49 223.30	99.59 (15.64
7	8.67 (142.15	.0676 (31.00	.56 (258.40	.50 (227.40	99.60 15.64
8	7.98 (130.80	.0436 (20.00	.50 230.70	.46 210.70	99.57 (15.64
9	8.51 (139.32	.0698 (32.00	.55 (252.60	.48 220.60	99.59 15.64
10	8.51 (139.32	.0698 (32.00	.56 (255.90	.49 223.90	99.59 (15.64
11	8.33 (136.49	.0698 (32.00	.54 (250.50	.47 218.50	99.58 15.64
12	7.98 (130.80	.0436 (20.00	.49 (227.50	.45 207.50	99.57 15.64
13	8.67 (142.15	.0698 (32.00	.56 (257.30	.49 225.30	99.60 15.64
14	8.16 133.65	.0698 (32.00	.53 (245.00	.47 213.00	99.58 15.64
15	7.47 (122.33	.0436 (20.00	.47 (214.20	.42 194.20	99.54 15.64

Table 2.3: Calculation of Unit Weight

TEST 2

CAN NO.	VOLUME OF CAN in³ (cm³)	WEIGHT OF CAN Lbs (g)	WEIGHT OF CAN AND SOIL Lbs (g)	NET WEIGHT Lbs (g)	UNIT WEIGHT Lb/ft³ (KN/m³)
1	9.36 (153.47)	.0677 (31.00)	.60 (277.80)	.54 (246.80)	99.67 (15.65)
2	8.16 (133.65)	.0436 (20.00)	.51 (234.80)	.47 (214.80)	99.58 (15.64)
3	8.16 (133.65)	.0436 (20.00)	.51 (232.70)	.47 (212.70)	99.58 (15.64)
4	8.59 (139.32)	.0458 (21.00)	.53 (243.00)	.49 (222.00)	99.59 (15.64)
5	8.33 (136.49)	.0436 (20.00)	.52 (239.50)	.48 (219.50)	99.59 (15.64)
6	9.02 (147.82)	.0698 (32.00)	.59 (270.50)	.52 (238.50)	99.61 (15.65)
7	8.50 (139.32)	.0676 (31.00)	.56 (255.20)	.49 (224.20)	99.59 (15.65)
8	7.98 (130.82)	.0436 (20.00)	.50 (209.00)	.46 (209.00)	99.57 (15.64)
9	9.02 (147.82)	.0698 (32.00)	.58 (226.70)	.52 (234.70)	99.61 (15.65)
10	9.02 (147.82)	.0698 (32.00)	.58 (266.60)	.52 (234.60)	99.61 (15.65)
11	8.84 (144.98)	.0698 (32.00)	.57 (261.20)	.51 (229.20)	99.61 (15.65)
12	8.16 (133.65)	.0436 (20.00)	.51 (234.00)	.47 (214.00)	99.58 (15.64)
13	8.85 (144.98)	.0698 (32.00)	.58 (264.60)	.51 (232.60)	99.61 (15.65)
14	8.50 (139.32)	.0698 (32.00)	.56 (255.30)	.49 (223.30)	99.59 (15.64)
15	7.96 (130.82)	.0436 (20.00)	.49 (228.10)	.46 (208.10)	99.57 (15.64)

Table 2.4 Calculation of Unit Weight

TEST 3

CAN NO.	VOLUME OF CAN in³ (ft³)	WEIGHT OF CAN LBS (g)	WEIGHT OF CAN AND SOIL LBS (g)	NET WEIGHT LBS (g)	UNIT WEIGHT LB/ft³ (KN/m³)
1	8.85 144.98	.0677 31.00	.57 260.11	.51 229.11	99.61 15.65
2	.95 130.26	.0437 20.00	--------	--------	--------
3	8.51 139.32	.0437 20.00	.52 240.10	.49 220.10	99.59 15.65
4	8.33 136.49	.0458 21.00	.52 237.30	.48 216.30	99.59 15.65
5	8.33 136.49	.0437 20.00	.52 239.60	.48 219.60	99.59 15.65
6	9.19 150.64	.0698 32.00	.59 270.30	.53 240.30	99.62 15.65
7	8.51 139.30	.0677 31.00	.55 253.20	.49 222.20	99.59 15.64
8	8.16 133.69	.0437 20.00	.52 238.20	.47 218.20	99.58 15.64
9	9.36 153.47	.0698 32.00	.59 270.50	.54 242.50	99.63 15.65
10	9.36 153.47	.0698 32.00	.61 227.80	.54 245.80	99.63 15.65
11	9.19 150.64	.0698 32.00	.59 271.00	.53 239.00	99.62 15.65
12	8.85 144.98	.0437 20.00	.55 250.20	.51 230.20	99.60 15.64
13	9.19 150.64	.0698 32.00	.59 270.60	.53 238.60	99.62 15.65
14	8.85 144.98	.0698 32.00	.58 265.10	.51 233.10	99.61 15.65
15	8.16 133.69	.0437 20.00	.57 232.50	.47 212.50	99.57 15.64

Table 2.5: Calculation of Unit Weight

And knowing that:

$$G_s = 2.662,\ e_{max} = .815 \text{ and } e_{min} = .590$$

The relative density in these tests was 63.33%. From Figure 2.6 this corresponds to an angle of friction of 41.2% (direct shear test).

CHAPTER 3

EXPERIMENTAL RESULTS

Pressure transducers were indispensable for the measurement of the normal pressure acting on the face of the plate: In particular, the integration of these pressures yielded the total passive earth pressure and consequently, the ultimate load. Calibration of the pressure transducers was achieved inside a special pressure chamber and the transducers were independently subjected to air pressure on their frontal surfaces. Thus, calibration curves were obtained for exitation versus pressure (see Figures 3.1-a to 3.1-h).

The load cell in the present investigation primarily served the two following purposes: First, as monitoring device for possible malfunctioning of the pressure transducers, and second, to determine frictional resistance produced in every test (see Figures 3.2-a and 3.2-b). By means of stress control procedure, the calibration of the load cell was carried out and incremental loads were added up to a total of 500 pounds. The curve thus obtained plots exitation versus load (see Figure 3.3).

Curves of the ultimate load per anchor for all tests are shown in Figures 3.4-a to 3.4-c. In addition to these, the transducer readings made feasible the drawing of curves which depict the relation between

TRANSDUCER NO. 10

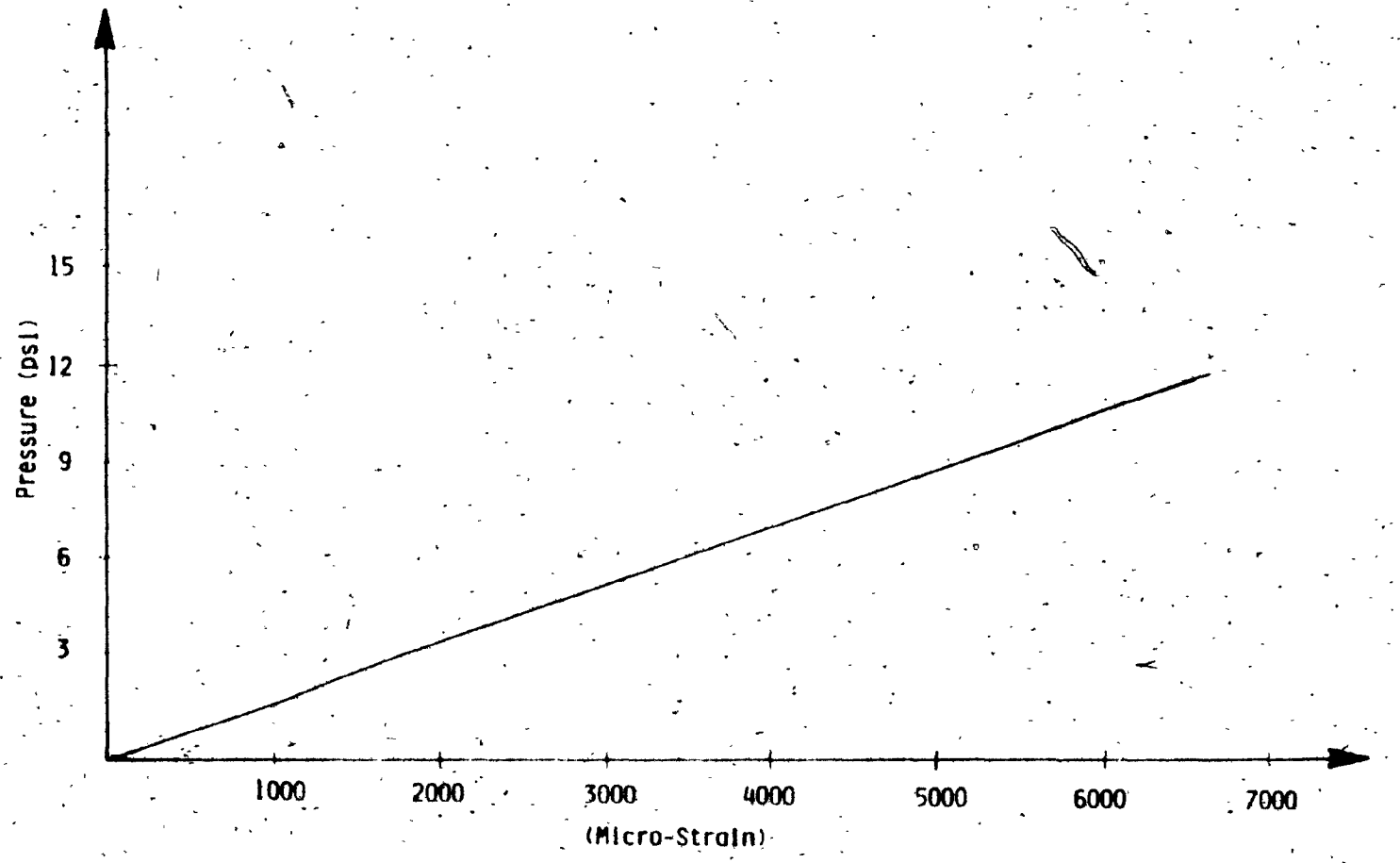

Figure 3.1-a : Calibration Curve

TRANSDUCER NO. 11

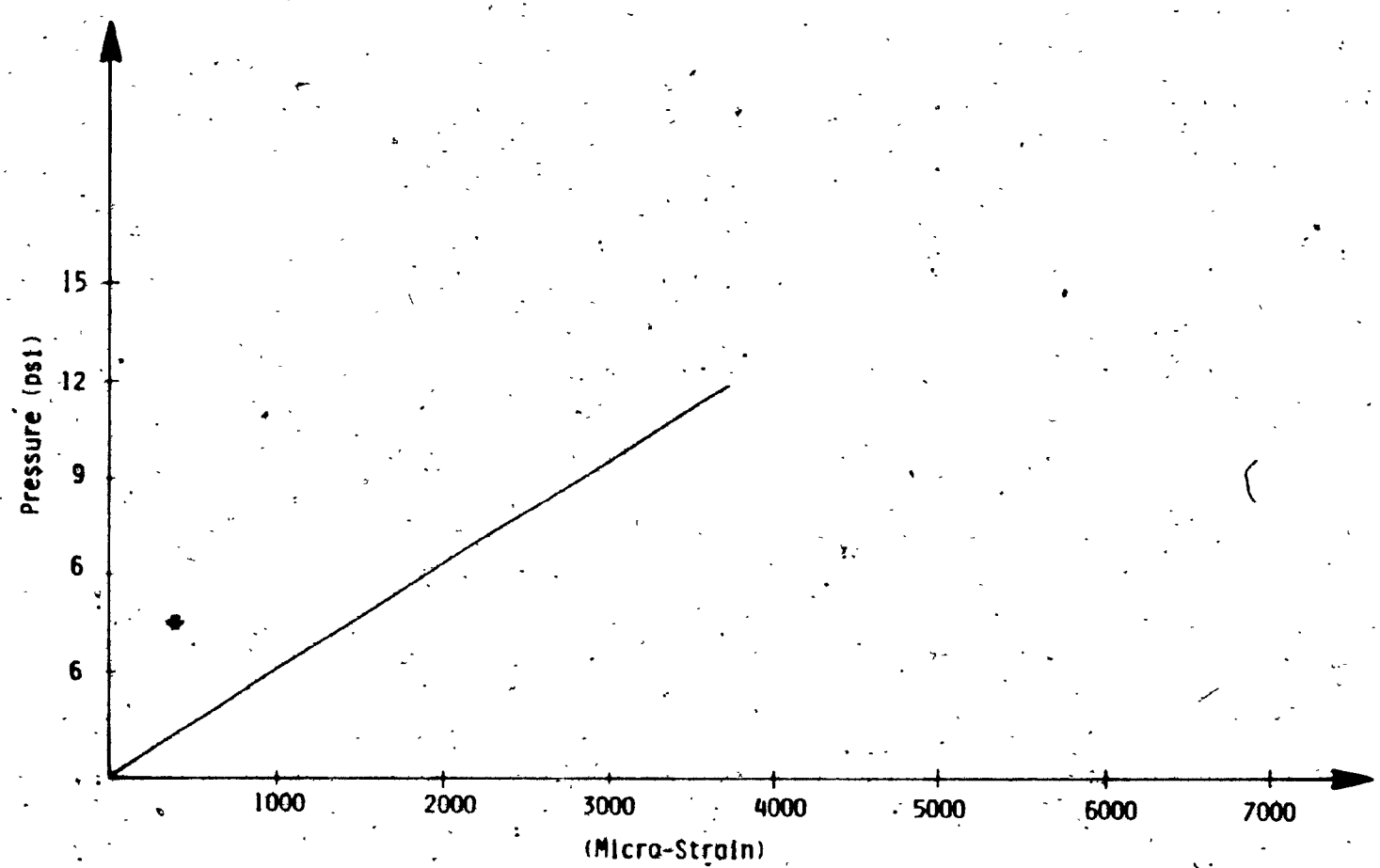

Figure 3.1-b : Calibration Curve

TRANSDUCER NO. 12

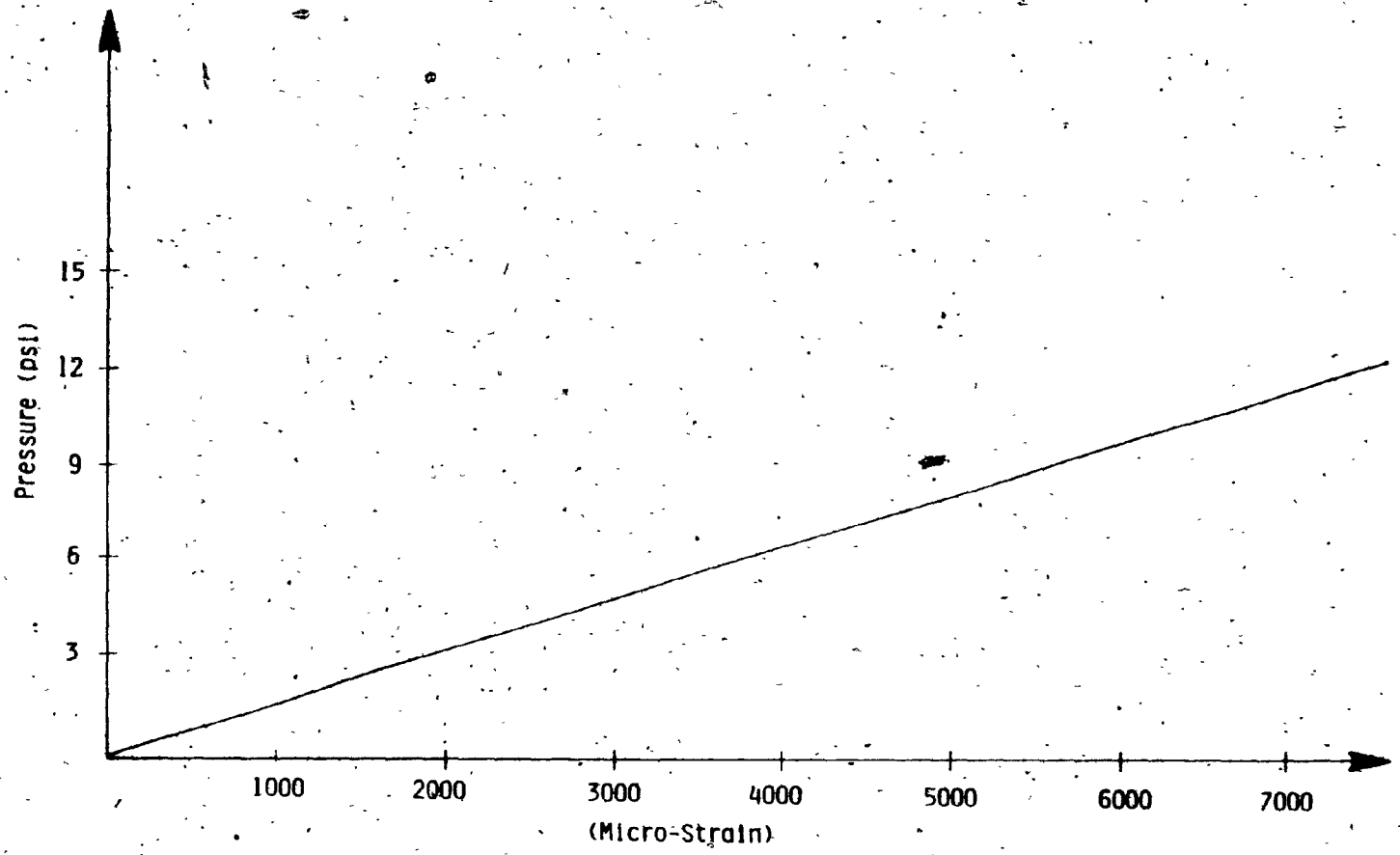

Figure 3.1-c : Calibration Curve

TRANSDUCER NO. 13

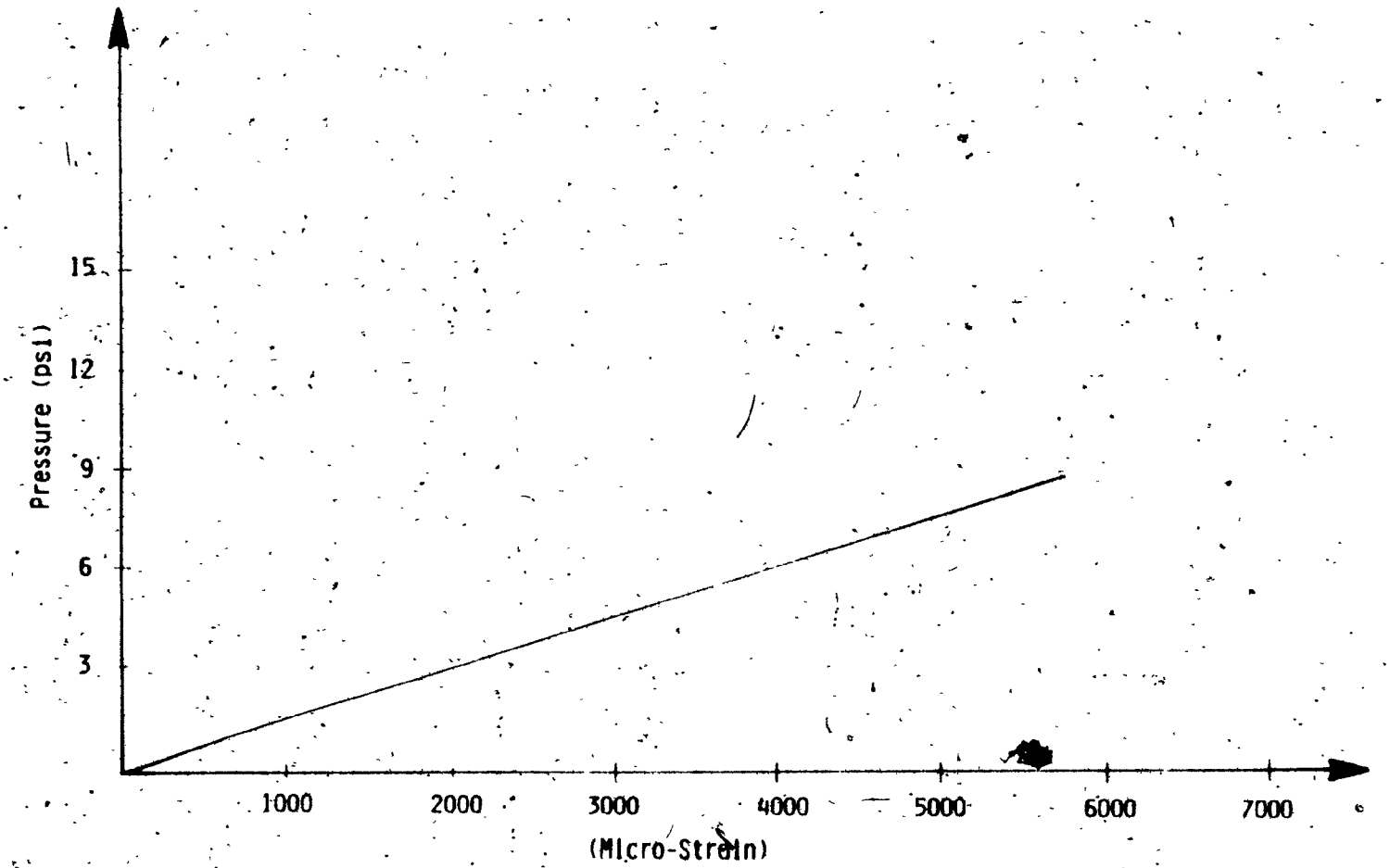

Figure 3.1-d: Calibration Curve

TRANSDUCER NO. 14

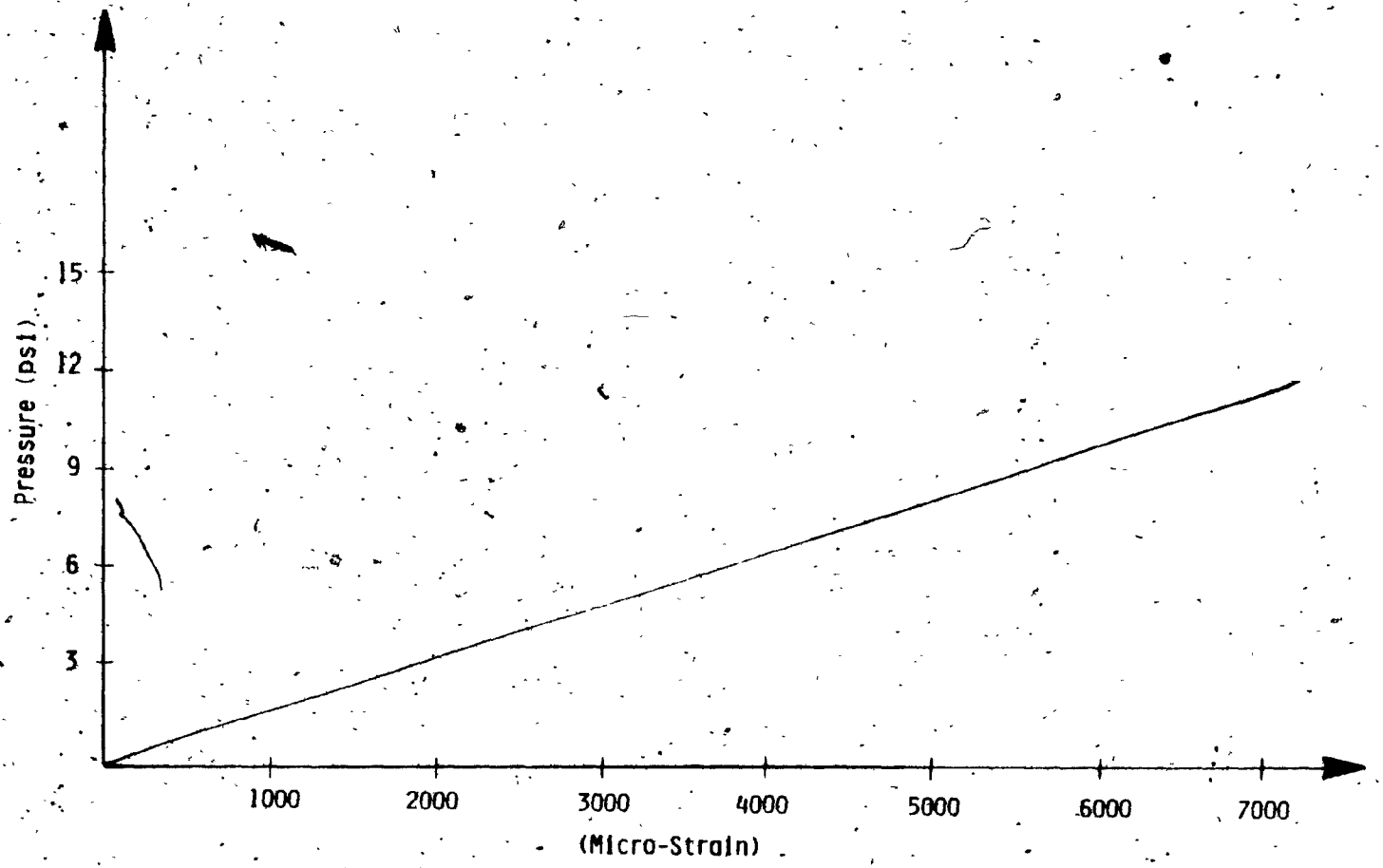

Figure 3.1-e : Calibration Curve

TRANSDUCER NO. 15

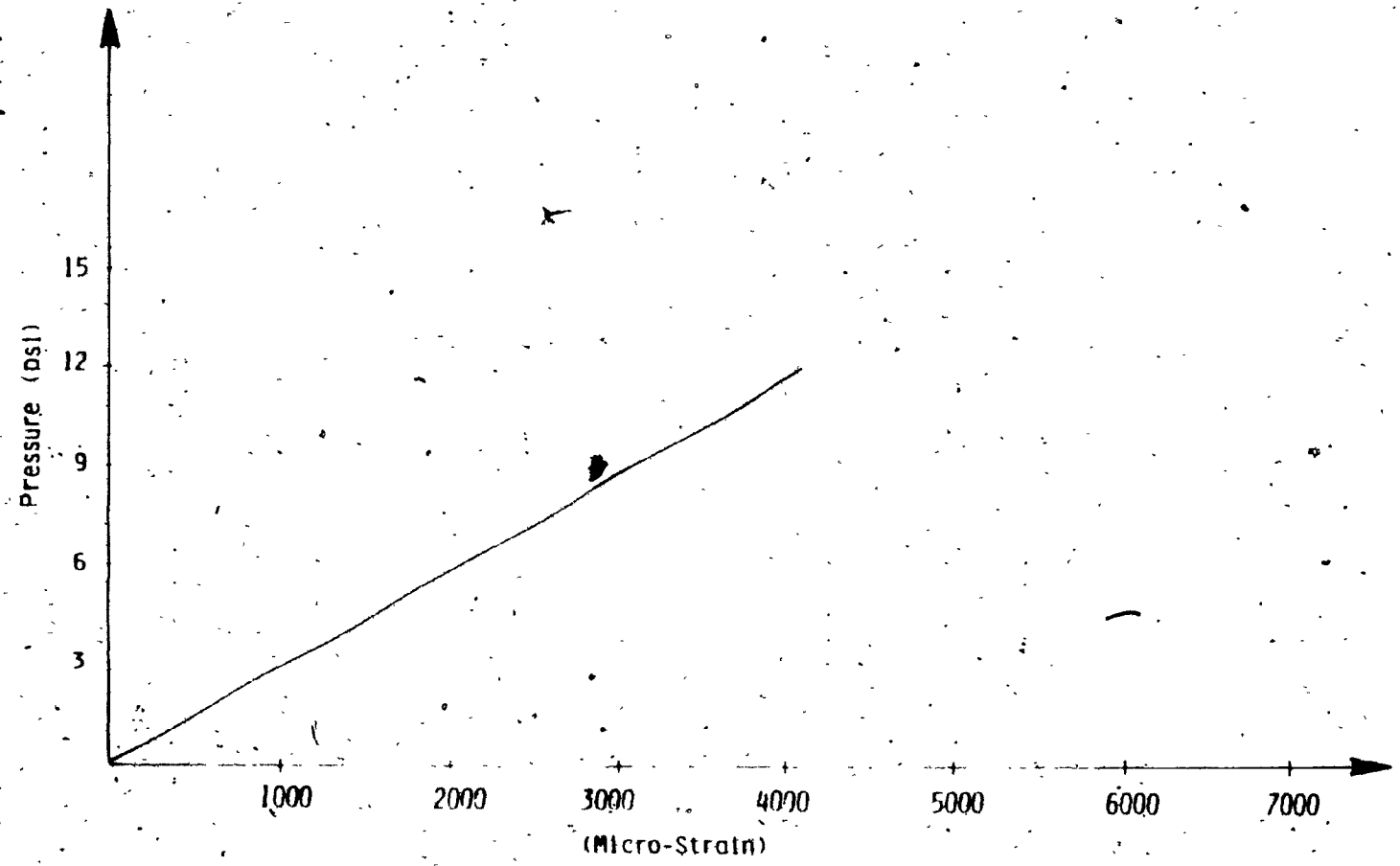

Figure 3.1-f : Calibration Curve

TRANSDUCER NO. 16

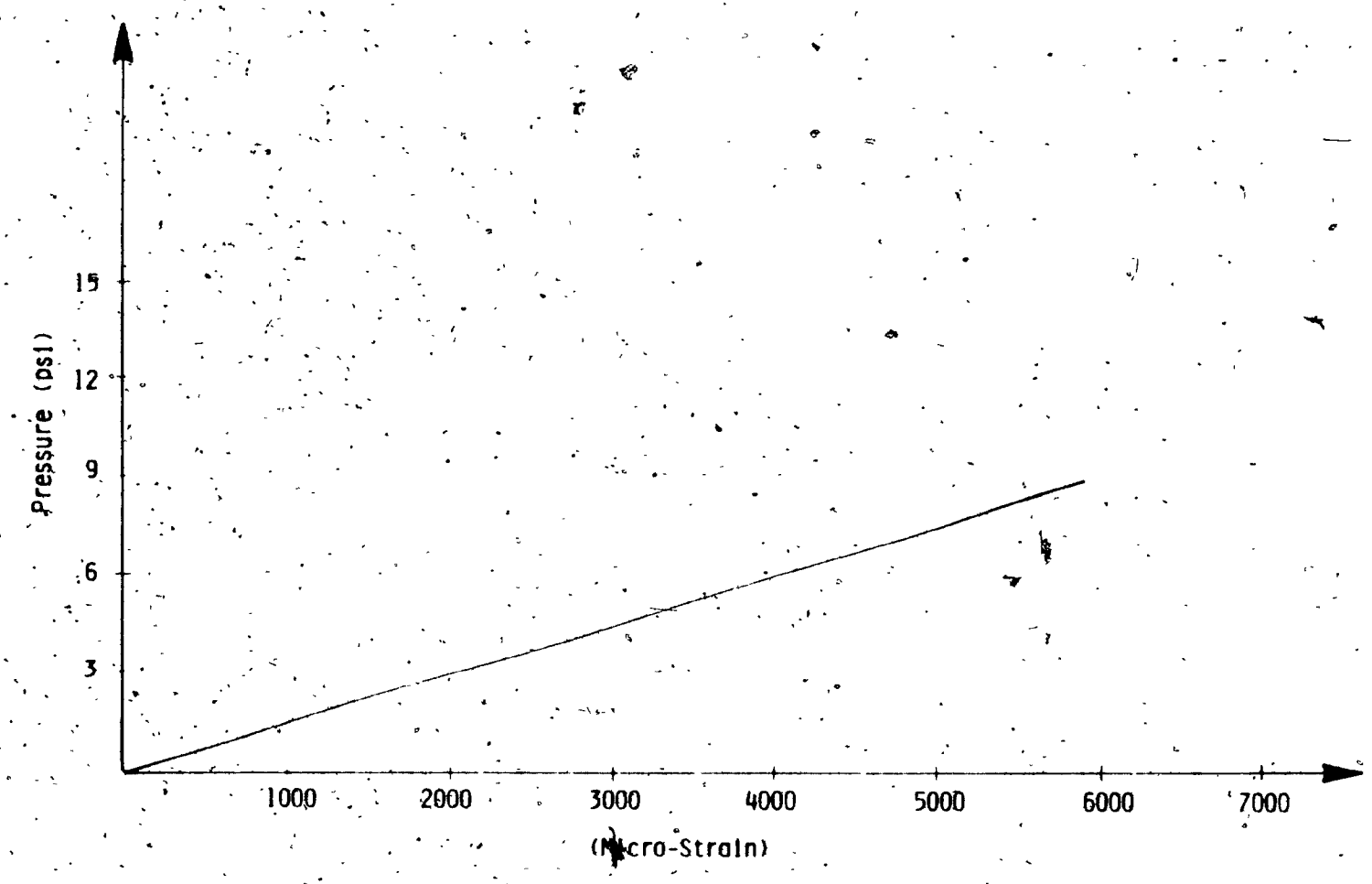

Figure 3.1-g: Calibration Curve

TRANSDUCER NO. 17

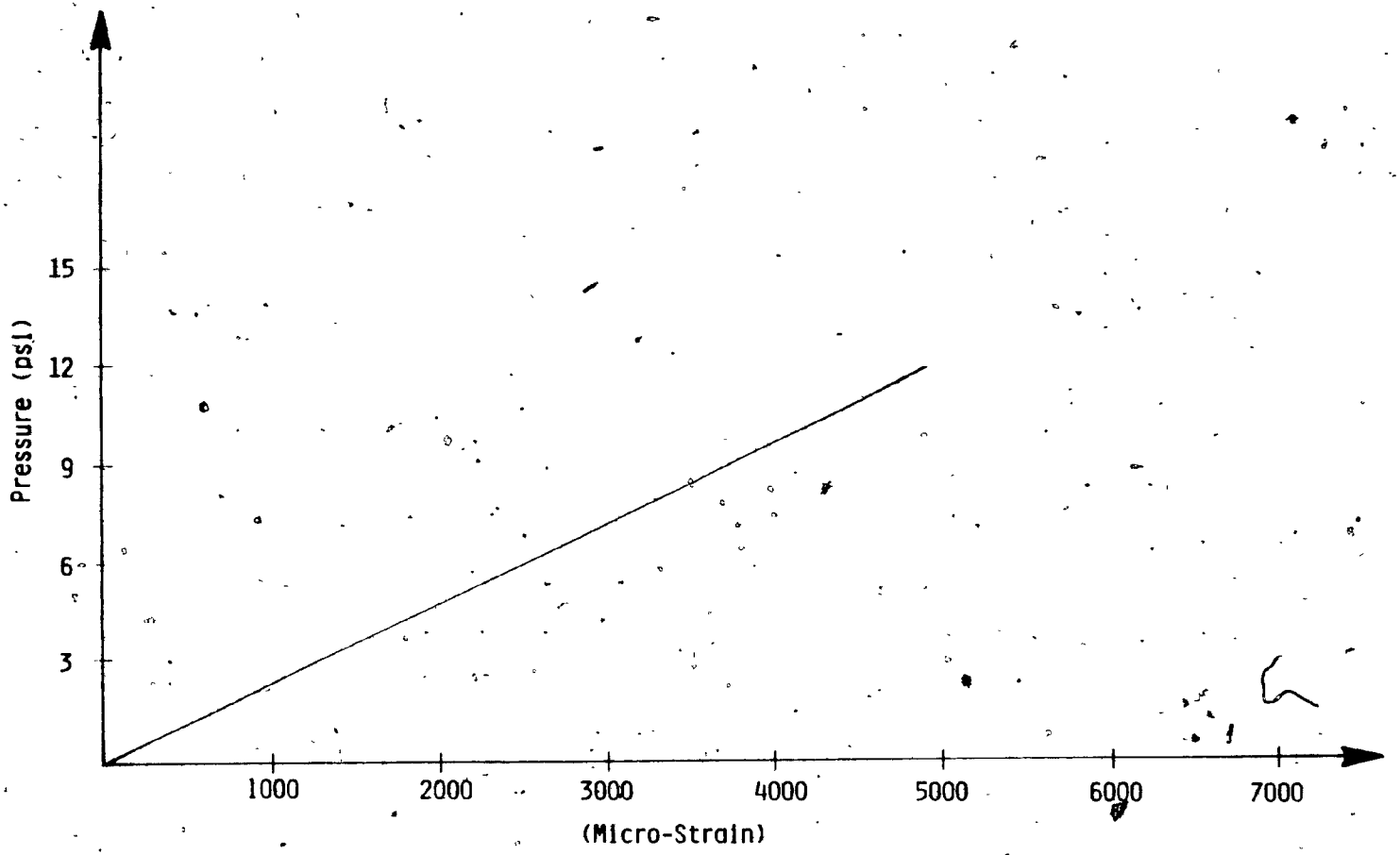

Figure 3.1-h : Calibration Curve

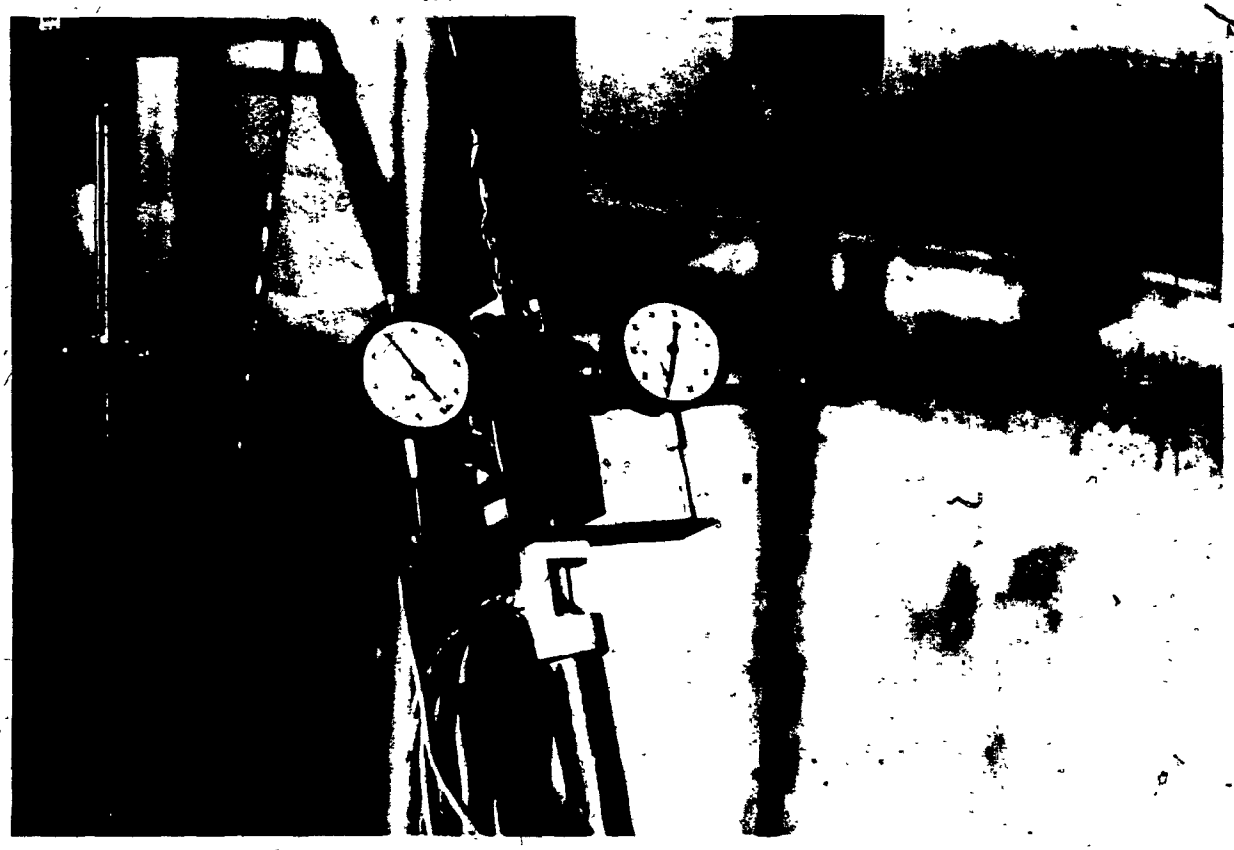

Figure 3.2-a: Load Cell Used in the Monitoring of Frictional Resistance

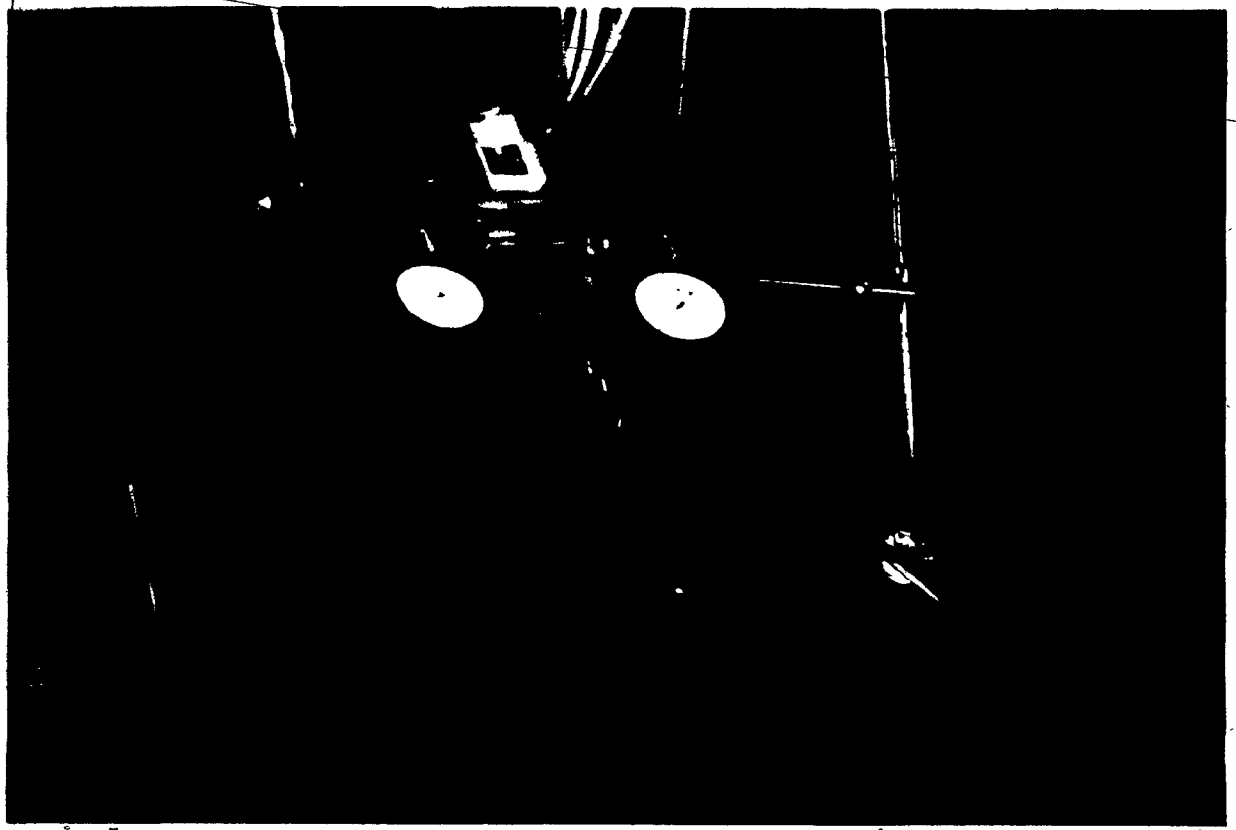

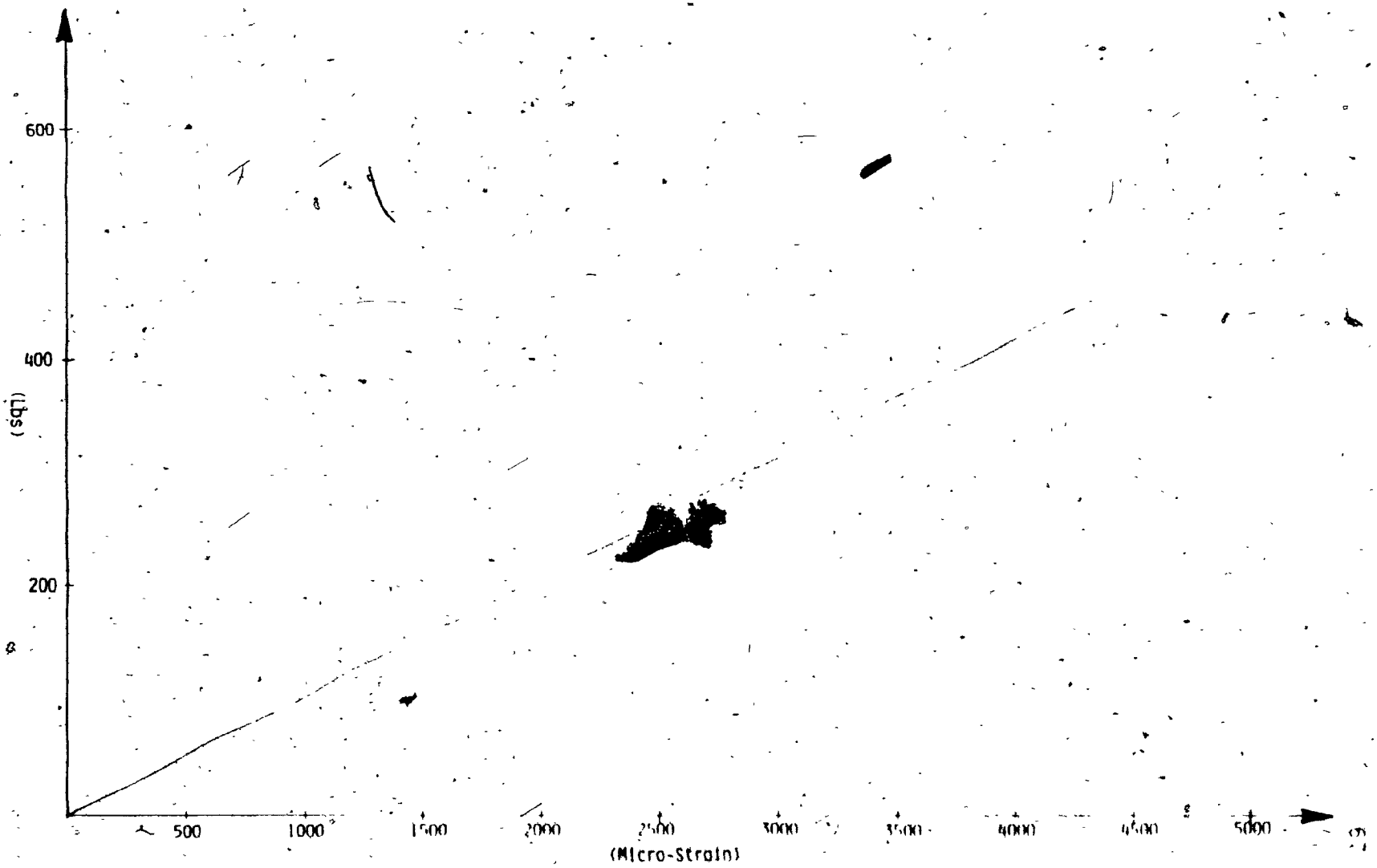

Figure 3.3: Load Cell Calibration Curve

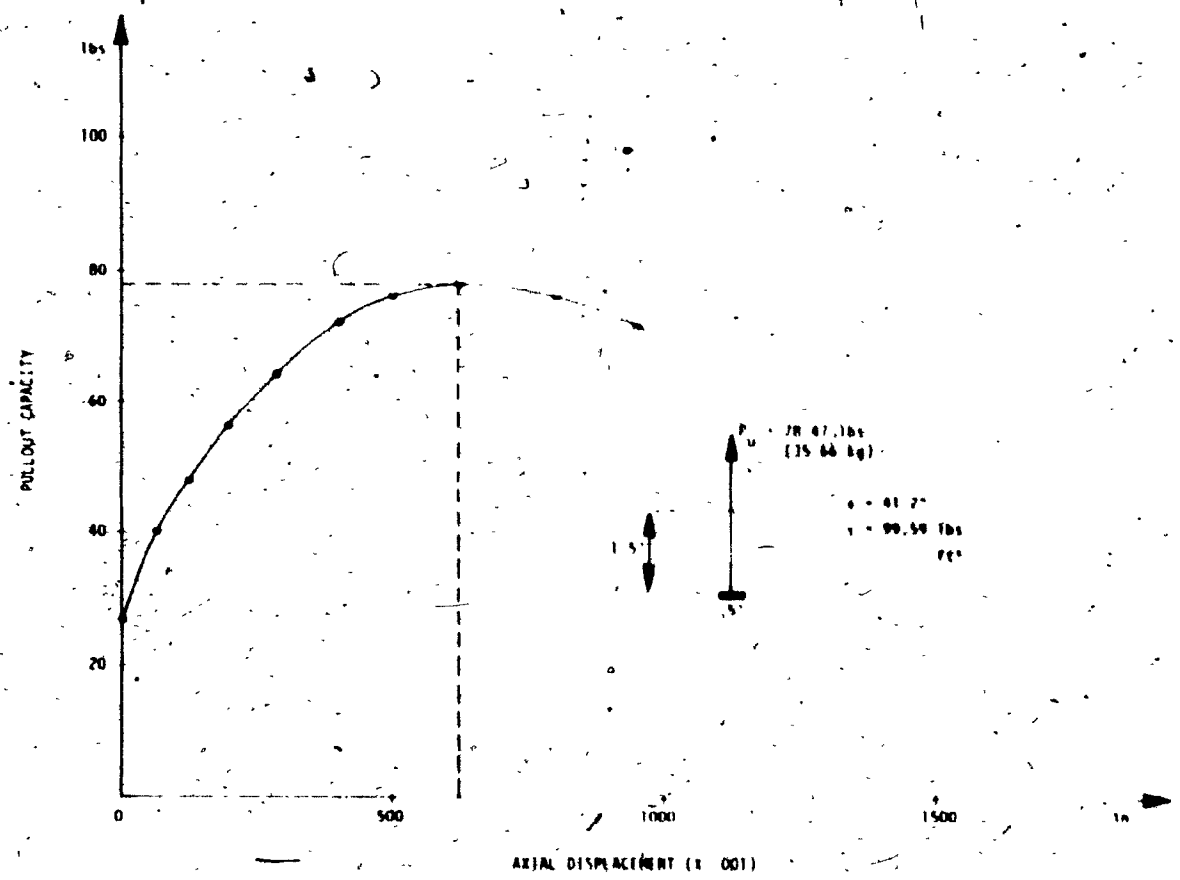

Figure 3.4-a Curve of Pullout Capacity Versus Axial Displacement

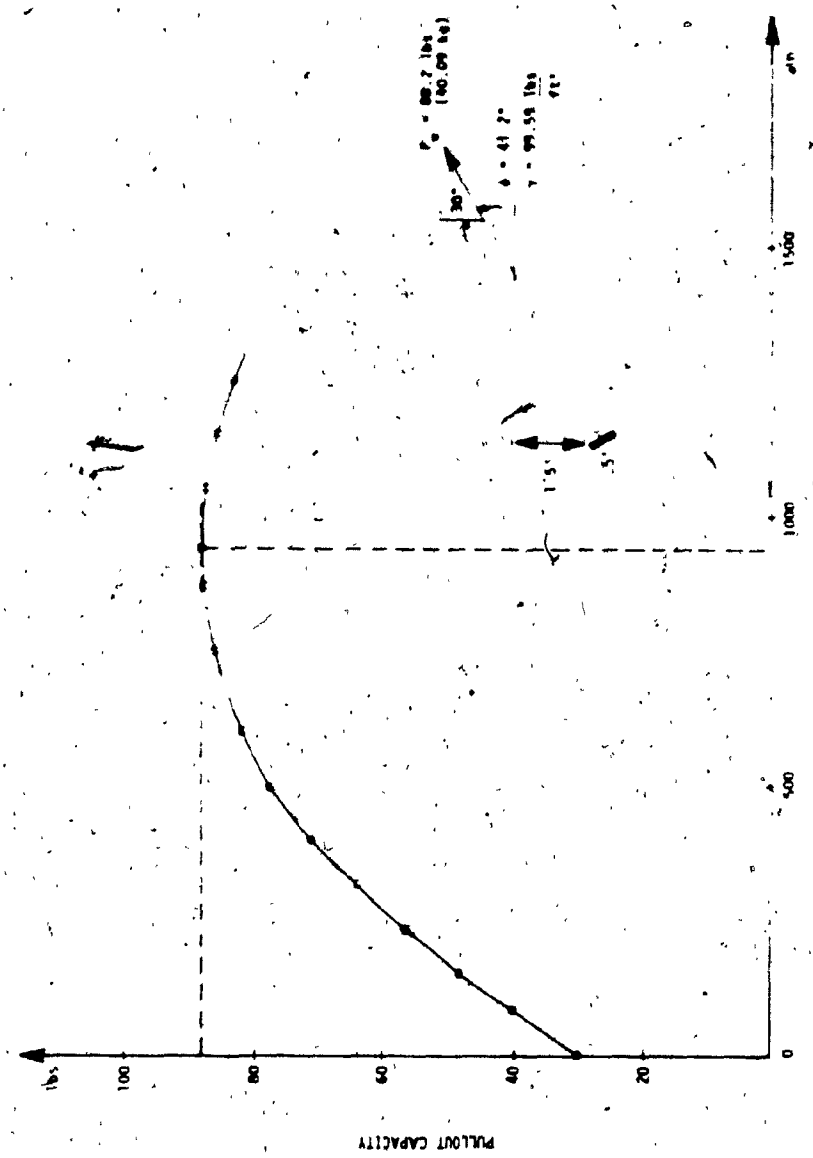

Figure 3.4-b. Curve of Pullout Capacity Versus Axial Displacement

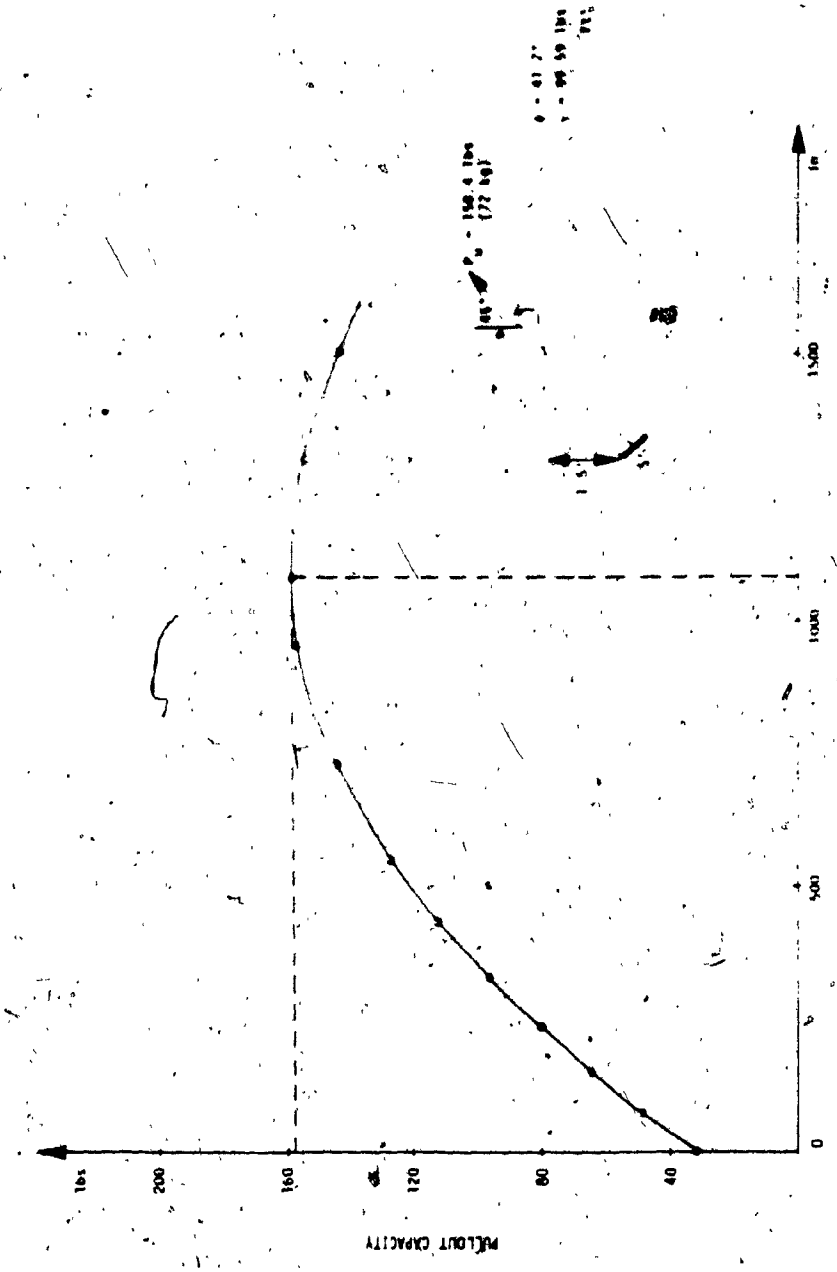

Figure 1.4-c. Curve of Pullout Capacity Versus Axial Displacement

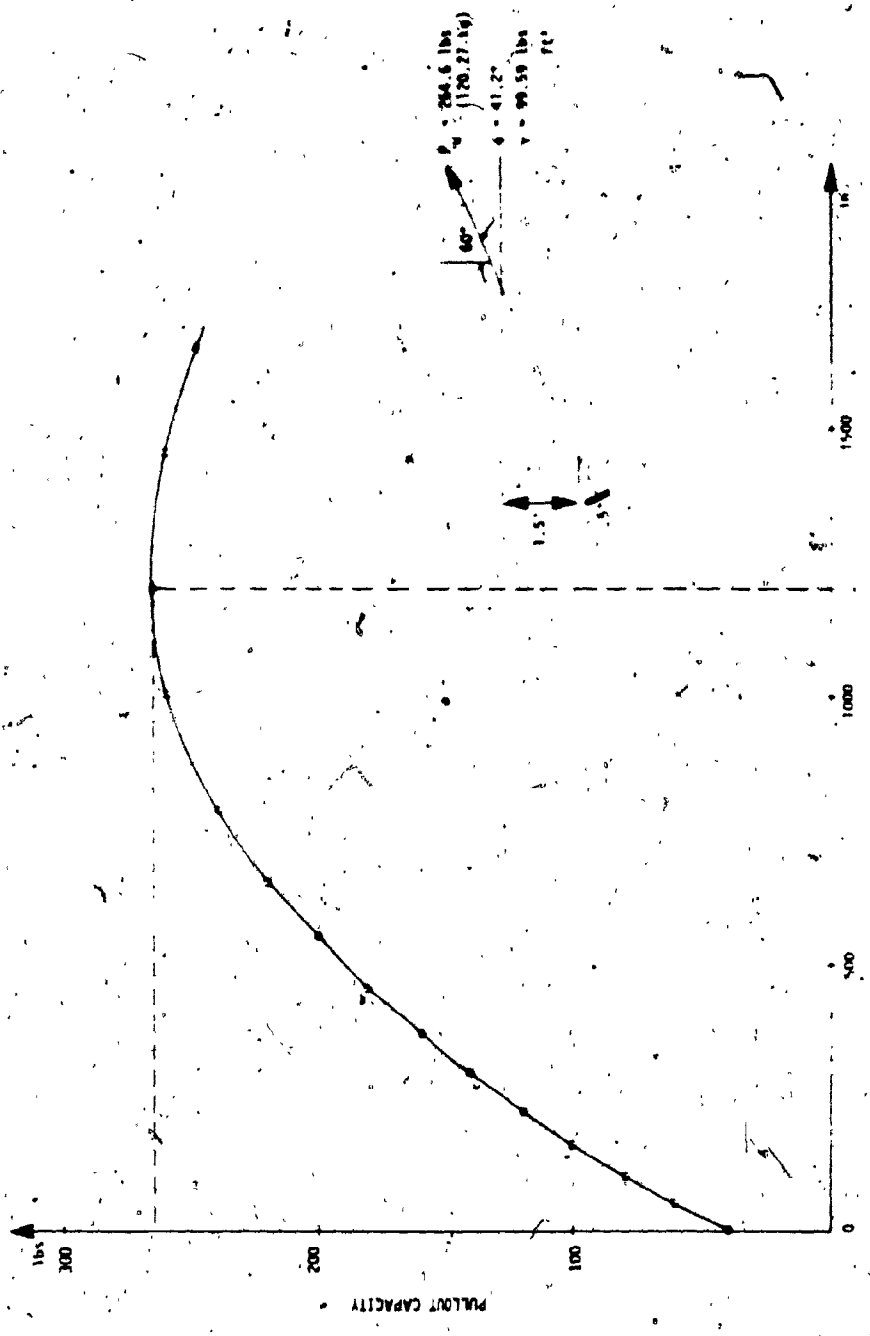

Figure 3.4-d Curve of Pullout Capacity Versus Axial Displacement

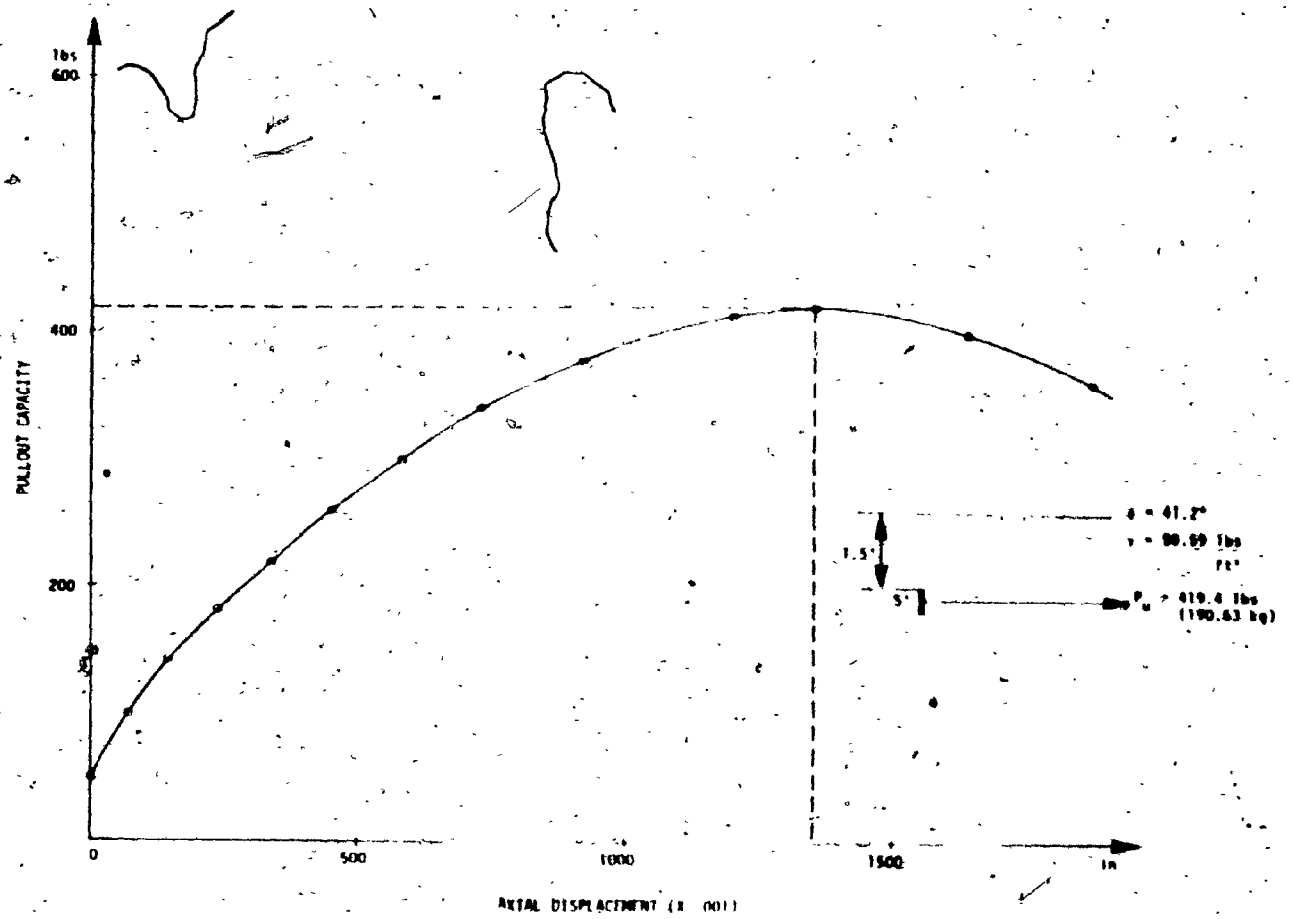

Figure 3.4-e Curve of Pullout Capacity Versus Axial Displacement

the passive earth pressure and displacement of plate. Figures 3.5-a to 3.5-d show such a curve for the special case where the anchor is subjected to horizontal pull. Furthermore, refer to Figures 3.6-a to 3.6-e for the distribution of pressure acting on the plate in the vertical direction (plotted for all tests).

The test results clearly indicate an increase in the ultimate pullout load as the angle of pull α_v increases. The increase is less significant, however, from 0 to 30 degrees than for angles greater than 30 degrees.

The obtained results lead to the following conclusions:

1. The pressure distribution follows the well established classical pattern, although some insignificant irregularities (due to transducer difficiencies) are present.

2. There is no significant difference between the initial pressure distribution and the pressure distribution at the stage of soil failure.

3. The graph of the pressure distribution does not change under increase of pullout load and plate displacement.

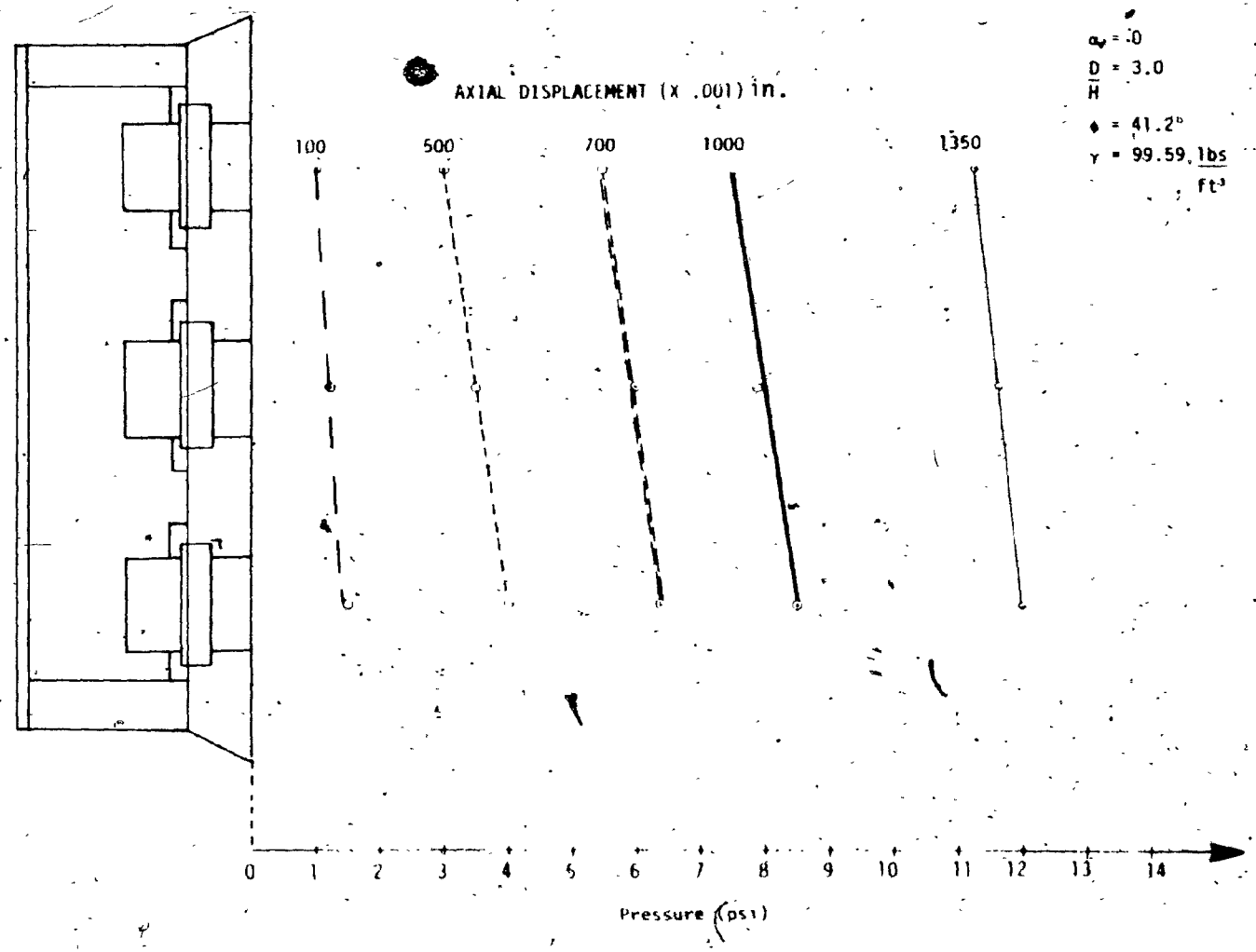

Figure 3.5-a: Distribution of Passive Earth Pressure

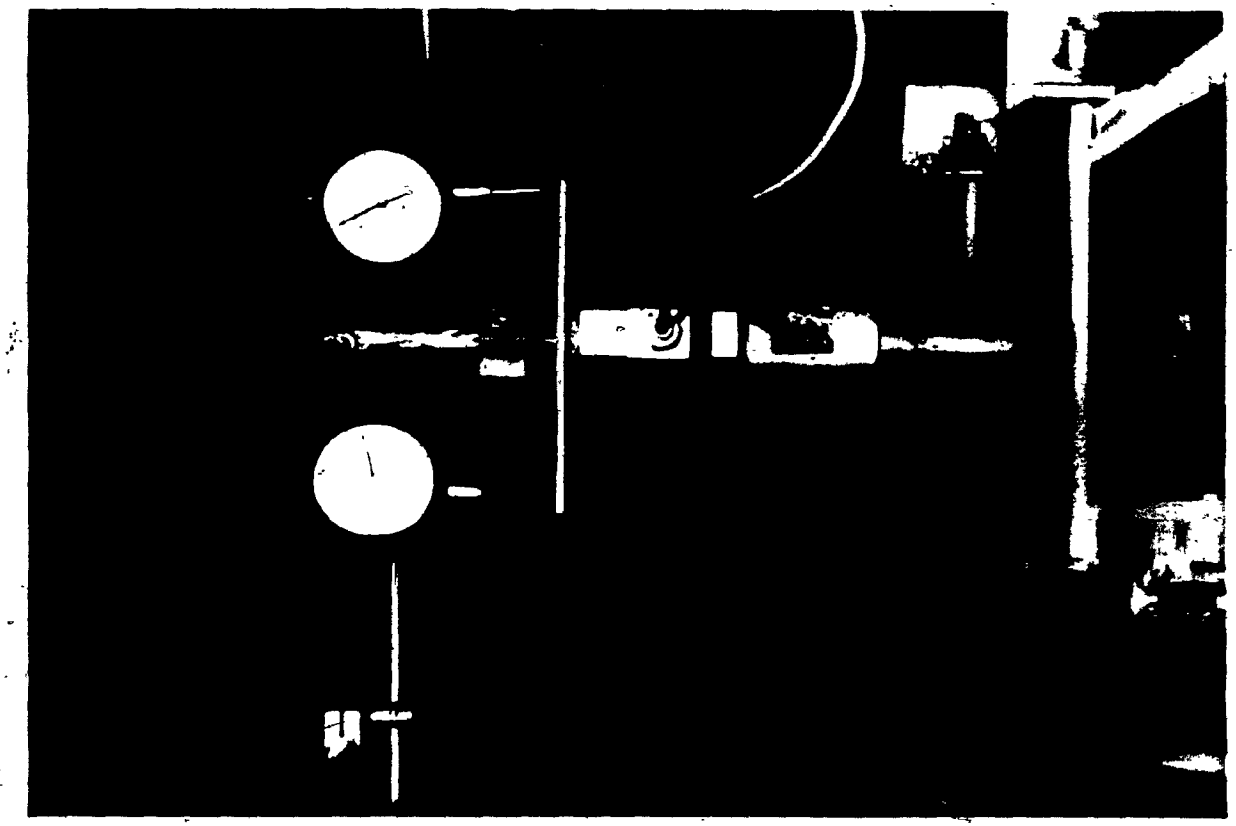

Figure 3.5-b Top View of Anchor Subject to Horizontal Pull

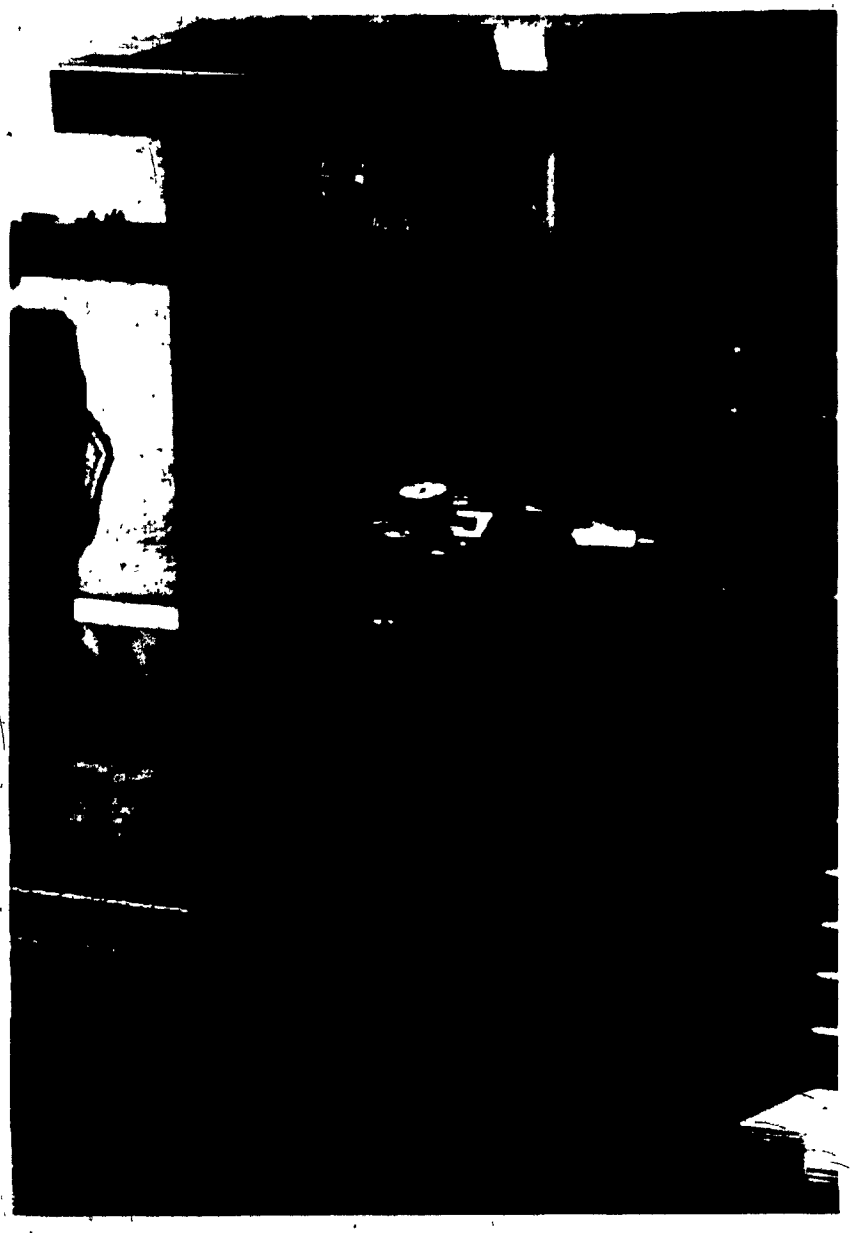

Figure 3.5-c: Side View of Anchor Subject to Horizontal Pull

Figure 3.5-d: Lateral View of Anchor Subject to Horizontal Pull

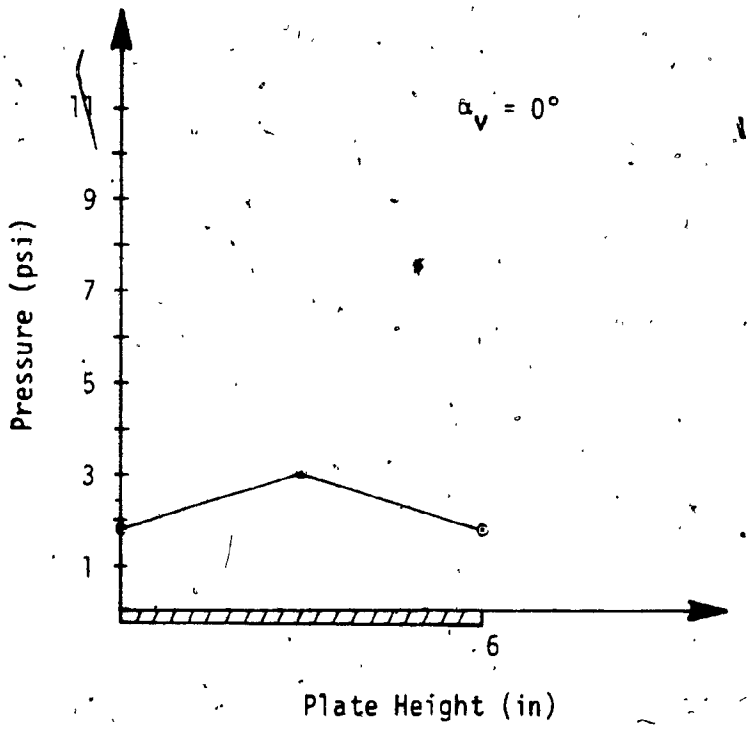

Figure 3.6-a: Pressure Distribution on Plate's Frontal Surface at Failure

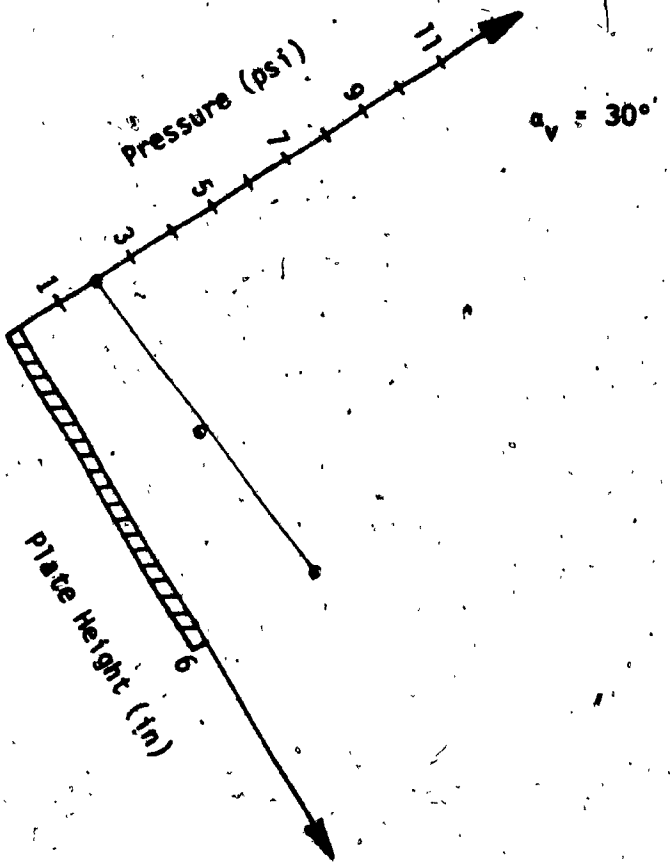

Figure 3.6-b: Pressure Distribution on Plate's Frontal Surface at Failure

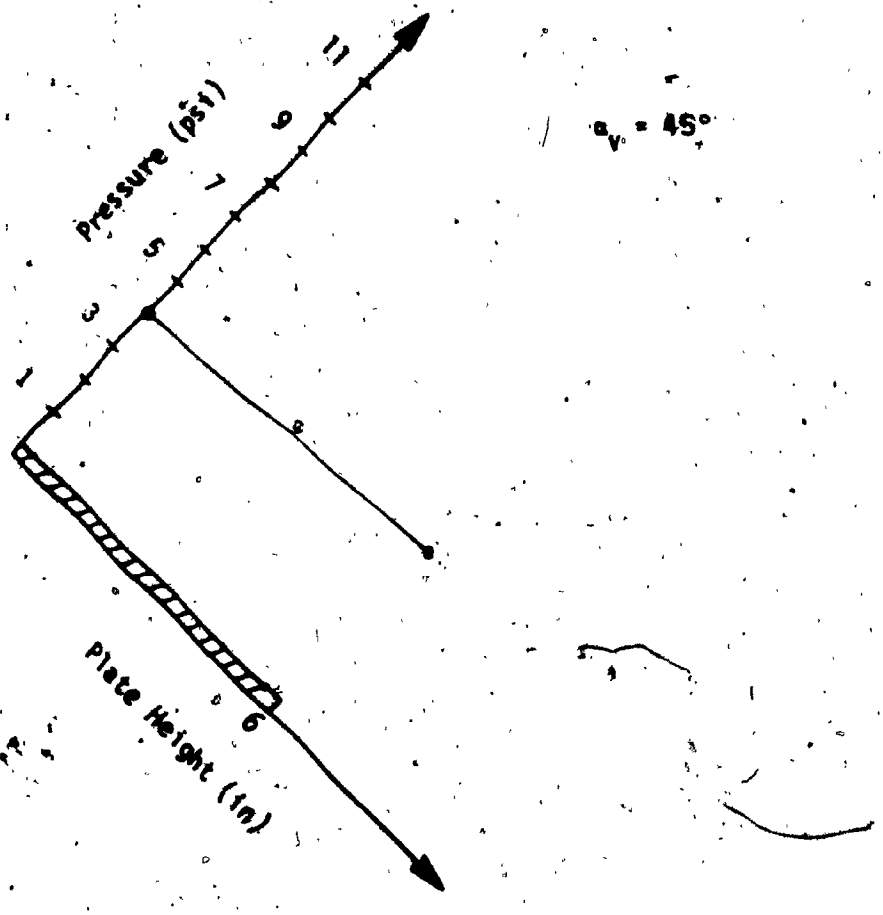

Figure 3.6-c: Pressure Distribution on Plate's Frontal Surface at Failure

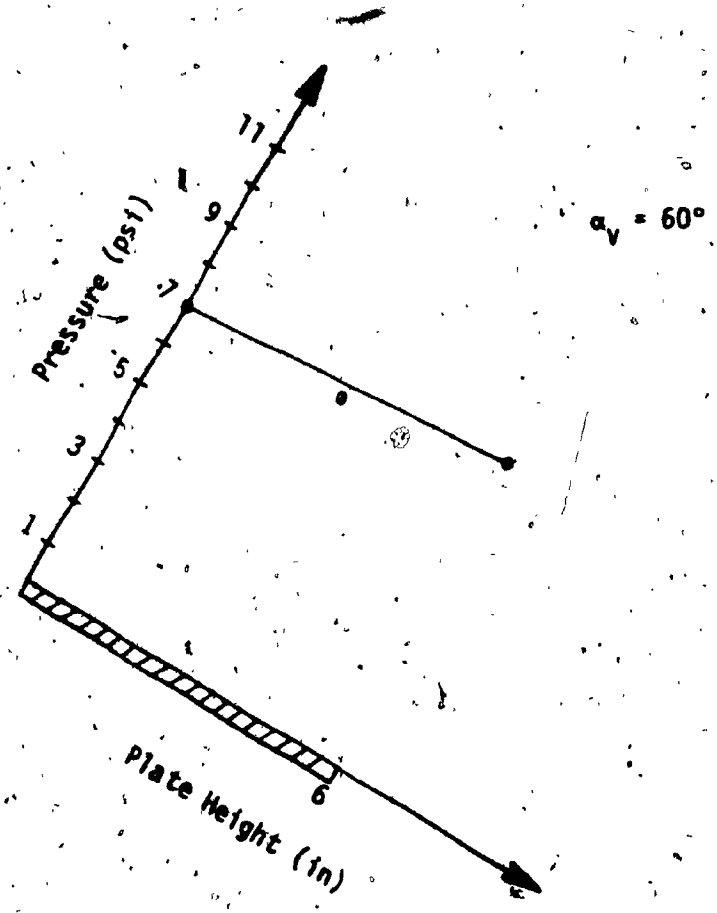

Figure 3.6-d: Pressure Distribution on Plate's Frontal Surface at Failure

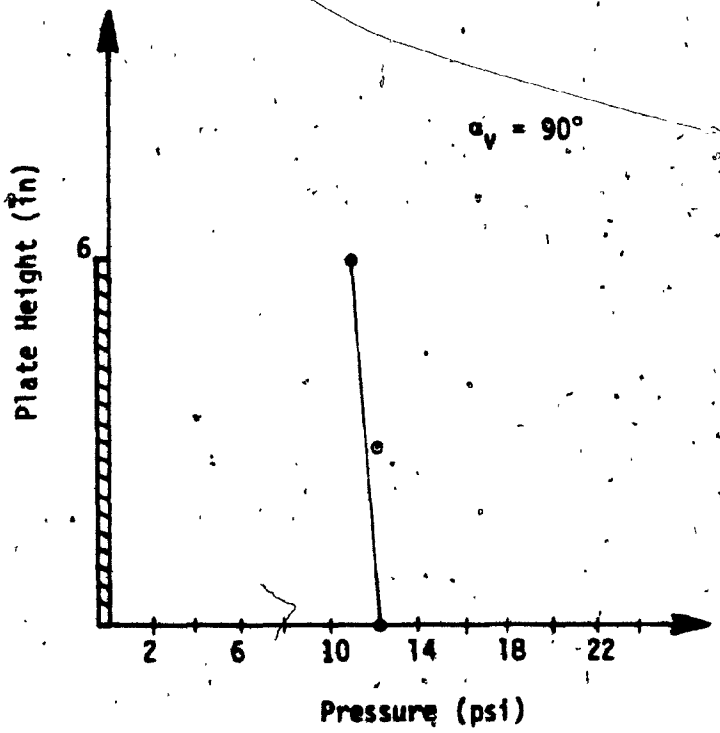

Figure 3.6-e: Pressure Distribution on Plate's Frontal Surface at Failure

SIDE EFFECTS

The contribution from side friction in plane strain tests is considered significant. Figure 3.7 indicates that the total passive resistance P_p is the sum of three components, P_1, P_2 and P_3. Intrinsically, force P_1 results from the resistance provided by the slip plane B, C, F, E, whereas P_2 is due to the frictional resistance of the two vertical side planes, G, D, C, E and H, A, B, F. On the other hand, P_3 is produced by the "trapping" of sand particles between the plate and the two vertical sides of the tank. Summarizing, $P_p = P_1 + P_2 + P_3$. Many investigators failed to separate these three effects. Some (Terzaghi, 1948, Tschebotarioff, 1973, Biarez et al 1965 and Kezdi, 1972) investigated the total passive resistance while neglecting the influence of the three separate components. Others (for example, Schofield, 1961) evaluated the side friction P_2 utilizing the articulated walls. None of these investigators considered the effect of friction caused by the "trapping" of sand particles between the side of the plate and the wall.

In the present investigation, the value of the total passive earth pressure was calculated by integrating the pressure transducer readings on the face of the plate. The difference between the load cell value and total passive load equals the sum of the apparatus resistance value, soil friction (against the pulling shaft), any active earth pressure

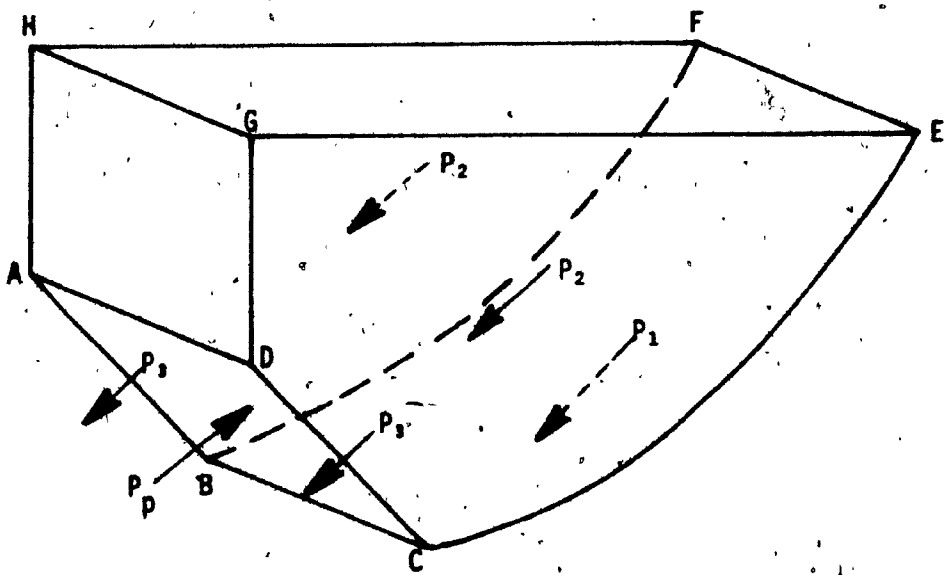

Figure 3.7: Forces Acting on Sand Mass

(from the opposite part of plate) and additional side effect (see Table 3.1). From the Table, one can conclude that the frictional resistance increases with increasing angle from the vertical. This is attributed to the fact that the surface of shear increases and more soil is mobilized on the plexiglass sand interface as the inclination of the anchor increases. This also increases the "trapping" component of the frictional resistance.

	LOAD CELL READING P_{TOT}	INTEGRATION OF PRESSURES (TRANSDUCERS) P_p	FRICTIONAL RESISTANCE P_f
0	94.68 lbs (42.99 kg)	78.47 lbs (35.67 kg)	16.11 lbs (7.32 kg)
30	105.31 lbs (47.86 kg)	88.2 lbs (40.09 kg)	17.11 lbs (7.77 kg)
45	178.96 lbs (81.35 kg)	158.4 lbs (72 kg)	20.56 lbs (9.34 kg)
60	286.94 lbs (130.43 kg)	264.6 lbs (120.27 kg)	22.34 lbs (10.15 kg)
90	444.67 lbs (202.13 kg)	419.4 lbs (190.63 kg)	25.27 lbs (11.48 kg)

$$\phi = 41.2$$

$$\gamma = 99.59 \frac{lbs}{ft^3}$$

$$\frac{D}{H} = 3.0$$

Table 3.1: Calculation of Frictional Resistance

CHAPTER 4

THEORETICAL ANALYSIS (LIMIT EQUILIBRIUM APPROACH)

The analyzed anchor had length much larger than its height; consequently, it was necessary to treat it as a plane strain problem. Figure 4.1 depicts a strip anchor of height H buried to a depth D in dense sand subjected to axial vertical loads, whereas Figures 4.2-a and 4.2-b show the same anchor subjected to central inclined loads at angle α_v with the vertical axis. To expedite calculations, ab and cd were assumed to be the failure planes. Thus, the mobilized angle δ of shearing resistance along the assumed failure planes must be less than the angle ϕ of shearing resistance of the sand.

According to Meyerhof (1973), the ultimate load acts normal to the anchor base; hence, the difference between the corresponding passive and active earth pressures yields the shearing resistance on the surfaces through the anchor perimeter. From earth pressure theories, it becomes evident that the magnitude of the passive pressure, and consequently the shearing stress acting on the assumed failure planes, will have a triangular distribution P_1 due to the weight component. Further, the passive pressure on a plane inclined at angle $-\alpha$ is greater than for one inclined at angle $+\alpha$. Nevertheless, observation during testing indicated that failure takes place in the loading direction, while the

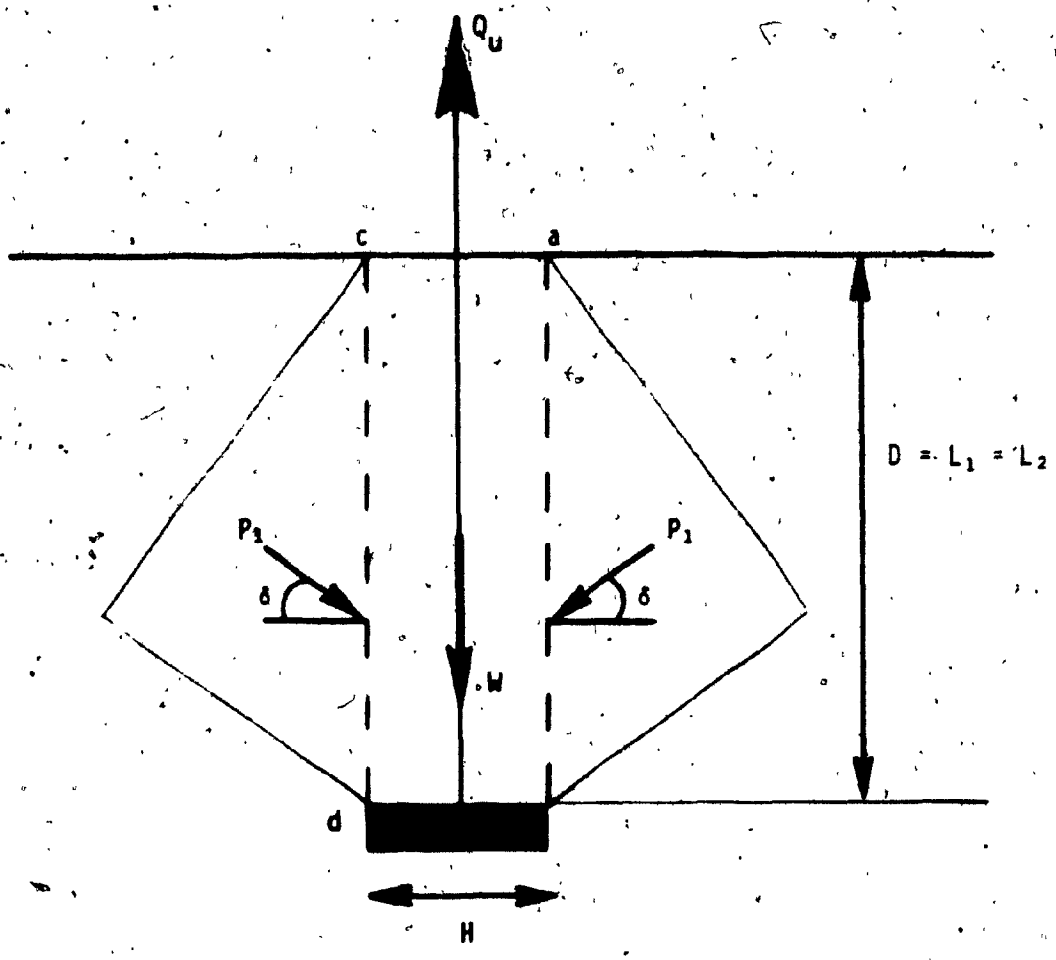

Figure 4.1: Stress Diagram - Strip Anchor Plate Under Vertical Load

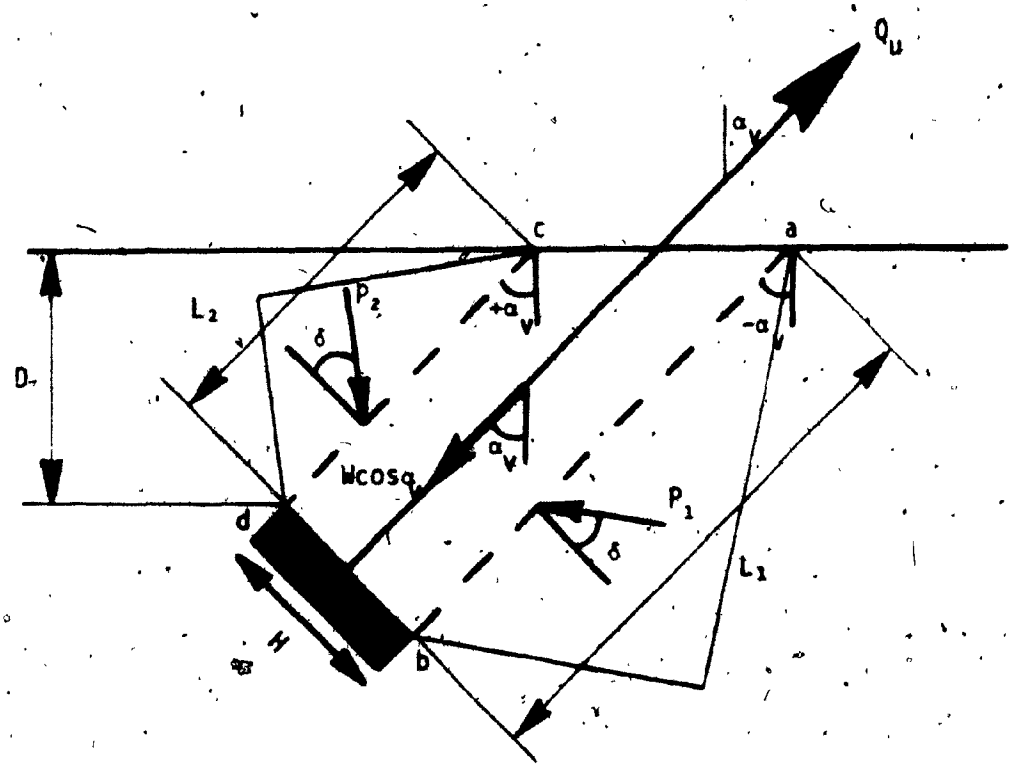

Figure 4.2-a: Stress Diagram - Strip Anchor Plate Under Inclined Load From Vertical

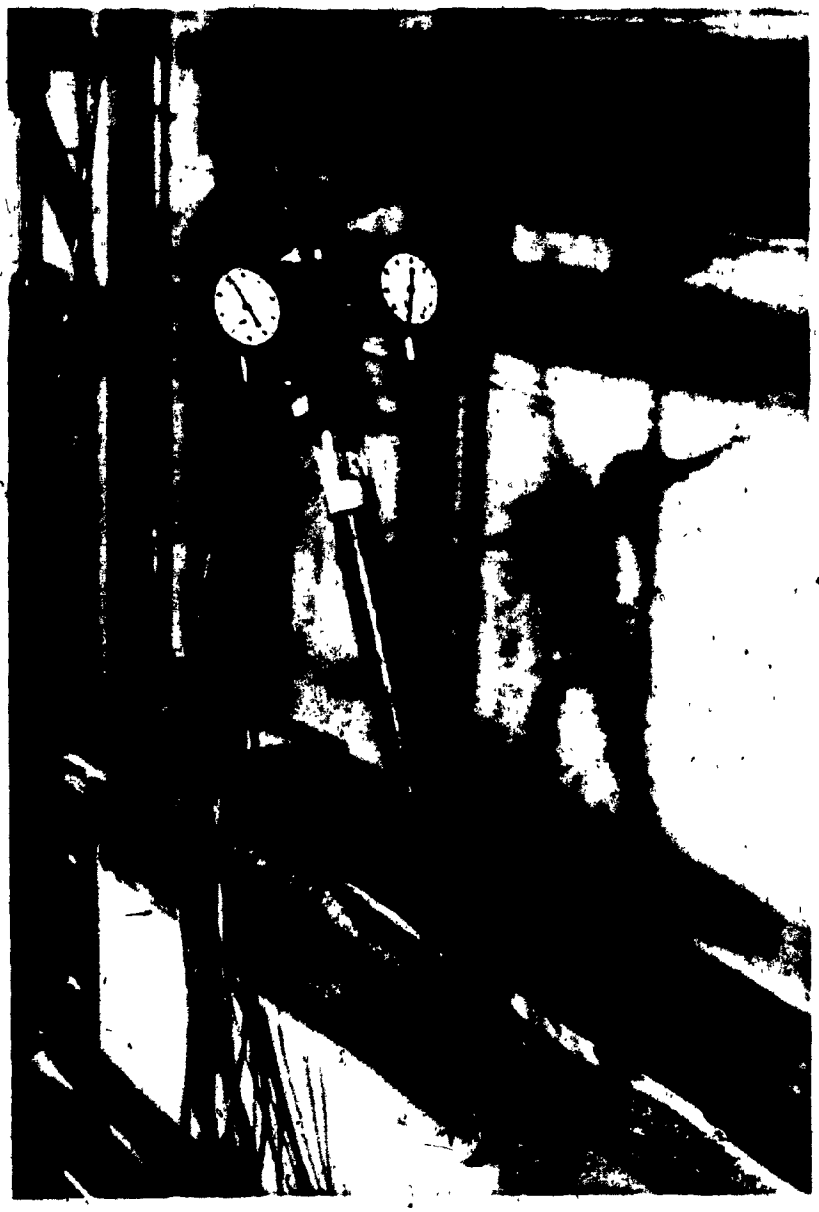

Figure 4.2-b: Experimental Setup of Anchor Subject to Inclined Load From Vertical Axis

equilibrium conditions must be satisfied in a direction normal to the failure plane. This condition is justifiable only if the mobilized passive pressures are the same on both sides of the assumed failure planes, so that the pressure on the plane inclined at $+\alpha$ dominates. The passive earth pressure coefficient $k_{p\gamma}$ due to weight component, as developed by Caquot and Kérisel (1948 and 1968), have been used for positive α for the case $\delta = \phi$. For the case of δ less than ϕ, the reduction factor R_γ, introduced by Caquot and Kérisel (1948 and 1968), has been applied. Since the failure mechanism varies extensively as the inclination of the anchor increases, we proceed to develop two equations as follows. Take the block (a b c d) of the dense sand (see Figures 4.2-a and 4.2-c) as a free body, and write the equilibrium equations of the external forces acting on this block and in the direction of the assumed failure plane. For the case of a strip anchor subjected to inclined pull from the vertical and horizontal axes, the equilibrium equations are respectively as follows:

$$Q_u = P_1 \sin\delta + P_2 \sin\delta + W\cos\alpha_v \quad (0 \leq \alpha_v \leq 45), \qquad 4.1$$

where Q_u = Ultimate pullout load,

$P_1 = 1/2\, R_\gamma\, k_{p\gamma} \cdot \gamma \cdot L_1^2$,

$P_2 = 1/2\, R_\gamma\, k_{p\gamma} \cdot \gamma \cdot L_2^2$,

α_v = Angle of applied load with the vertical axis,

δ = The average mobilized angle of shearing resistance on the assumed failure plane,

W = Weight of soil block ABCD and own weight of the anchor, and

γ = Initial Unit Weight of Sand;

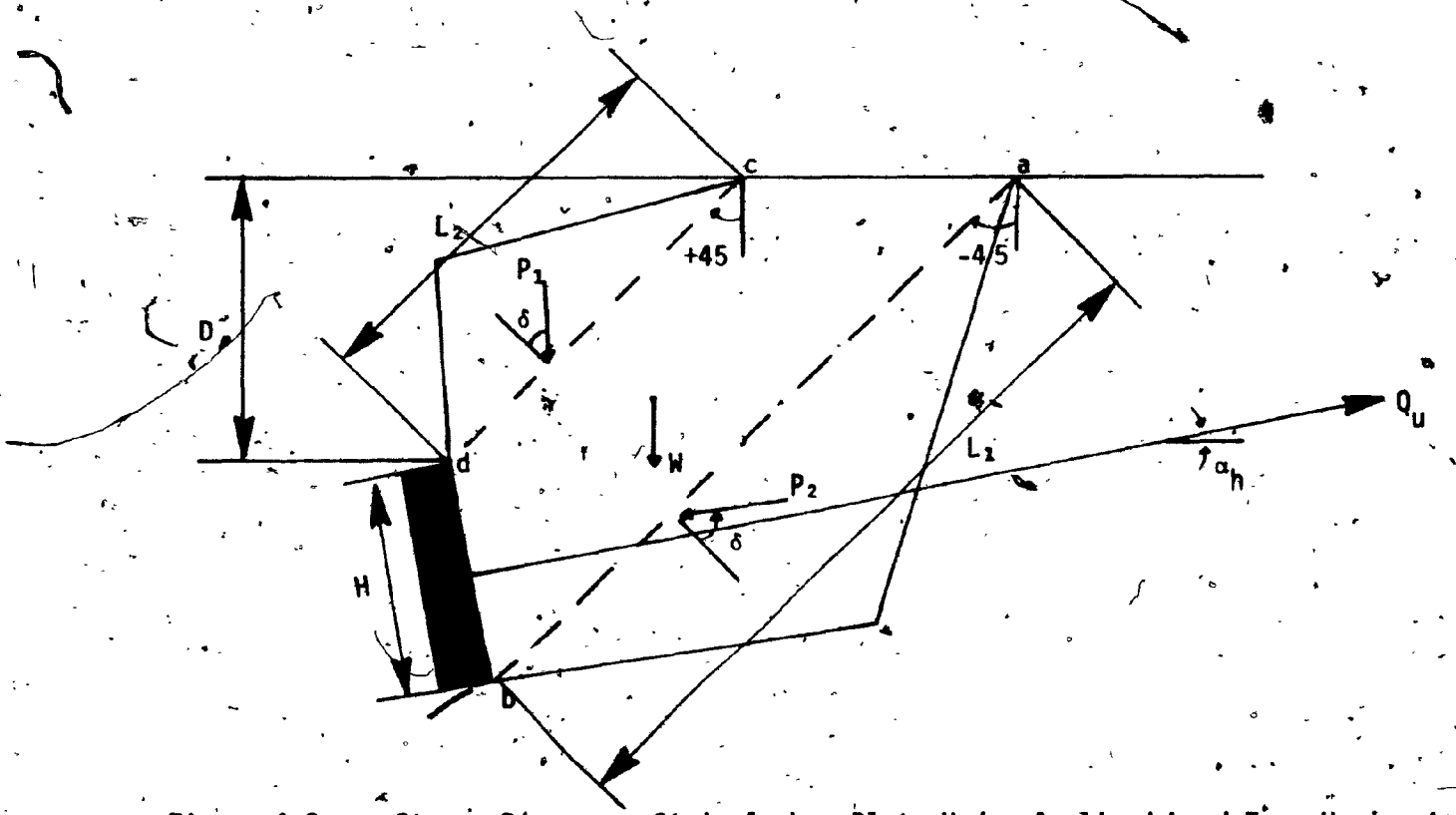

Figure 4.2-c: Stress Diagram - Strip Anchor Plate Under Inclined Load From Horizontal

and

$$Q_u \cos(45 - \alpha_h) = P_1 \sin\delta + P_2 \sin\delta + W \cos 45 \quad (0 \le \alpha_h \le 45), \qquad 4.2$$

where Q_u = Ultimate pullout load,

$P_1 = 1/2\, R_\gamma\, k_{p\gamma} \cdot \gamma \cdot L_1^2$,

$P_2 = 1/2\, R_\gamma\, k_{p\gamma} \cdot \gamma \cdot L_2^2$,

α_h = Angle of the applied load with the horizontal axis,

δ = The average mobilized angle of shearing resistance on the assumed failure plane,

W = Weight of the soil block ABCD and own weight of anchors, and

γ = Unit weight of dense sand.

Equations 4.1 and 4.2 are solved stepwise as follows:

(i) We rewrite Equation 4.1 as

$$\frac{Q_u - 1/2\,(L_1 + L_2) \cdot H \cdot \gamma \cdot \cos\alpha_v}{1/2\gamma\,(L_2^2 + L_1^2)} = k_{t\gamma}, \text{ where } k_{t\gamma} = R_\gamma\, k_{p\gamma} \sin\delta \qquad 4.3$$

(ii) The left-hand side of equation 4.3 is determined from the test data.

(iii) Appearing on the right side of Equation 4.3, $k_{t\gamma}$ is evaluated by assuming the values for δ/ϕ. Different values for δ/ϕ are substituted until both sides of Equation 4.3 are equal.

By employing Equations 4.1 and 4.2 as well as data from Figures 3.4-a to 3.4-e, the experimental δ/ϕ were computed, which yielded the experimental values of $k_{t\gamma}$.

It is evident from Figure 4.5 that the ratio δ/ϕ and consequently the coefficient $k_{t\gamma}$ is an increasing function of α_v (inclination of load from the vertical axis). This increasing nature indicates that the actual and assumed failure planes approach each other as the inclination increases. From Figure 4.5, it is also clear that the deduced ratio δ/ϕ from the present experimental investigation is usually less than unity. For a constant angle of friction ϕ, this ratio depends primarily on the inclination angle and to a lesser extent on the depth. These behaviors are explained as follows:

1. If the analyses is made on the actual plane AB of failure (see Figure 4.3), then the angle of friction δ will be equal to ϕ. On the other hand, if the analyses is made on the assumed plane AC, then the angle of friction δ mobilized must be less than ϕ, since failure has not taken place on the assumed planes (Hanna 1978).

2. The shear failure in the soil in front of the anchor is a phenomenon of progressive rupture at variable stress levels (Muhs 1965 and Hanna 1978). Thus, when the slip line AB

(see Figure 4.3) reaches B, it mobilizes the peak shear strength at point B and hence the soil strength at the beginning of the slip line (point A) must be less than that at B. In other words, the angle of shearing resistance at point A is less than that at point B. This behaviour is reflected in the δ values.

3. The mobilized passive earth pressure on the assumed failure plane is an increasing function of the inclination angle of the axial load (from the vertical). This is due to the fact that with increasing inclination, the assumed planes and actual failure planes approach each other. Therefore, the lateral movement causes maximum mobilization of the passive pressure (corresponding to the angle of shearing resistance ϕ).

Mathematical verification of these arguments is cumbersome and perhaps impossible. An obstacle is the separation of the preceding effects (1 to 3) for the purpose of evaluating the average mobilized angle of shearing resistance δ and consequently, the mobilized passive pressure on the assumed failure planes. However, such difficulties may be overcome by the following assumptions. First, assume the average angle of shearing resistance δ to be less than the angle of shearing resistance ϕ ; and secondly, angle δ is directly proportional to ϕ. Thus, the conclusions in arguments 1, 2 and 3 become valid in these analyses. These δ/ϕ values are determined experimentally for design purpose as shown in Figure 4.5. It may be added that the ratio δ/ϕ tends to

unity as the inclination of the anchor increases. This is explained by the fact that the assumed planes and true failure planes approach each other. On these planes, therefore, the mobilized angle of shearing resistance δ equals the angle of shearing resistance ϕ of the soil - i.e., $\delta/\phi = 1$.

Based on the fact that the locally mobilized angle of shearing resistance δ_z on the assumed plane at point A equals the angle of shearing resistance (since it is located on the assumed as well as on the real failure planes), we argue as follows. Moving upward from the point A to C on the assumed plane, the angle δ_z decreased to the minimum value of $\lambda\phi$ at the point C on the soil surface, where λ depends on the inclination of the anchor. Hence, the variation of the locally mobilized angle of shearing resistance δ_z in terms of depth z is linear or non-linear as depicted by curves (1), (2) and (3) respectively (see Figure 4.3).

In order to predict the distribution of the locally-mobilized angle of shearing resistance δ_z on the assumed planes, together with the value of the coefficient λ, a computer program was developed to perform such analyses. In each case, the total passive earth pressure P_p was calculated from the following equation:

$$P_p = \int_0^{L_f} \gamma \, k_{pz} \, z \, dz \qquad 4.4$$

The value of P_p that was determined from Equation 4.4 was later equated to the value given by Equations 4.1 and 4.2 in order to determine the average mobilized angle of shearing resistance δ. The solution was conducted by trial and error, assuming a value of δ and then determining the corresponding value of k_p from the tables of Caquot and Kérisel until both sides agreed.

A comparison between the deduced angle of shearing resistance δ, from experimental data with the theoretical values will enable the determination of the existing δ_z distribution together with the corresponding value of the coefficient λ.

Trial calculations using values 0, 0.1, 0.2,...; 1.0 for λ indicate that the relationship represented in curve no. 1 (see Figure 4.3) overestimates the average mobilized angle of shearing resistance δ along the assumed plane AC with respect to the deduced values from the present investigation. After several trials on different curves with factor λ ($0 \leq \lambda \leq 1$), the deduced average angles of shearing resistance may be evaluated provided the following two conditions:

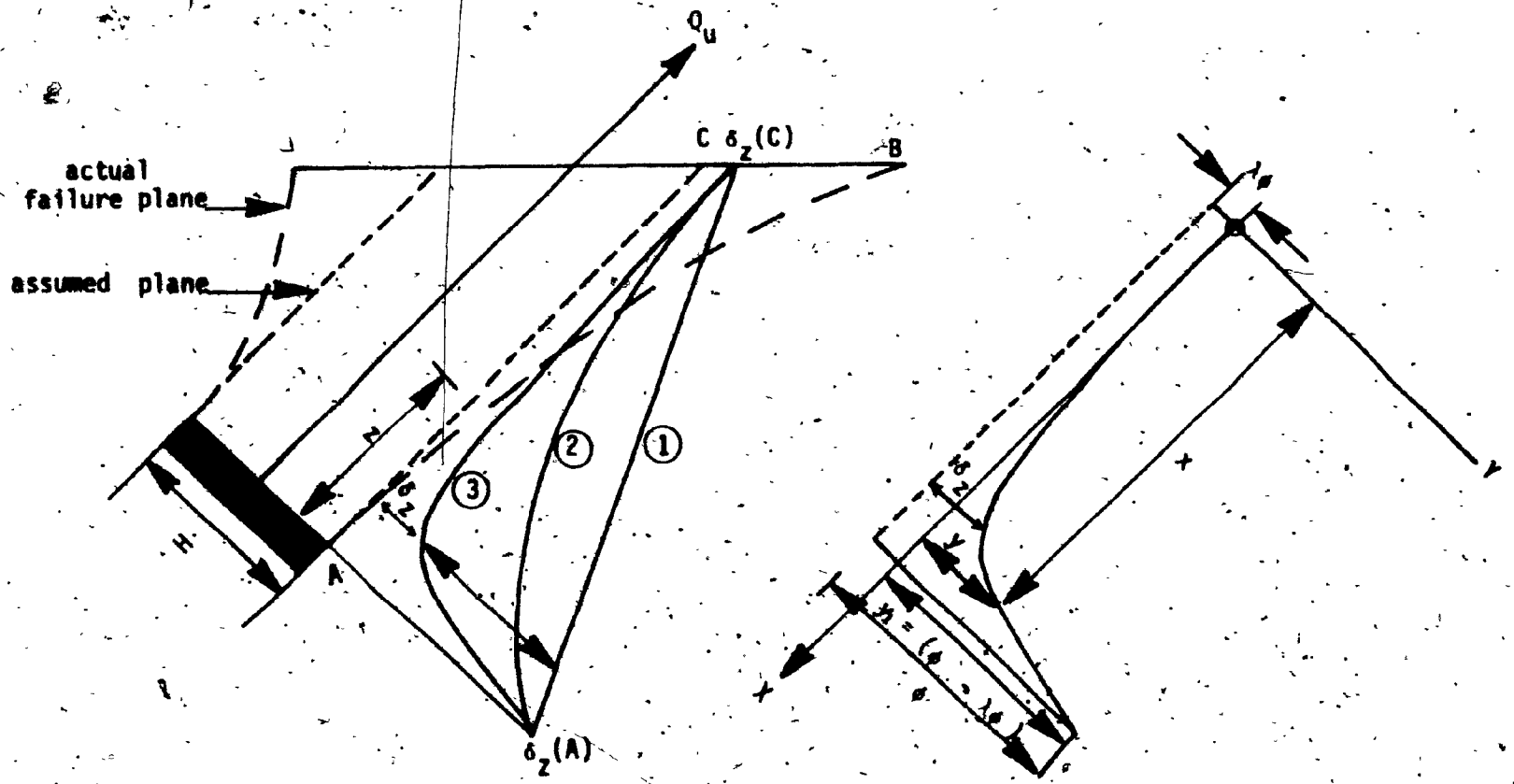

Figure 4.3: Distribution of the Local Angle of Shearing Resistance on the Assumed Failure Plane

(1) λ is assumed to be a function of the angle of friction and anchor inclination, where

$$\lambda = (\alpha_v/90)^3 + e^{-5\tan\phi}. \qquad 4.5$$

(2) Relationship represented by curve no. 3 is a hyperbola with equation

$$y = \frac{ax}{1 - bx} \qquad 4.6$$

having origin at the soil interface, where the assumed failure plane and the interface plane are assigned by the x-y axes respectively and constants a and b given by

$$a = \frac{\phi}{\beta} \qquad b = \frac{1}{\beta}.$$

In addition, an alternate suitable form for the localized angle δ_z of friction was found to be

$$y = \frac{ax^2}{1 + bx^2} \qquad 4.7$$

The test results, compared with the theory, are given in Figures 4.4-a and 4.4-b for strip anchors. These figures show the variation of the ultimate pullout capacity with angle of inclination. As would be expected, the observed pullout capacity increases with increasing inclination from the vertical.

The computer program referred to earlier was used again utilizing Equations 4.5 and 4.6 which express the distribution of the locally-mobilized angle of shear resistance δ_z and the coefficient λ. The purpose of this procedure was to determine the average mobilized angle of shearing resistance δ for given angles of shearing resistance.

It is interesting to note in Figure 4.5 that the δ/ϕ values tend to unity where the assumed planes approach the actual failure planes very closely. Thus, the average mobilized angle of shearing resistance on these planes must be equal to the angle of shearing resistance of the soil, i.e. $\delta/\phi = 1$. Setting $k_s \sin\phi = k_p \sin\delta$ in which k_s = the uplift coefficient, and substituting into Equations 4.1 and 4.2 leads to:

$$Q_u = 1/2\gamma\, k_s \sin\phi\, (L_1^2 + L_2^2) + 1/2\,(L_1 + L_2)\, H\gamma \cos\alpha_v \quad 0 \le \alpha_v \le 45 \qquad 4.8$$

and

$$Q_u = \frac{1/2\,\gamma k_s \sin\phi\,(L_1^2 + L_2^2) + 1/2\,(L_1 + L_2)\,\gamma H \cos(45 - \alpha_h)\cos 45}{\cos(45 - \alpha_h)}, \quad 0 \le \alpha_h \le 45 \qquad 4.9$$

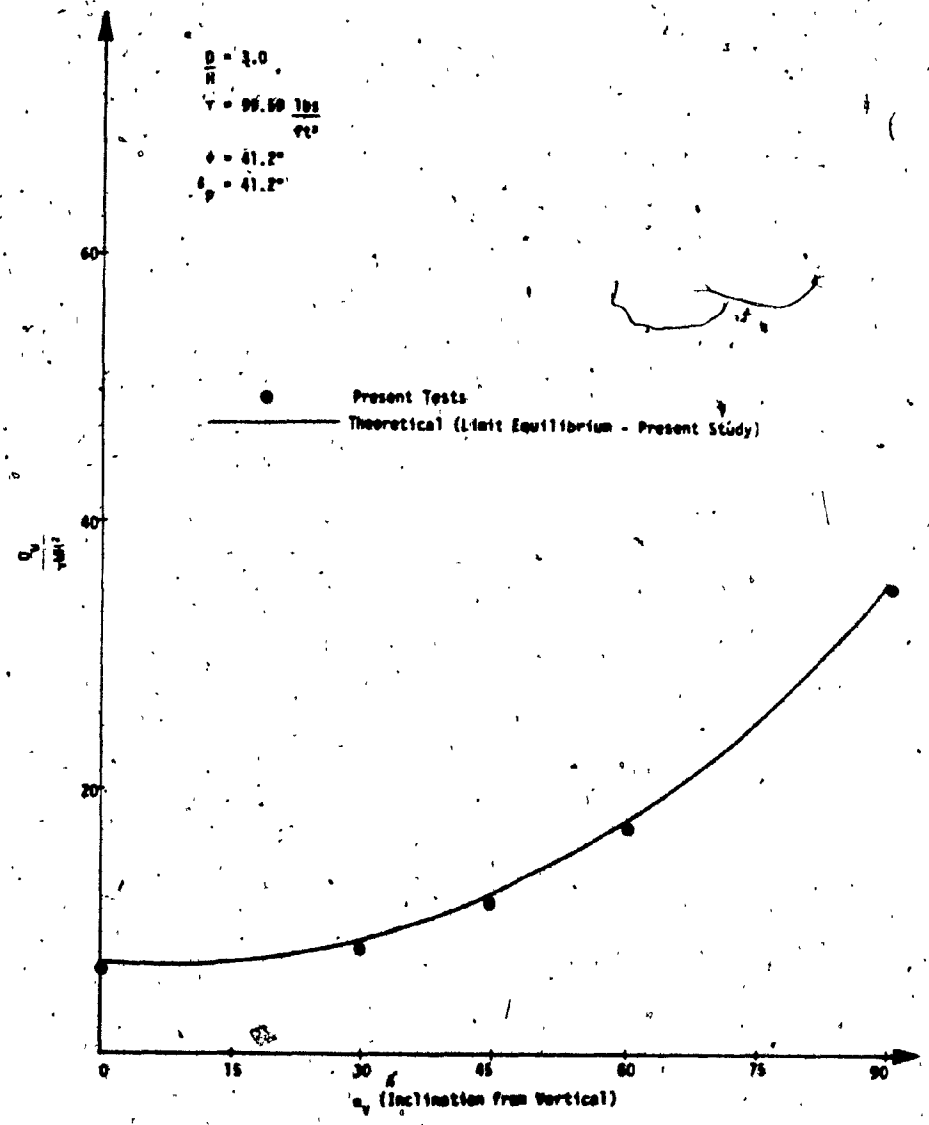

Figure 4.4-a: Present Tests Versus Theoretical (Limit Equilibrium - Present Study)

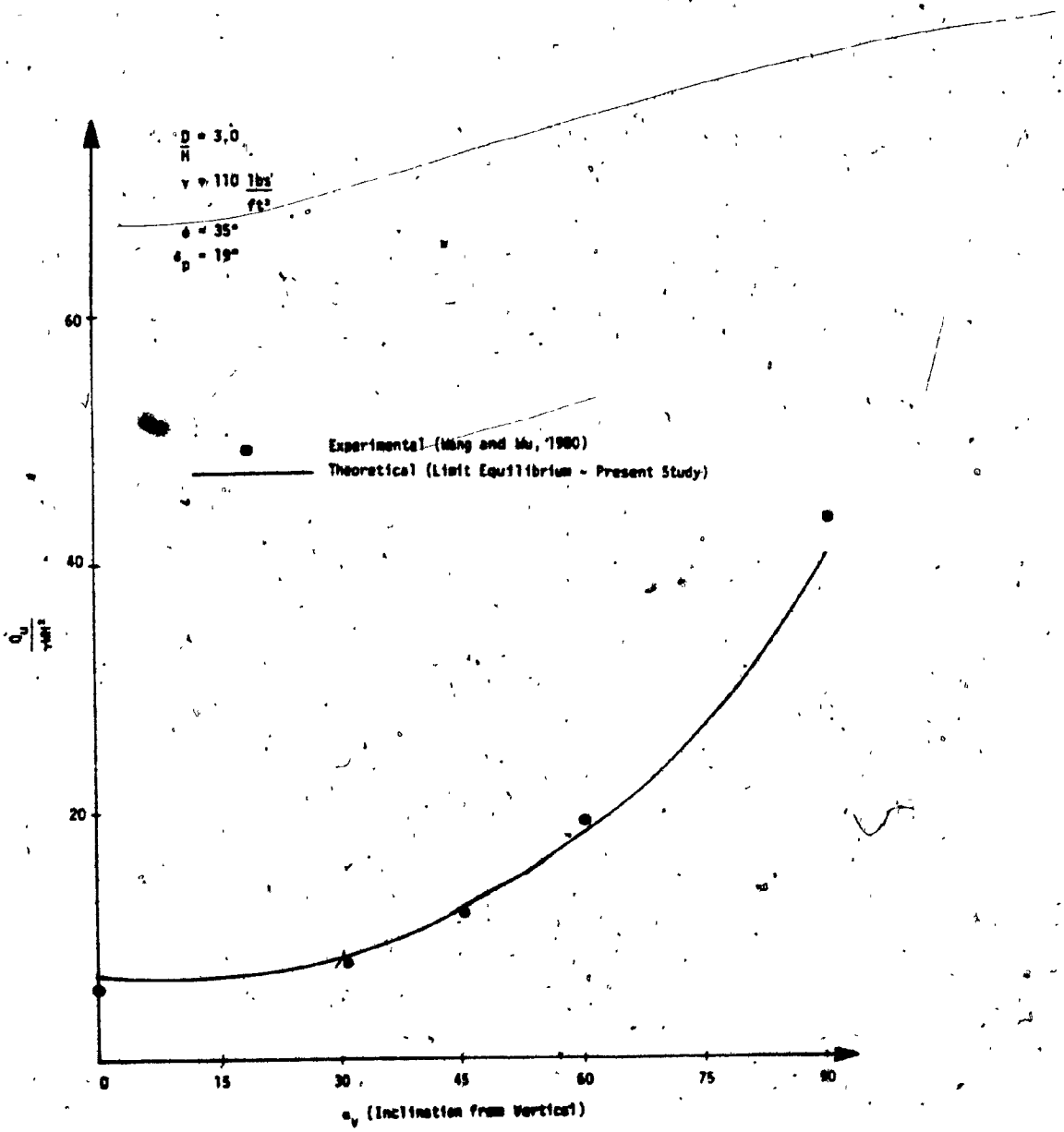

Figure 4.4-b: Experimental (Wang & Wu, 1980) Versus Theoretical (Limit Equilibrium - Present Study)

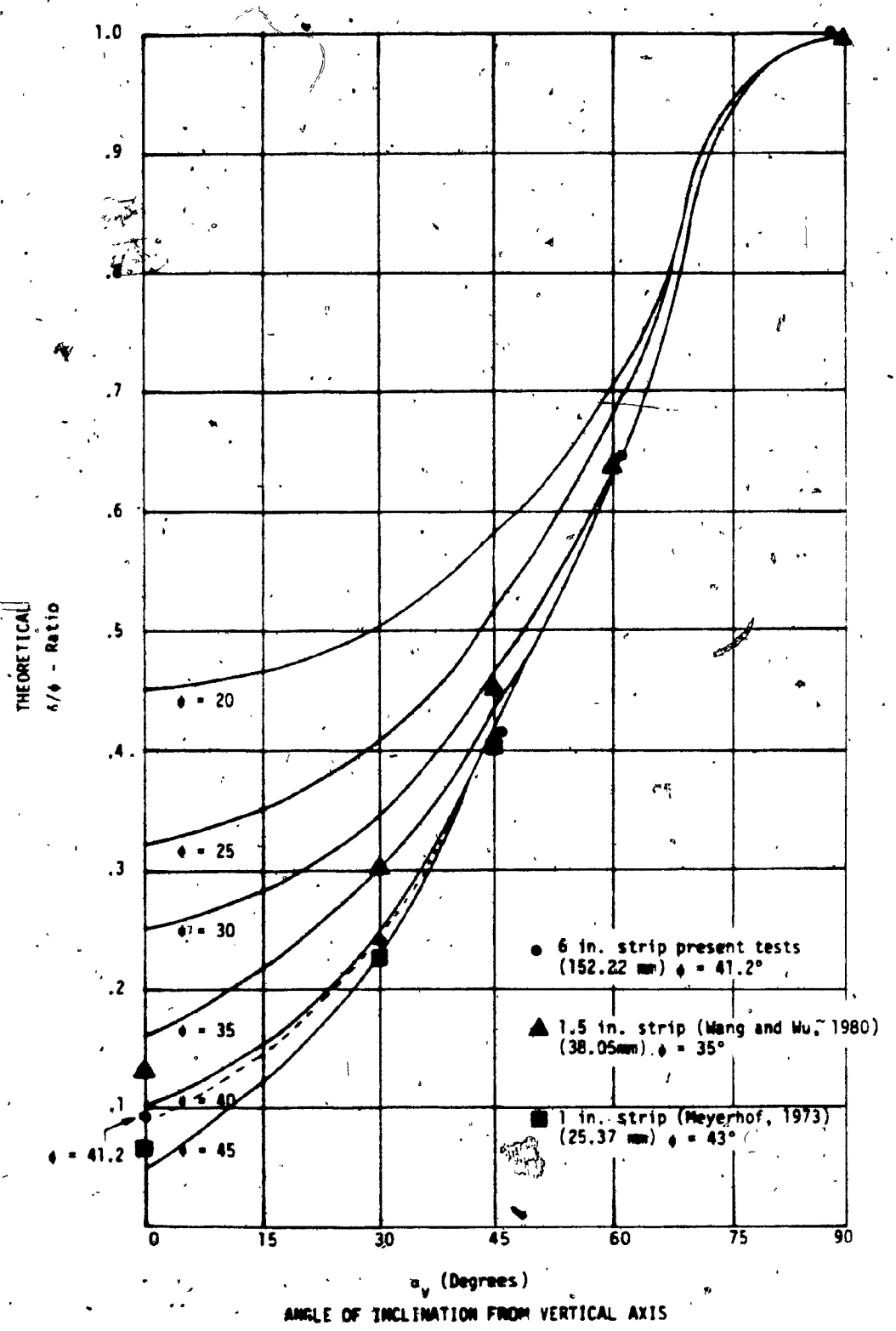

Figure 4.5: δ/ϕ Ratios for Strip Anchors in Sand

A theoretical (limit equilibrium) and experimental investigation of the ultimate pullout capacity on strip anchors has been presented.

From the design chart introduced (see Figure 4.6), the uplift coefficient can be determined from known values of the angles of shearing resistance ϕ. These angles may be determined from plane strain shear test results, however, for conservative design, shear box test results may be used. The uplift coefficient can be used in conjunction with the proposed ultimate pullout capacity equations (4.8 and 4.9) to predict the ultimate pullout capacity of a strip anchor.

The theory given in this section may also be utilized to determine the depth of sand provided artificially to increase the ultimate pullout load to a desired design value.

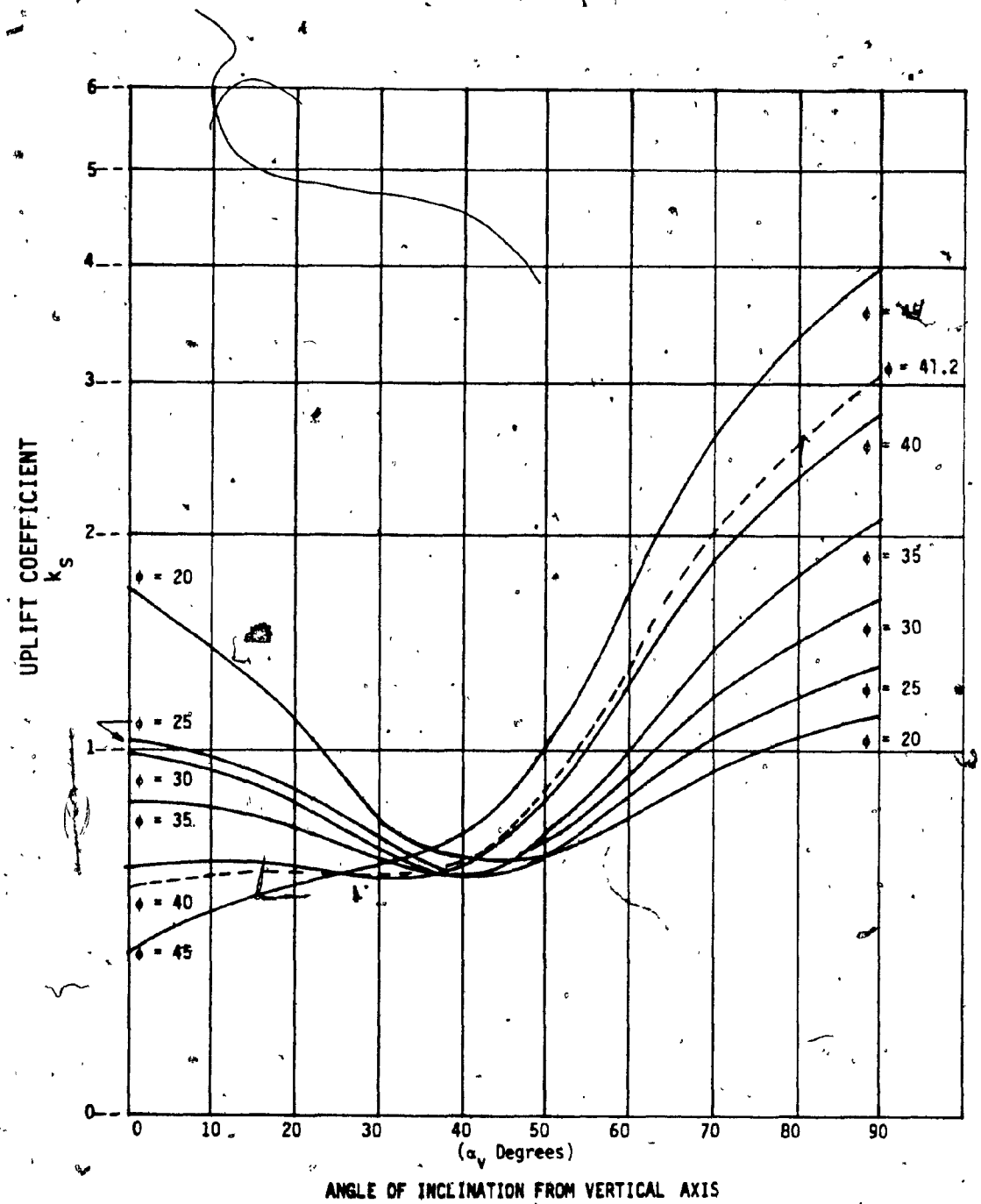

Figure 4.6: Design Chart for Determining Uplift Coefficient k_s

CHAPTER 5

THEORETICAL ANALYSES (UPPER BOUND LIMIT ANALYSES)

For a given failure mechanism described by n independent parameters, the ultimate load of the anchor is

$$Q_u = \min \left\{ 1/2\ \gamma\ H^2\ k_{p\gamma}(\theta_1, \theta_2, \ldots \theta_n) : \right.$$
$$\left. \theta_i \text{ suitably constrained } (1 \le i \le n) \right\}, \qquad 5.1$$

where $k_{p\gamma}$ represents the effects of weight. Because H and γ are independent of θ_i $(1 \le i \le n)$, the above minimization reduces to

$$Q_u = 1/2\ \gamma\ H^2 \min \left\{ k_{p\gamma}\ (\theta_1, \theta_2, \ldots \theta_n) \right\}. \qquad 5.2$$

The Multi-Stage Monte-Carlo Optimization Technique, henceforth referred to as MSMCO, shall yield the corresponding critical load. Based on the preceding laboratory study, the failure mechanism is representable by means of a triangle-quadrilateral mechanism (see Figures 5.1-a and 5.1-b), wherein, for simplicity sake, the modified convention of Chen (1975) is used.

An anchor with a friction angle δ_p less than ν is called smooth, whereas an anchor with an angle δ_p greater than or equal to ν is called rough, where ν is the angle of dilatancy. Moreover, we call particular cases "perfectly smooth" or "perfectly rough" according as $\delta_p = 0$ or $\delta_p = \nu$ respectively.

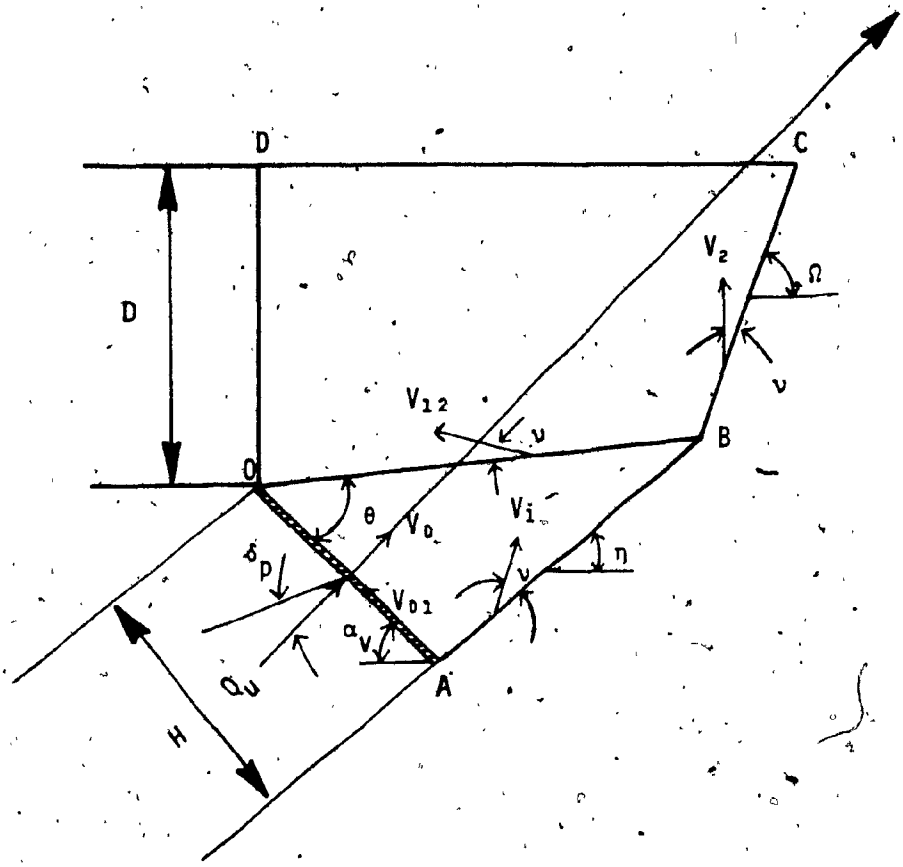

Figure 5.1-a: Smooth Anchor

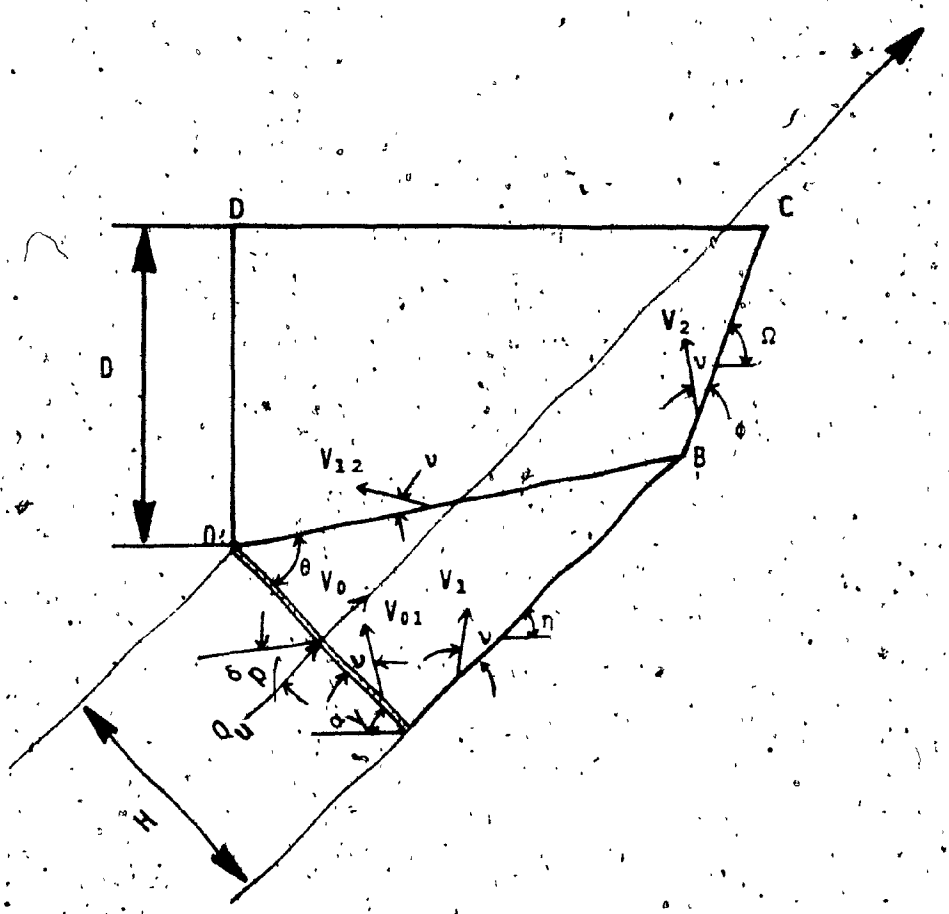

Figure 5.1-b: Rough Anchor

In addition, we note that the rate of external work due to self-weight in any region, is the product of the vertical component of velocity (in that region) with the weight of the region. Denoting the external work performed by regions OAB, OBCD and by the moving anchor load by W_{OAB}, W_{OBCD} and $W_{m.a.l.}$ respectively, we have

$$W_{OAB} = \frac{-1/2\gamma \; H^2 \; V_1 \sin\theta \sin(\alpha_v + \eta) \sin(\nu + \eta)}{\sin(\alpha_v + \eta - \theta)}$$

$$W_{OBCD} = -1/2\gamma \; H^2 \; V_2 \left\{ \frac{2D \cos(\alpha_v - \theta) \sin(\alpha_v + \eta)}{H \sin(\alpha_v + \eta - \theta)} + \right.$$

$$\frac{\cos(\alpha_v - \theta) \sin^2(\alpha_v + \eta) \sin(\alpha_v - \theta)}{\sin^2(\alpha_v + \eta - \theta)} +$$

$$\left. \left[\frac{D + \sin(\alpha_v + \eta) \sin(\alpha_v - \theta) H}{\sin(\alpha_v + \eta - \theta)} \right]^2 \frac{\mathrm{ctg}\Omega}{H^2} \right\} \sin(\nu + \Omega)$$

and

$$W_{m.a.l.} = Q_u V_o \; .$$

For a smooth anchor ($\delta_p \leq \nu$) the dissipation of energy through sliding friction is

$$V_{01} \; Q_u \tan \delta_p$$

However, for a rough anchor ($\delta_p \geq \nu$), the dissipation of energy for cohesionless soil is zero. After utilizing suitable velocity diagrams (see Figure 5.1-c), all velocities of the mechanism are expressible in terms of the anchor translational velocity V_0. If V_1 and V_2 denote the region velocities of OAB and OBCD respectively, then "for the case of smooth anchors ($\delta_p < \nu$)".

$$V_1 = \frac{V_0}{\sin (\nu + \eta + \alpha_v)}$$

$$V_2 = \frac{\sin (2\nu + \eta + \alpha_v + \theta)}{\sin (2\nu + \Omega + \alpha_v - \theta) \sin (\nu + \eta + \alpha_v)}$$

$$V_{01} = -\text{ctg} (\nu + \eta + \alpha_v) V_0$$

and

$$V_{12} = \frac{\sin (\Omega - \eta) V_0}{\sin (2\nu + \Omega + \alpha_v - \theta) \sin (\nu + \eta + \alpha_v)}$$

SMOOTH ANCHORS $\delta_p < \nu$

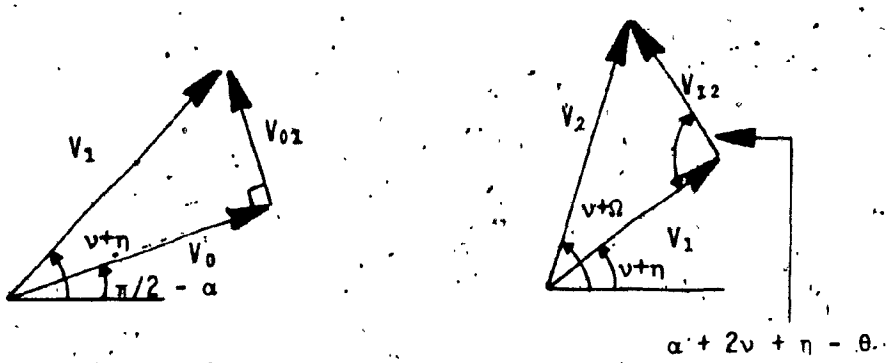

ROUGH ANCHORS $\delta_p \geq \nu$

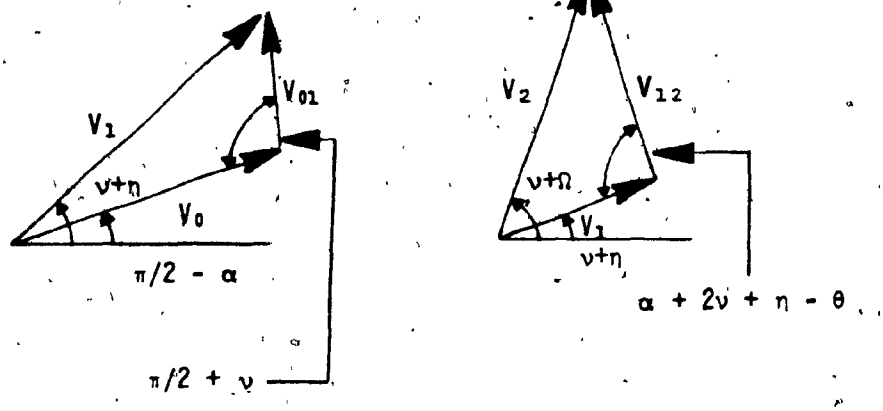

Figure 5.1-c: Velocity Diagrams

where V_{01} stands for the relative velocity between region OAB and the anchor, and V_{12} is the relative velocity between regions OAB and OBCD. On the other hand, however, for the case of rough anchors ($\delta_p \geq \nu$), the above-defined velocities assume the following formulas:

$$V_1 = \frac{\cos\nu \, V_0}{\sin(2\nu + \eta + \alpha_v)}$$

$$V_2 = \frac{\sin(\alpha_v + 2\nu + \eta - \theta)\cos\nu \, V_0}{\sin(2\nu + \Omega + \alpha_v - \theta)\sin(2\nu + \eta + \alpha_v)}$$

$$V_{01} = \frac{-\cos(\nu + \eta + \alpha_v) V_0}{\sin(2\nu + \eta + \alpha_v)}$$

and

$$V_{12} = \frac{\sin(\Omega - \eta)\cos\nu \, V_0}{\sin(2\nu + \Omega + \alpha_v - \theta)\sin(2\nu + \eta + \alpha_v)}$$

In consequence of the Plastic Limit Theorem, we equate the rate of external work to the rate of internal energy dissipation and, thus, obtain for a smooth anchor ($\delta_p < \nu$):

$$k_{pr} = \left\{ \frac{\sin\theta \sin(\alpha_v + \eta) \sin(\nu + \eta)}{\sin(\alpha_v + \eta - \theta) \sin(\nu + \eta + \alpha_v) \left[\tan\delta_p \operatorname{ctg}(\nu + \eta + \alpha_v) + 1.0\right]} + \right.$$

$$\left[\frac{2D \cos(\alpha_v - \theta) \sin(\alpha_v + \eta)}{H \sin(\alpha_v + \eta - \theta)} + \right.$$

$$\frac{\cos(\alpha_v - \theta) \sin^2(\alpha_v + \eta) \sin(\alpha_v - \theta)}{\sin^2(\alpha_v + \eta - \theta)} + \left[\frac{D}{H}\right]^2 \operatorname{ctg}\Omega +$$

$$\left. \frac{2D \sin(\alpha_v + \eta) \sin(\alpha_v - \theta) \operatorname{ctg}\Omega}{H \sin(\alpha_v + \eta - \theta)} + \frac{\sin^2(\alpha_v + \eta) \sin^2(\alpha_v - \theta) \operatorname{ctg}\Omega}{\sin^2(\alpha_v + \eta - \theta)} \right]$$

$$\left. \left[\frac{\sin(\alpha_v - \theta + 2\nu + \eta) \sin(\nu + \Omega)}{\sin(\Omega + 2\nu + \alpha_v + \eta) \sin(\nu + \eta + \alpha_v) \left[\tan\delta_p \operatorname{ctg}(\nu + \eta + \alpha_v) + 1.0\right]} \right] \right\}$$

5.3

and for a rough anchor ($\delta_p \geq \nu$)

$$k_{p\gamma} = \left\{ \frac{\sin\theta \sin(\alpha_v + \eta) \sin(\nu + \eta) \cos\nu}{\sin(\alpha_v + \eta - \theta) \sin(2\nu + \eta + \alpha_v)} + \left[\frac{2D \cos(\alpha_v - \theta) \sin(\alpha_v + \eta)}{H \sin(\alpha_v + \eta - \theta)} + \right.\right.$$

$$\frac{\cos(\alpha_v - \theta) \sin^2(\alpha_v + \eta) \sin(\alpha_v - \theta)}{\sin^2(\alpha_v + \eta - \theta)} + \left[\frac{D}{H}\right]^2 \operatorname{ctg}\Omega +$$

$$\left. \left. \frac{2D \sin(\alpha_v + \eta) \sin(\alpha_v - \theta) \operatorname{ctg}\Omega}{H \sin(\alpha_v + \eta - \theta)} + \frac{\sin^2(\alpha_v + \eta) \sin^2(\alpha_v - \theta) \operatorname{ctg}\Omega}{\sin^2(\alpha_v + \eta - \theta)} \right] \right.$$

$$\left. \left[\frac{\sin(\alpha_v + 2\nu + \eta - \theta) \cos\nu}{\sin(\Omega + 2\nu + \alpha_v - \theta) \sin(2\nu + \eta + \alpha_v)} \right] \right\}$$

5.4

The respective critical loads for smooth ($\delta_p < \nu$) and rough ($\delta_p \geq \nu$) anchors is obtained by minimizing the respective expressions for k_{pY} with respect to the parameters θ, η and Ω of the mechanism subjected to the following constraints:

$$(D + H \sin \alpha_v) - \frac{H \sin \theta \sin \eta}{\sin (\alpha_v + \eta - \theta)} > 0 ,$$

$$\nu + \eta > 90 - \alpha_v$$

and

$$\eta > \Omega .$$

This was achieved via the complete search of feasible solutions through the technique MSMCO. This entailed the construction of sufficiently large rectangles inside the feasible solution region. Within these rectangles, hundreds of feasible random solutions were read, the best minimum results were stored and rectangles were recentered. For these new recentered rectangles, the above search procedure was repeated to obtain better minimums. This entire process was iterated 20 times to obtain the numerical results stated in this thesis (see Appendix).

Theoretical results for the special case of a horizontal anchor at the soil surface (vertical wall) show good agreement with the classical earth pressure theories (see Table 5.1). It could be observed that the passive pressure coefficient increases rapidly with the friction angle ϕ. For high values of this angle ($\phi \geq 40°$), the value of the coefficient is not in full agreement with the classical earth pressure theories. This can be explained by the fact that the generated soil particle displacement pattern, conventionally referred to as the velocity field, is different from the stress characteristics pattern on which the stresses have maximum obliquity of the angle ϕ. As reported by Poorooshasb (1967), the overall shape of the stress characteristics pattern is similar to the shape of the velocity characteristics but bigger, for the passive case. This is due to the dilation angle ν of the soil which is generally smaller than the internal frictional angle ϕ. It is found that the effect of dilatancy on earth pressure coefficients increases rapidly with the friction angle ϕ. In practice, however, the value of ν of soil generally increases with ϕ only to a maximum of about $\nu = \phi/2$ for very dense soils, when the earth pressure coefficients are roughly midway between the lower limit $\nu = 0$ and the upper limit for $\nu = \phi$.

Results of the theoretical analyses are compared with the experimental data. The results are well within the bounds of $\nu = \phi$ and $\nu = \phi/2$ (see Figures 5.2-a and 5.2-b). This indicates that, indeed, the velocity field is different from the stress characteristics and that

ϕ_o	δ_p	Caquot & Kérizel	Chen	Coulomb	Sokolovskii	Present Theory	
						$\delta_p < \phi$	$\delta_p \geq \phi$
0	0	1.00	1.00	1.00	1.00	1.00	
10	0	1.42	1.42	1.42	1.42	1.42	
10	5	1.55	1.56	1.57	1.56	1.55	
10	10	1.64	1.68	1.73	1.66	1.65	1.70
20	0	2.04	2.04	2.04	2.04	2.04	
20	10	2.59	2.58	2.63	2.55	2.54	
20	20	3.01	3.17	3.52	3.04	2.98	3.31
30	0	3.00	3.00	3.00	3.00	3.00	
30	15	4.78	4.71	4.98	4.62	4.55	
30	30	6.42	7.10	10.10	6.55	6.29	7.14
40	0	4.59	4.60	4.60	4.60	4.59	
40	20	10.36	10.10	11.77	9.69	9.50	
40	40	17.50	20.90	---	18.20	23.23	25.49

Table 5.1: Earth Pressure Coefficient $k_{p\gamma}$ For a Vertical Wall and Horizontal Soil Surface

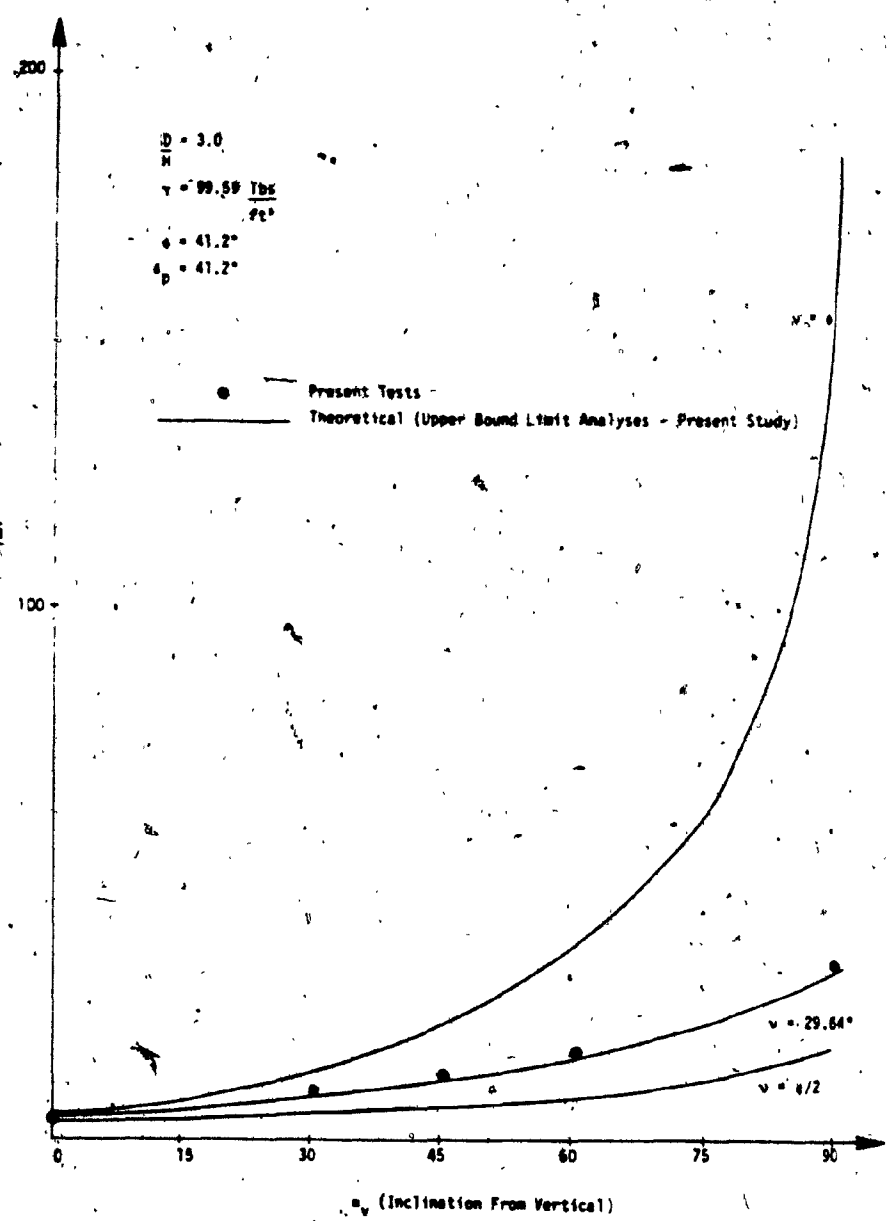

Figure 5.2-a: Test Results - Present Tests Versus Present Study (Upper Bound Limit Analyses)

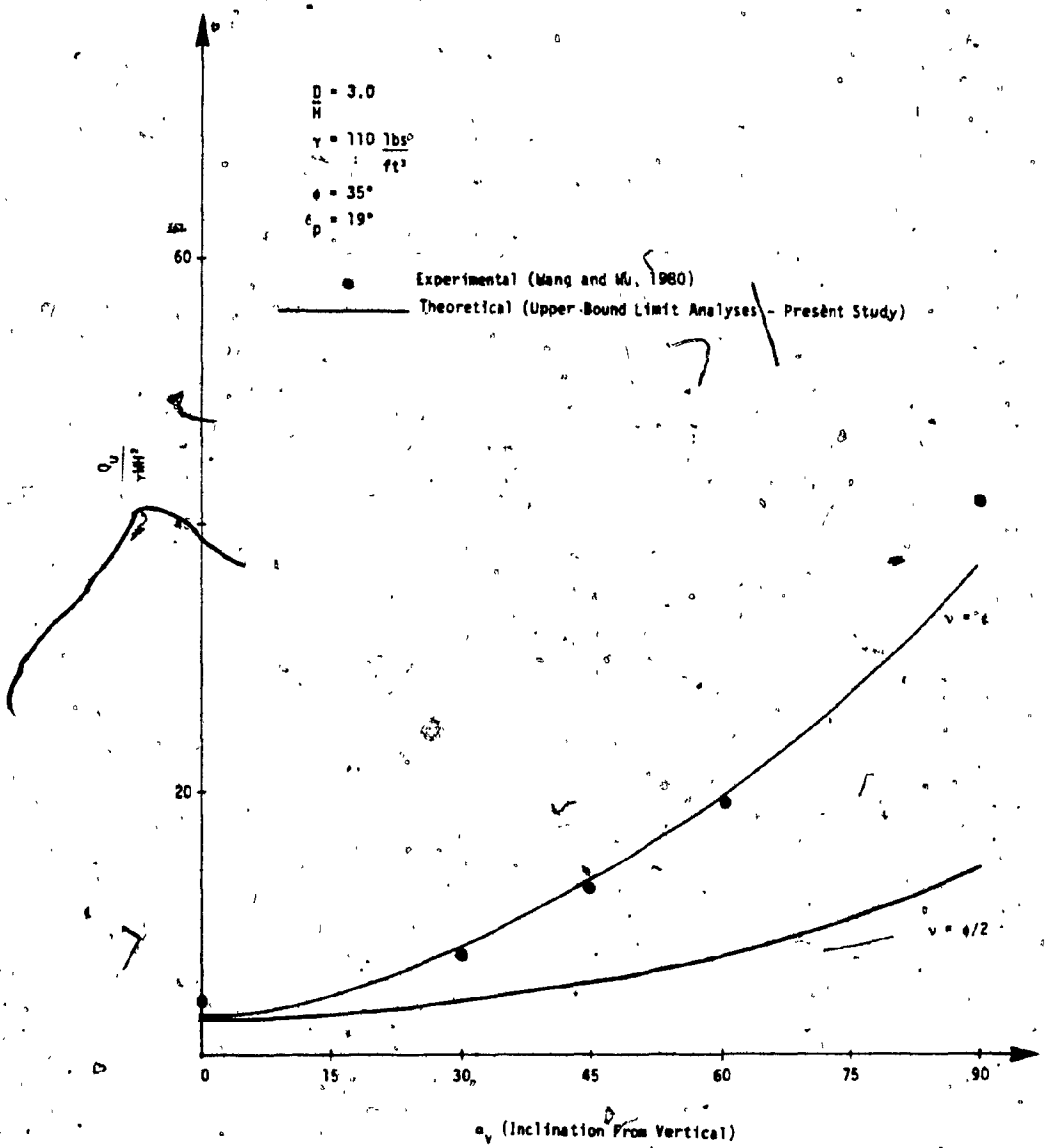

Figure 5.2-b: Test Results - Experimental (Wang & Wu, 1980) versus Theoretical (Present Study - Upper Bound Limit Analyses)

the difference is more pronounced as the angle ϕ increases. For low friction angles, the difference is less significant (see Table 5.1). The data agrees fairly well with the theory when the angle of dilatancy is used (see Figure 5.2-a).

One can conclude from the test results that for a constant D/H ratio, the pullout resistance increases with an increase in the angle of inclination. This behavior was also confirmed by the theory. It can be attributed to the fact that the surface of shear enlarges as the anchor inclination increases. From Figures 5.1-a and 5.1-b, one can see that as the angle increases, the difference in the extent of the ruptured soil zone becomes more pronounced.

CHAPTER 6

CONCLUSION

The pullout capacity of inclined anchors in sand investigated theoretically, as well as experimentally, was theoretically derived via the methods of upper bound limit analyses and limit equilibrium. The results of the analyses strongly agree with the obtained experimental data. The conclusions for the experimental study of the model anchor plate are as follows:

1- The pressure distribution on the face of the plate corroborates other previously well-established results, although some insignificant deviations are present.

2- There is no significant difference between the initial pressure distribution of the tests and in the stages of soil failure.

3- The graph of the pressure distribution is invariant with respect to increase of pullout load and displacement of the plate.

4- For ratio D/H fixed, the pullout resistance increases as the angle of inclination from vertical increases.

5- The rate of increase in pullout capacity increases as the inclination angle from the vertical increases.

6- The contribution from the side effect in plane strain tests becomes more significant as the inclination angle from the vertical increases.

7- The rotational behavior of the anchor plate tested in this thesis was not studied in detail. It should be noted that the passive resistance of an anchor plate has some significant effect on the rotational stability of the plate.

Thus, further studies are required to investigate the effect of anchor embedment, angle of shearing resistance of the soil and anchor soil friction. Also, the rotational behavior of the anchor plate should be investigated.

REFERENCES

1 - Adams, J.I. and Hayes, D.C. (1967). "The Uplift Capacity of Shallow Foundations", Ontario Hydro Research Quarterly, 19,1.

2 - Adams, J.I. and Klym, T.W. (1972). "A Study of Anchorages for Transmission Tower Foundations", Canadian Geotechnical Jnl, Vol 9, p. 89.

3 - Afram, A. (1984). "Pullout Capacity of Battered Piles in Sand", M. Engr. Thesis, Concordia University, Montreal, Canada.

4 - Arthur, J.R.F. and Roscoe, K.H. (1965). "An Examination of Edge Effects in Plane Strain Model Earth Pressure Tests", Proc. 6th Int. Conf. on Soil Mech. 2, pp. 363-368.

5 - Baker, W.H. and Kondner, R.L.(1966). "Pullout Load Capacity of a Circular Earth Anchor Buried in Sand", Highway Research Record 108.

6 - Balla, A. (1961). "The Resistance to Breaking Out of Mushroom Foundations for Pylons", Proc. 5th Int. Conf. on Soil Mech. and Found. Engr. 1.

7 - Bhalla, S.J.S. (1970). "Uplift Capacity of Inclined Piles in Sand", M. Engr. Thesis, Nova Scotia Tech. College, Halifax, Nova Scotia, Canada.

8 - Biarez, J. (1962). "Contribution à l'étude des propriétés mécaniques des sols et des matériaux pulvérulents", Thèse de Doctorat en Science, Grenoble, France.

9 - Biarez, J., Baucraut, L.M. and Negre, R. (1965). "Equilibre limit d'écrans verticaux soumis à une translation ou une rotation", Proc. 6th Int. Conf. on Soil Mech. and Found. Engr., Montreal, Canada, p. 368.

10 - Biarez, J., Grosjean, PH. et Trān-Vō-Nhiem (1970). "Force de soulèvement d'une fondation en fonction de la force normale aux parois latérales en milieu pulvérulent bidimensionnel", Comptes-rendus de l'Académie des Sciences, Paris, France.

11 - Brinch-Hansen, J. (1953). "Earth Pressure Calculation", Copenhagen, Denmark.

12 - Caquot, A. and Kérisel, L. (1966). "Traité de mécanique des sols", Gauthier-Villars, Paris, France.

13 - Caquot, A. and Kérisel, L. (1948). "Tables de poussée et butée", Gauthier-Villars, Paris, France.

14 - Casbarian, A.O.P. (1967). "Ultimate Lateral Resistance of Anchor Plates in Cohesionless Soils", Third Pan-American Conf. on Soil Mech. and Found., Caracus, Venezuela, Vol. II, Div. 4.

15 - Chen, W.F. (1975). "Limit Analyses and Soil Plasticity", Elsevier Scientific Publishing Company, New York, N.Y.

16 - Colb, J.L. and Herbich, J.B. (1972). "Effects of Inclined and Eccentric Load Application on the Breakout Resistance of Objects Embedded in the Sea Floor", Sea Grant Publication, No. TAMU-SG-72-204, Coastal and Ocean Engr. Div., Report No. 153, Texas A & M University.

17 - Conley, Williams (1984). "Computer Optimization Techniques - Revised Edition", Petrocelli Books Inc., New York, Princeton.

18 - Das, B.M. (1975). "Pullout Resistance of Vertical Anchors", Proc. ASCE, Vol. 100, No. GT1.

19 - Das, B.M. (1975). "Pullout Resistance of Vertical Anchors", Jnl of the Geotechnical Engr. Div., ASCE, Vol. 101, No. GT1, Proc. Paper 11040, pp. 87-91.

20 - Das, B.M. and Seeley, G.R. (1975). "Passive Resistance of Inclined Anchors in Sand", Jnl of the Geotechnical Engr. Div., ASCE, Vol. 101, No. GT3, Proc. Paper 1152, pp. 353-356.

21 - Donovan, H.L. (1961). "Deep Foundations and Sheet Piling", Concrete Publications Ltd., London, England.

22 - Douglas, D.J. and Davis, E.H. (1964). "The Movement of Buried Footings Due to Movement and Horizontal Load and the Movement of Anchor Plates", Géotechnique 14, No. 2, pp. 115-132.

23 - Hanna, A.M. (1978). "Bearing Capacity of Footings Under Vertical and Inclined Loads on Layered Soils", Doctor of Philosophy Thesis, Nova Scotia Tech. College, Halifax, Nova Scotia, Canada.

24 - Hueckel, S. (1957). "Model Tests on Anchoring Capacity of Vertical and Inclined Plates", Proc. 4th Int. Conf. on Soil Mech., London, England, Vol. 2, p. 203.

25 - Hueckel, S., Kwasniewski, J. and Baran, L. (1965). "Distribution of Passive Earth Pressure on the Surface of a Square Vertical Plate Embedded in Soil", Proc. 6th Int. Conf. on Soil Mech. and Found. Engr., Canada, Vol. II.

26 - James, R.G. and Bransby, P.L. (1971). "A Velocity Field for Some Passive Earth Pressure Problems", Géotechnique 21, No. 1, pp. 61-83

27 - James R.G. and Bransby, P.L. (1970). "Experimental and Theoretical Investigation of a Passive Earth Pressure Problem", Géotechnique, London, England, Vol. 20, No. 1, pp. 17-37.

28 - Kananyan, A.S. (1966). "Experimental Investigation of the Stability of Bases of Anchor Foundations", Soil Mech. and Found. Engr., Moscow, U.S.S.R., Vol. 3, No. 6, p. 9.

29 - von Keviczky, A.B. (1982). "Besonderheiten radialwirkender linearer Integraloperatoren in $H^p(\pi^+)$", Math. Nachr., Vol. 108, pp. 331-355.

30 - Kezdi, A. (1972). "Earth Pressure Measurement", Proc. 5th European Conf. on Soil Mech., Vol. 1, Madrid, Spain, pp. 157-162.

31 - Kondner, R.L. (1963). "Hyperbolic Stress-Strain Response: Cohesive Soils", Jnl of the Soil Mech. and Found. Div., ASCE, Vol. 89, No. SMI, Proc. Paper 3429, pp. 115-143.

32 - Kostyukov, V.D. (1967). "Distribution of the Density of Sand in the Sliding Wedge in Front of Anchor Plates", Soil Mech. and Found. Engr., No. 1, pp. 12-13.

33 - Mariupol'skii, L.G. (1965). "The Bearing Capacity of Anchor Foundations", Osnovaniya Fundamenty i Mekhanika Gruntov, Vol. 3, No. 1, pp. 14-18. (Available in English translation from Consultants Bureau, New York, N.Y., pp. 26-32.)

34 - Meyerhof, G.G. (1973). "The Uplift Capacity of Foundations Under Oblique Loads", Canadian Geotechnical Jnl, Vol. 10, No. 1, pp. 64-70.

35 - Meyerhof, G.G. (1973). "Uplift Resistance of Inclined Anchors and Piles", Proc. 8th Int. Conf. on Soil Mech. and Found. Engr., Vol. 2, Moscow, U.S.S.R., pp. 167-172.

36 - Meyerhof, G.G. and Adams, J.I. (1968). "The Ultimate Uplift Capacity of Foundations", Canadian Geotechnical Jnl, Vol. 5, p. 225.

37 - Muhs, H. (1965). "On the Phenomenon of Progressive Rupture in Connection With the Failure Behavior of Footings in Sand", Discussion of the Proc. of the 6th Conf. on Soil Mech. and Found. Engr., Montreal, Canada, Vol. 3, pp. 419-421.

38 - Neely, W.J. et al (1973). "Failure Loads of Vertical Anchor Plates in Sand", Proc. ASCE, Vol. 99, No. SM2.

39 - Neely, W.J., Stuart, J.C. and Graham, J. (1973). "Failure Loads of Vertical Anchor Plates in Sand", Jnl of Soil Mech. and Found. Div., ASCE, Vol. 99, No. 9, pp. 669-685.

40 - Ovesen, N.K. (1964). "Anchor Slabs Calculation Methods and Model Tests", Danish Geotechnical Inst., Copenhagen, Denmark, Bull. No. 16, p. 5.

41 - Poorooshasb, H.B., Hobulec, I. and Sherbourne, A.N. (1967). "Yielding and Flow of Sand in Triaxial Compression", Canadian Geotechnical Jnl, Vol. IV, No. 4.

42 - Ranjan, G. and Kaushal, Y.P. (1977). "Load Deformation Characteristics of Model Anchors Under Horizontal Pull of Sand", Geotechnical Engineering, Bangkok, Thailand, p. 68.

43 - Ranjan, G. and Kaushal, Y.P. (1975). "Behavior of Vertical Anchors in Sand", Proc. 5th Asian Regional Conf. on Soil Engr., Bangalore, India, Vol I.

44 - Rowe, R.K. (1978). "Soil Structure Interaction Analyses and its Application to the Prediction of Anchor Behavior", Doctor of Philosophy Thesis, University of Sydney, Australia.

45 - Schofield, A.N. (1961). "The Development of Lateral Force of Sand Against the Vertical Face of a Rotating Model Foundation", Proc. 5th Int. Conf. on Soil Mech., Paris, France, Vol. 2, p. 479.

46 - Terzaghi, K. (1948). "Theoretical Soil Mechanics in Engineering Practice", Wiley, New York.

47 - Trân-Vô-Nhiem (1971). "Force portante limite des fondations superficielles et résistance maximale à l'arrachement des ancrages profonds", Thèse de Docteur-Ingénieur, Grenoble, France.

48 - Trân-Vô-Nhiem and Biarez, J. (1971). "Force maximale de soulèvement des fondations d'ancrages en milieu pulvérulent bidimensionel", Proc. 4th Asian Regional Conf. on Soil Mech., Bangkok, Thailand.

49 - Tschebotarioff, G.D. (1973). "Foundations, Retaining and Earth Structures - Second Edition", pp. 536-542.

50 - Vesic, A.S. (1972). "Expansion of Cavities in Infinite Soil Mass", Jnl of the Soil Mech. and Found. Div., ASCE, Vol. 98, No. SM3, Proc. Paper 8790, pp. 265-290.

51 - Vesic, A.S. (1971). "Breakout Resistance of Objects Embedded in Ocean Bottoms", Proc. ASCE, Vol. 97, No. SM9.

52 - Wang, M. C. and Wu, A.H. (1980). "Yielding Load of Anchor in Sand", Symposium on Limit Equilibrium, Plasticity, and Generalized Stress Strain Applications in Geotechnical Engineering, Hollywood, Florida, pp. 291-307.

APPENDIX

```
      PROGRAM THE2(INPUT,OUTPUT,TAPE5=INPUT,TAPE6=OUTPUT)
C-----A THREE VARIABLE
C-----NONLINEAR SYSTEM
C-----MONTE CARLO OPTIMIZATION
      INTEGER Z
      REAL X(3),B(3),M,P,L(3),R
      REAL N(3),AU(3),A(3)
      PI=3.1415927
      ALPHA=90.0
      PHY=10.0
      D=0.0
      H=1.0
      DELTA=5.0
      DO 76 IB=1,20
      F=1.5
      DO 1 I=1,3
      B(I)=0.0
      A(I)=45.0
      N(I)=90.0
      M=1.0E70
      DO 19 J=1,12
      Z=30
      DO 3 II=1,Z
      DO 4 K=1,3
      IF (A(K)-N(K)/F**J.LT.B(K)) GO TO 50
      GO TO 60
50    L(K)=B(K)
      GO TO 65
60     L(K)=A(K)-N(K)/F**J
65    IF (A(K)+N(K)/F**J.GT.N(K)) GO TO 80
      GO TO 90
80    AU(K)=N(K)-L(K)
      GO TO 100
90    AU(K)=A(K)+N(K)/F**J-L(K)
100   CONTINUE
      X(K)=L(K)+RANF()*AU(K)
4     CONTINUE
      R1=ALPHA+X(2)-X(1)
      R2=PHY+X(2)+ALPHA
      R3=X(3)+2*PHY+ALPHA-X(1)
      R4=D+H*SIN(ALPHA*PI/180.0)
      R5=H*SIN(X(1)*PI/180.0)*SIN(X(2)*PI/180.0)
      R6=SIN(R1*PI/180.0)
      IF((R4-R5/R6).LE.0.0) GO TO 3
      IF ((PHY+X(2)).LE.(90.0-ALPHA)) GO TO 3
      IF (X(2).GE.X(3)) GO TO 3
      IF (SIN(R1*PI/180.0).GE.0.999) GO TO 3
      IF (SIN(R1*PI/180.0).LE.0.001) GO TO 3
      IF (SIN(R2*PI/180.0).GE.0.999) GO TO 3
      IF (SIN(R2*PI/180.0).LE.0.001) GO TO 3
      IF (SIN(R3*PI/180.0).GE.0.999) GO TO 3
      IF (SIN(R3*PI/180.0).LE.0.001) GO TO 3
      IF (ABS(TAN(DELTA*PI/180.0)/TAN(R2*PI/180.0)+1.0)
     * LE. 0.001) GO TO 3
      CALL FCN(PI,ALPHA,PHY,D,H,DELTA,X,P)
```

```
56                IF (P .LE. 0.0) GO TO 3
57                IF (P.LT.M) GO TO 200
58                GO TO 3
59           200  CONTINUE
60                M=P
61                DO 11 I1=1,3
62                A(I1)=X(I1)
63            11  CONTINUE
64             3  CONTINUE
65            19  CONTINUE
66                WRITE(6,300) M
67           300  FORMAT(1H ,E20.8)
68                WRITE(6,302) A(1),A(2),A(3)
69           302  FORMAT(1H ,3F16.7)
70            76  CONTINUE
71                STOP
72                END
```